Max-Planck-Institut für Meteorologie
Max Planck Institute for Meteorology

MAX-PLANCK-GESELLSCHAFT

Impact of small-scale fluctuations on climate sensitivity and its stochastic analysis

Rita Seiffert

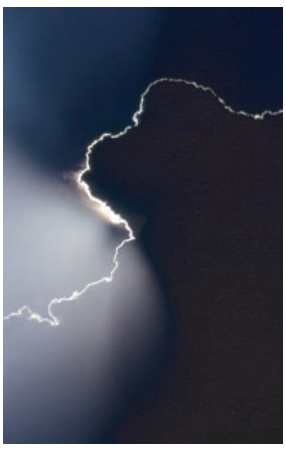

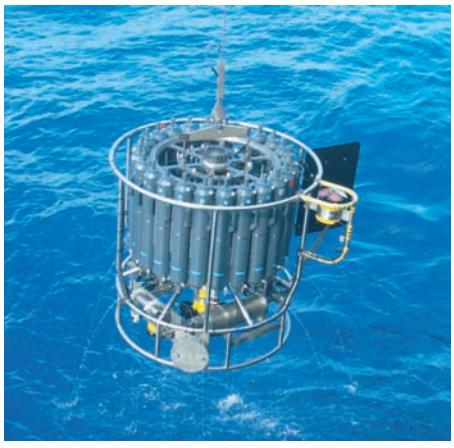

Berichte zur Erdsystemforschung 58/2009

Reports on Earth System Science

Hinweis

Die Berichte zur Erdsystemforschung werden vom Max-Planck-Institut für Meteorologie in Hamburg in unregelmäßiger Abfolge herausgegeben.

Sie enthalten wissenschaftliche und technische Beiträge, inklusive Dissertationen.

Die Beiträge geben nicht notwendigerweise die Auffassung des Instituts wieder.

Die "Berichte zur Erdsystemforschung" führen die vorherigen Reihen "Reports" und "Examensarbeiten" weiter.

Notice

The Reports on Earth System Science are published by the Max Planck Institute for Meteorology in Hamburg. They appear in irregular intervals.

They contain scientific and technical contributions, including Ph. D. theses.

The Reports do not necessarily reflect the opinion of the Institute.

The "Reports on Earth System Science" continue the former "Reports" and "Examensarbeiten" of the Max Planck Institute.

Anschrift / Address

Max-Planck-Institut für Meteorologie
Bundesstrasse 53
20146 Hamburg
Deutschland

Tel.: +49-(0)40-4 11 73-0
Fax: +49-(0)40-4 11 73-298
Web: www.mpimet.mpg.de

Layout:

Bettina Diallo, PR & Grafik

Titelfotos:
vorne:
Christian Klepp - Jochem Marotzke - Christian Klepp
hinten:
Clotilde Dubois - Christian Klepp - Katsumasa Tanaka

Berichte zur Erdsystemforschung 58/2009

Impact of small-scale fluctuations on climate sensitivity and its stochastic analysis

Dissertation zur Erlangung des Doktorgrades der Naturwissenschaften
im Departement Geowissenschaften der Universität Hamburg
vorgelegt von

Rita Seiffert

aus Berlin

Hamburg 2008

Reports on Earth System Science 58/2009

ISSN 1614-1199

Rita Seiffert
Max-Planck-Institut für Meteorologie
Bundesstrasse 53
20146 Hamburg
Germany

Als Dissertation angenommen
vom Department Geowissenschaften der Universität Hamburg

auf Grund der Gutachten von
Prof. Dr. Jochem Marotzke
und
Dr. Jin-Song von Storch

Hamburg, den 28. Oktober 2008
Prof. Dr. Jürgen Oßenbrügge
Leiter des Departments für Geowissenschaften

ISSN 1614-1199

Impact of small-scale fluctuations on climate sensitivity and its stochastic analysis

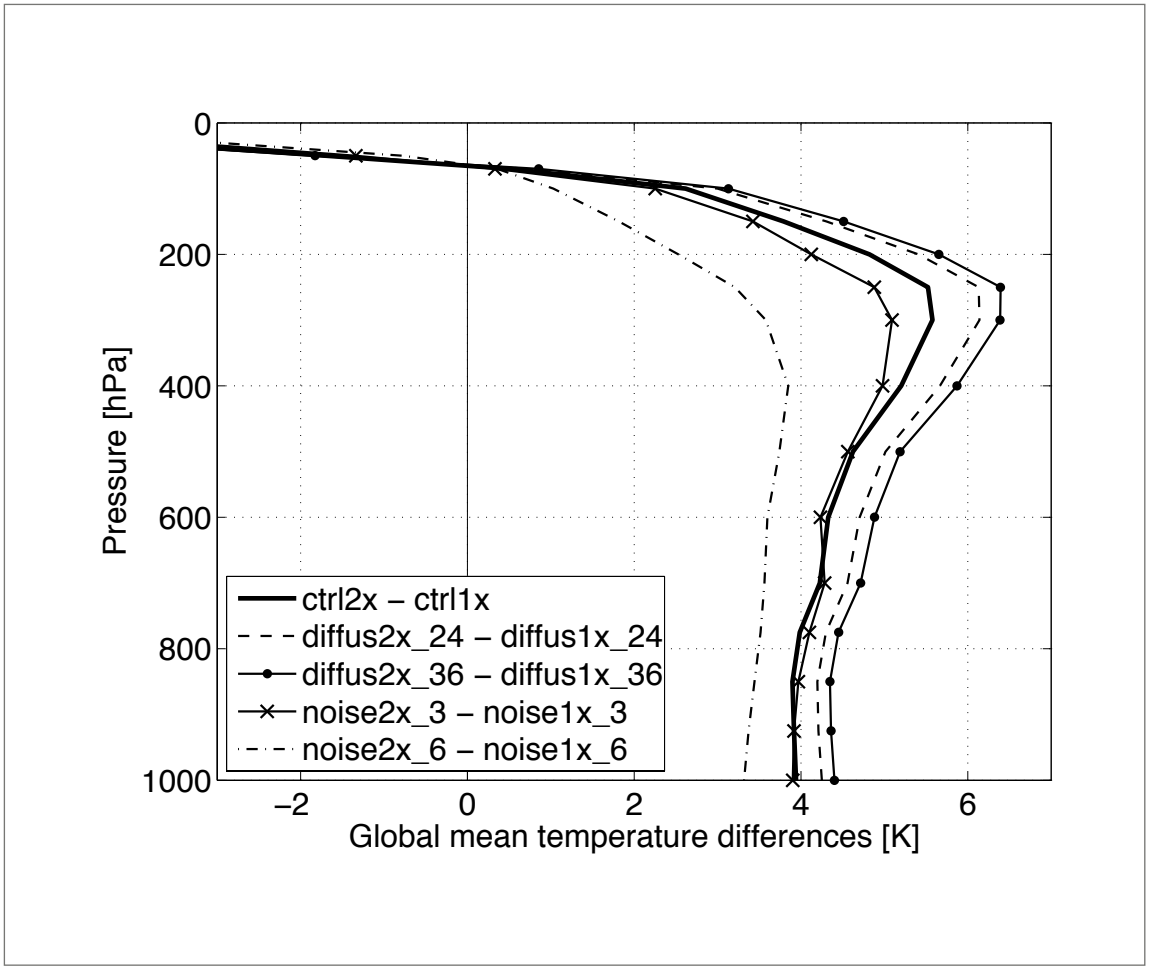

Rita Seiffert

Hamburg 2008

The figure on the previous page shows: Temperature response to doubled CO_2 concentration (i.e., $T2\times CO_2$ –$T1\times CO_2$) obtained from experiments with different representations of small scale fluctuations. The results are based on the temperature means over the last 50 years of the integrations.

Abstract

One of the main challenges in climate research is the estimation of the climate response to increasing greenhouse gas concentrations. Such an estimation is often made with the aid of a climate model. Although climate models are forced in the same way, they simulate different climate sensitivities. Model errors caused by the representations of feedback processes related to water vapour, clouds, temperature lapse rate and surface albedo are known to account for the high uncertainty of the modelled climate sensitivity. But also the representation of dynamical small-scale processes could affect the modelled climate sensitivity. All climate models have finite spatial and temporal resolutions. The impact of unresolved processes is often parameterised without taking the variability induced by subgrid-scale processes into account.

The aim of this study is to investigate the impact of enhanced small-scale atmospheric fluctuations on the modelled climate response to increased CO_2 concentration. Using a coupled atmosphere-ocean-sea ice general circulation model (ECHAM5/MPI-OM) we carried out experiments with enhanced small-scale fluctuations. To enhance small-scale fluctuations we reduced the horizontal diffusion or added white noise to spectral coefficients with high total wavenumbers.

Whereas the reduction of the horizontal diffusion hardly affects the mean state of the pre-industrial climate, the additional noise alters the climate considerably. The climate response to a doubling of the CO_2 concentration is influenced by both methods used to enhance the small-scale fluctuations. Reducing the horizontal diffusion by a factor of 3 leads to an increase of the equilibrium climate sensitivity at the surface by 13%. If white noise is added to the small scales, the surface climate sensitivity tends to weaken. In general, the largest changes in responses occur in the upper troposphere.

To better understand how small-scale fluctuations alter the climate sensitivity we used a simple stochastic model. We fitted a Langevin equation to the global mean temperature time series at 300 hPa. The analysis based on the stochastic model enables us to distinguish between two mechanisms influencing the climate sensitivity. Enhanced small-scale fluctuations can influence the climate sensitivity via altering feedback and interaction processes which are present in the unper-

turbed system and/or via altering processes which are only occurring in response to the CO_2 increase. Whereas reducing the horizontal diffusion changes the climate sensitivity via the second mechanism, the additional noise initiates both mechanisms.

Although the impact of the enhanced small-scale fluctuations on the modelled climate sensitivity is not as large as, e.g., the impact of different cloud parameterisations, it is not a negligible source of uncertainty for the determination of the future climate change.

Contents

1 Introduction

1.1 Motivation

Due to the industrialisation atmospheric greenhouse gas concentrations (e.g., of carbon dioxide (CO_2), methane (CH_4), and nitrous oxide (N_2O)) increase remarkably. The unnatural high greenhouse gas concentrations affect the climate. To assess the future climate change we use comprehensive climate models. For example, we want to know how much the globally averaged surface temperature will rise due to the increased greenhouse gas concentrations until the end of the 21st century.

When using comprehensive climate models to answer the above question we come across two major sources of uncertainty. a) The models themselves are no one-to-one representations of the real climate system. b) We force the models with prescribed emission scenarios, which describe only a few possible future developments of the greenhouse gas emissions. In this study we want to focus on the first source of uncertainty, i.e., the question of how model errors influence the climate response.

The results published in the 4th Assessment Report (AR4) of the Intergovernmental Panel on Climate Change (IPCC) show that the simulated increase of temperature largely depends on the climate model applied. Although the comprehensive climate models are all forced in the same way, e.g. according to the A1B scenario, they show different climate responses. The projected globally averaged surface warming at the end of the 21st century ranges from 1.7 K to 4.4 K (IPCC, 2007). This transient climate response is closely related to the equilibrium climate sensitivity of each model. The equilibrium climate sensitivity is generally defined as the equilibrium change in global surface temperature due to a doubling of CO_2 concentration.

Several attempts have been made to quantify the degree of uncertainty of the equilibrium climate sensitivity. Murphy et al. (2004), Piani et al. (2005), and Knutti et al. (2006) determine the uncertainty of the climate sensitivity due to model errors by estimating probability density functions of the climate sensitivity. They use perturbed physics ensembles. That means, the same climate model is run

many times with different set of parameters to explore the widest possible range of model responses to CO_2 doubling. Their results suggest that the equilibrium climate sensitivity lies between 1.5 K and 6.8 K. These values depend, however, strongly on the explicit method used to estimate the probability density functions.

Thermodynamical feedback processes

Model errors caused by parameterisations of processes related to nonlinear thermodynamical feedbacks are generally called to account for the high uncertainty of the climate sensitivity. These feedbacks involve interactions of water vapour, clouds, temperature lapse rate and surface albedo with the earth's radiation budget (Bony et al., 2006). Several studies (e.g., Colman (2003), Soden and Held (2006), Webb et al. (2006)) have estimated the strength of the feedback processes in different climate models and provided valuable insight into the origins of varying model sensitivities. Especially, the cloud feedback is found to be a large source of uncertainty.

Dynamical small-scale processes

In this study we do not concentrate on model errors originating, e.g., from cloud parameterisations, sea ice modelling, or other thermodynamical feedback processes, rather we investigate the effect of the representation of dynamical small-scale processes on the modelled climate sensitivity. The climate system is not only determined by the interactions of complex thermodynamical processes but also by nonlinear dynamical coupling of various scales of motion. As a consequence of the limited model resolution in space and time, the governing equations are truncated at a certain scale. Dynamical processes below this scale cannot be adequately represented in the models and have to be parameterised. Such parameterisations generally do not take the variability into account, which is induced by the subgrid-scale processes. Especially, the variability near the truncation scale is neglected (Seiffert et al., 2006), and this variability can affect the behaviour of large-scale processes (von Storch, 2004).

Climate response experiments with different model resolutions indicate that the model sensitivity to increased CO_2 concentration depends on the model resolution and with it on the representation of small-scale processes. Kiehl et al. (2006) found that the climate sensitivity of the Community Climate System Model 3 (CCSM3) increases with increased horizontal resolution. The equilibrium climate sensitivity of the high-resolution version (T85) is 17% higher than the model sensitivity of the low-resolution version (T31). In contrast, the atmospheric general

circulation model ECHAM5 of the Max Planck Institute (MPI) for Meteorology coupled to a fixed-depth (50m) mixed layer ocean and a thermodynamical sea ice module experiences a reversed trend (E. Roeckner, personal communication, 2007). The results of May and Roeckner (2001), who used an earlier version of the present MPI model, ECHAM4, also suggest a weaker climate response to increased CO_2 concentration when changing the resolution from T42 to T106. The opposite trends in the two models, CCSM3 and ECHAM, can be ascribed to many factors. The different parameterisations of complex thermodynamical processes in the two models certainly play an important role. Since parameterisations in general depend on the chosen model resolution, it is hard to distinguish between the effect of changed parameterisations due to different resolution and the effect of additional resolved small-scale processes on the climate sensitivity. Hence, to investigate the impact of changes in the representation of dynamical small-scale processes we do not change the model resolution in this study.

Fluctuation dissipation theorem

From a more theoretical point of view we find arguments how the representation of the small-scale fluctuations could influence the climate sensitivity by considering the fluctuation dissipation theorem. The fluctuation dissipation theorem (FDT) originates from statistical physics. It states that the response of a system to a changed external forcing can be deduced from the statistical properties of the unperturbed system. Leith (1975) first proposed that the FDT might be applicable to the climate system. Since Leith's paper several studies applied the FDT to climate-like systems (Bell (1980), North et al. (1993), Cionni et al. (2004), Langen and Alexeev (2005), Gritsun and Branstator (2007)).

Bell (1980) gives a nice illustrative example of the idea, how the properties of the undisturbed system are related to the system's response to a changed external forcing. He considers an oscillating mass suspended at the end of a spring. The average height of the mass above the ground represents the mean 'climate state' of the undisturbed system (e.g., a climate system in the equilibrium state with pre-industrial CO_2 concentration). If we increased, e.g., the gravitational force, the average height would decrease. The difference between the average heights in the system with normal gravitational force and in the system with stronger gravitational force is the mean response of the spring-mass-system to the change in external forcing. It represents a measure for its 'climate sensitivity'. The change in average height depends generally on the spring constant describing the elasticity of the spring. The spring constant can be determined by observing the undisturbed

oscillation. Hence we are able to deduce the system's response to a changed external forcing just by observing the undisturbed system. That, however, also means, if the spring constant of the system is altered, the system's response will change. For a complex system like climate, the 'spring constant' results from internal feedbacks and scale-interactions. Due to the dynamical coupling between small and large scales, small-scale variability can affect the statistics of large-scale variables (von Storch, 2004) and with it the climate system's 'spring constant'. Hence neglecting small-scale variability could have an influence on the model sensitivity to CO_2 forcing.

1.2 Thesis objective

Although all climate models have finite resolution in space and time, up to now no study explicitly investigated the impact of the representation of dynamical small-scale processes near the truncation scale on the modelled climate sensitivity. The purpose of this study is to systematically address the question of whether and how small-scale atmospheric fluctuations affect the modelled climate sensitivity to increased CO_2 concentration. Using the coupled atmosphere-ocean-sea ice climate model ECHAM5/MPI-OM we want to answer, in particular, the following questions:

- What influence do enhanced small-scale fluctuations have on the mean climate state?
- Do enhanced small-scale fluctuations influence the modelled climate sensitivity?
- If the small-scale fluctuations affect the climate sensitivity, do the small-scale fluctuations influence the 'spring constant' of the climate model and with it the climate sensitivity?

1.3 Thesis structure

Including this chapter the thesis is structured into seven chapters. Chapter 3, 4, 5, and 6 comprise the main results. Parts of Chapter 3 and 4 are published in Geophysical Research Letters (Seiffert and von Storch, 2008).

In **Chapter 2** the coupled atmospheric-ocean-sea ice model ECHAM5/MPI-OM is shortly introduced. Furthermore, we describe the model experiments carried

out. All experiments are done in pairs: one experiment with pre-industrial CO_2 concentration and one experiment with doubled CO_2 concentration. To enhance small-scale fluctuations we reduce the horizontal diffusion or add white noise to spectral coefficients with high total wavenumbers.

In **Chapter 3** we investigate the impact of the enhanced small-scale fluctuations on the mean climate state of the experiments with pre-industrial CO_2 concentration.

Chapter 4 focuses on the actual question of how enhanced small-scale fluctuations influence the modelled climate sensitivity. We compare the responses to the CO_2 doubling obtained from the experiments without and with enhanced small-scale fluctuations. We show that changing the representation of small-scale processes (i.e., enhancing the small-scale fluctuations) indeed affects the modelled climate response to CO_2 forcing.

In **Chapter 5** we introduce and test a simple stochastic model fitted to the global mean temperature at 300 hPa. We will need this stochastic model in Chapter 6.

Chapter 6 deals with the question whether the enhanced small-scale fluctuations change the modelled climate sensitivity by altering the 'spring constant' of the climate model.

The final chapter comprises the general conclusions and an outlook.

2 Model and experiments

2.1 The coupled model ECHAM5/MPI-OM

ECHAM5/MPI-OM is a comprehensive coupled atmosphere-ocean-sea ice general circulation model developed at the Max Planck Institute for Meteorology (MPI-M) in Hamburg (Germany). It consists of the atmosphere model ECHAM5 and the MPI-ocean model (MPI-OM). The interactions between the atmosphere model and the ocean model are realised via the Ocean-Atmosphere-Sea Ice-Soil (OASIS) coupler (Valcke et al., 2003). No flux-adjustment is needed to maintain a realistic steady climate. The model is used for a wide range of applications (e.g., Pohlmann et al. (2006), Bengtsson et al. (2007), IPCC (2007), Marotzke and Botzet (2007), Kloster et al. (2007), von Storch and Haak (2008)).

2.1.1 Atmosphere

The atmospheric model is the global general circulation model ECHAM5.2. The model consists of a spectral dynamical core based on the primitive equations and a comprehensive set of physical parameterisations. The prognostic variables temperature, vorticity, divergence, and the logarithm of the surface pressure are represented in the horizontal by finite series of spherical harmonics. In the vertical the atmosphere is divided into hybrid sigma-pressure levels reaching up to the pressure level of 10 hPa. Throughout this study we will mainly use the model version with the resolution T31L19. T31 denotes the truncation of the series of spherical harmonics at the zonal and total wavenumber $m_0 = l_0 = 31$ ($\approx 3.8° \times 3.8°$); L19 refers to the usage of 19 vertical levels. In Chapter 3 we also refer to the higher model resolution T63L31 indicating a truncation at $m_0 = l_0 = 63$ ($\approx 1.9° \times 1.9°$) and 31 vertical levels.

The set of physical parameterisations includes shortwave radiation, longwave radiation, cumulus cloud convection as well as stratiform cloud formation. Furthermore, parameterisations involving boundary layer processes and unresolved scale-interactions are implemented. For a more detailed description of ECHAM5 see Roeckner et al. (2003) or Roeckner et al. (2006). The latter provides also a

comparison of the simulated climate to reanalysis data.

2.1.2 Ocean

The ocean model MPI-OM is based on the primitive equations for a hydrostatic Boussinesq fluid on a rotating sphere. For horizontal discretisation an orthogonal curvilinear C-grid is used. The North Pole of the grid is located over Greenland and the South Pole is placed at the centre of Antarctica. In this way we avoid the numerical singularities associated with the convergence of the meridians at the geographical North Pole. The ocean model coupled to the T31L19-atmospheric model has a horizontal resolution of nominally 3 degrees (Arctic: ≈ 20 km, Tropics: ≈ 350 km). The T63L31-atmospheric model is coupled to the MPI-OM with a horizontal resolution of ≈ 1.5 degrees. In the vertical we use 40 unevenly spaced vertical z-levels.

The model includes subgrid-scale parameterisation such as vertical and along-isopycnal diffusion, eddy-induced isopycnal tracer mixing following Gent et al. (1995), vertical eddy viscosity and a bottom boundary layer slope convection scheme. Furthermore the effect of ocean currents on wind stress is taken into account. The MPI-OM also comprises a dynamic, thermodynamic sea-ice model. More technical details about the ocean model can be found in Marsland et al. (2003). A description of the mean ocean circulation for the high-resolution version is given by Jungclaus et al. (2006).

2.2 Experimental setups

2.2.1 Two approaches to modify the small-scale fluctuations

Using the low-resolution version of ECHAM5/MPI-OM (atmosphere: T31L19, ocean: 3°) we carry out idealised response experiments with enhanced small-scale fluctuations. Two different approaches are used to enhance the small-scale fluctuations.

The first method involves a modification of the horizontal diffusion in ECHAM5. The horizontal diffusion damps to a large extent the variability of small-scale components and can therefore be used to enhance small-scale variability. This parameterisation is implemented in ECHAM5 to incorporate the nonlinear interactions between subgrid scales and resolved scales. It is mainly used to ensure a realistic energy spectrum of the resolved scales.

The horizontal diffusion is applied in spectral space on the prognostic variables: temperature, vorticity and divergence. The time rate of change of the spectral coefficient $X_{l,m}$ caused by the horizontal diffusion is defined as

$$\left.\frac{\partial X_{l,m}}{\partial t}\right|_{\text{horizontal diffusion}} = -K_l X_{l,m} \tag{2.1}$$

with

$$K_l = \frac{1}{\tau_0}\left(\frac{l(l+1)}{l_0(l_0+1)}\right)^q. \tag{2.2}$$

The damping factor K_l depends strongly on the total wavenumber l. l_0 marks the truncation scale of the model (here $l_0 = 31$). The exponent q depends on the vertical level. q ranges from 2 in the uppermost three levels to 10 in the middle and lower troposphere. The damping time scale τ_0 controls the strength of the diffusion. In the low-resolution model version (T31L19) it is set to $\tau_0 = 12\,\text{h}$. An increase in τ_0 leads to a weaker damping and hence an enhancement of the variability of high wavenumber components.

In the second approach the horizontal diffusion remains unchanged. Instead we add noise to the smallest resolved scales. At each time step white noise is added to the spectral coefficients of temperature, divergence and vorticity with a total wavenumber $l \geq 26$. Note that the explicit representation of the small-scale processes related to wavenumbers close to the truncation scale ($l_0 = 31$) is not reliable anyway. The noise mimics a possible impact of unresolved processes. It does, however, not qualify for a realistic parameterisation of the subgrid-scale variability. Rather, it aims to isolate the impact of enhanced small-scale fluctuations on the climate sensitivity in the framework of idealised experiments.

2.2.2 Experiments

The experiments are carried out in pairs. Each set of experiments comprises one integration done with pre-industrial CO_2 concentration (280 ppm) and one integration with doubled CO_2 concentration. The difference of these two integrations can then be referred to as the response of the system to the increased CO_2 concentration. The doubled CO_2 concentration experiment was originally started from a state of the pre-industrial control integration. The $2\times CO_2$ concentration was achieved by a 1% per year increase until the final value of 560 ppm was reached. Holding the concentration constant, the model was further integrated for 930 years. The control experiment with pre-industrial CO_2 concentration has a total length of 1650 years.

	$1\times CO_2$	$2\times CO_2$
control experiments, τ_0=12 h, $\sigma_{noise} = 0$	`ctrl1x`	`ctrl2x`
reduced horiz. diffusion, τ_0=24 h	`diffus1x_24`	`diffus2x_24`
reduced horiz. diffusion, τ_0=36 h	`diffus1x_36`	`diffus2x_36`
moderate noise, $\sigma_{noise} = 3 \times 10^{-2}$ K ($3 \times 10^{-7}\,s^{-1}$)	`noise1x_3`	`noise2x_3`
high noise, $\sigma_{noise} = 6 \times 10^{-2}$ K ($6 \times 10^{-7}\,s^{-1}$)	`noise1x_6`	`noise2x_6`

Table 2.1: *Overview of the experiments carried out with ECHAM5/MPI-OM (atmosphere: T31L19, ocean:* 3°

Table 2.1 gives an overview of the experiments. Experiments `ctrl1x` and `ctrl2x` correspond to the control integrations of the standard model with no changes of the representation of the small-scale fluctuations. '`1x`' and '`2x`' denotes $1\times CO_2$ and $2\times CO_2$. For the analysis we considered the last 150 years of `ctrl1x` and of `ctrl2x`. The other experiments shown in Table 2.1 are 150 years long experiments which were branched off `ctrl1x` (at year 1500) and `ctrl2x` (at year 780 after reaching $2\times CO_2$). In these experiments we altered the model as described below.

In experiments `diffus1x_24`, `diffus2x_24`, `diffus1x_36`, and `diffus2x_36` the horizontal diffusion is reduced. The damping time τ_0 is increased by a factor of 2 or 3 from the standard value of 12 h to 24 h or 36 h. Figure 2.1 shows the damping factor K_l for the three configurations. Furthermore, four experiments with additional noise in the smallest resolved scales are carried out: `noise1x_3`, `noise2x_3`, `noise1x_6`, and `noise2x_6`. Here '`_3`' and '`_6`' distinguishes between two noise intensities. In the experiments `noise1x_3` and `noise2x_3` the standard deviation of the white noise σ_{noise} is 3×10^{-2} K for temperature and $3 \times 10^{-7}\,s^{-1}$ for vorticity and divergence. In the experiments `noise1x_6` and `noise2x_6` we use higher noise intensities: 6×10^{-2} K for temperature and $6 \times 10^{-7}\,s^{-1}$ for vorticity and divergence.

2.2.3 Discussion

Methods to enhance small-scale fluctuations

The implementation of horizontal diffusion into ECHAM5 is a simple and efficient way to ensure numerical stability and of parameterising subgrid-scale horizontal mixing and the energy-cascade into unresolved scales. The strength and the form of the horizontal diffusion are, however, under debate (e.g., Kaas et al. (1999)). Given the uncertainty of the form and strength of the horizontal diffusion, a

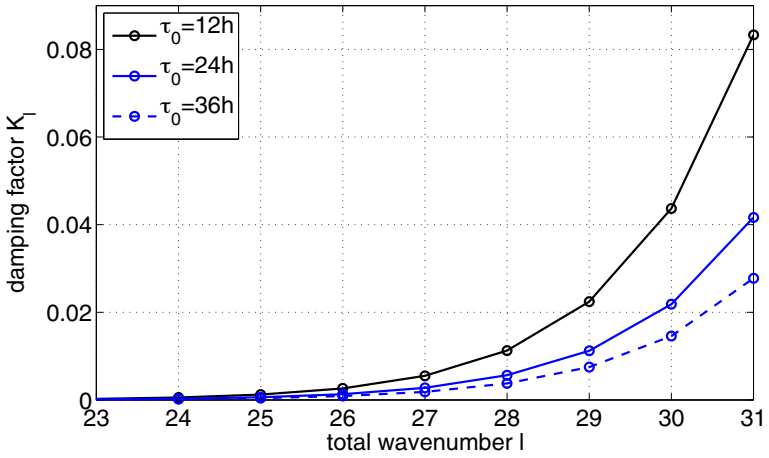

Figure 2.1: *Damping factor obtained from the horizontal diffusion in ECHAM5 (T31) for q=10 and different τ_0; black solid: τ_0=12 h, blue solid: τ_0=24 h, blue dashed: τ_0=36 h*

reduction of the horizontal diffusion to allow more small-scale fluctuations is not a drastic modification of the climate model.

Adding white noise to the smallest resolved scales can be seen as a simple approach to taking the effect of unresolved scales into account. In general, white noise is only appropriate if the time scales of the resolved variability are clearly separated from those of the dominant unresolved scales. Since the climate model resolves only time scales of hours and longer, the noise could represent fast atmospheric fluctuations occurring on time scales of minutes to seconds. Nevertheless, we should keep in mind that the white noise serves not as a realistic stochastic parameterisation of the subgrid-scale variability. A real stochastic parameterisation of the subgrid-scale variability would involve a more complex stochastic process (Buizza et al. (1999), Seiffert et al. (2006)). In this study we take the addition of white noise to the smallest resolved scales as a simple approach to enhancing small-scale fluctuations in a conceptual way.

Experimental design

Note that we do not carry out explicit response experiments for all pairs of experiments. That means, to estimate the response of the model with, e.g., reduced horizontal diffusion we do not slowly increase the CO_2 concentration (until 560 ppm) starting from `diffus1x_36`. Instead, we directly branch off a new experiment with reduced horizontal diffusion from the 2×CO_2 control experiment

`ctrl2x`. After some time the model run with reduced horizontal diffusion and $2\times CO_2$ concentration will reach a new equilibrium.

The advantage of this approach is the shorter computation time. If we increased the CO_2 concentration for each experiment with enhanced small-scale fluctuations individually, we would have to integrate the model each time over several hundred years. Since the enhancement of small-scale variability is only a minor change to the system compared to doubling the CO_2 concentration, the model adjusts more quickly.

The question arises whether our strategy will provide different results in comparison to the more straightforward way of increasing the CO_2 concentration in each setup individually. Assuming that each set of boundary conditions (such as the CO_2 concentration and the representation of the small scales) corresponds to one unique steady state, it should not matter how this steady state is reached. If it were crucial whether we first increased the CO_2 concentration and then reduced the horizontal diffusion or vice versa, we would find two different equilibria with the same boundary conditions. Since we do not expect that enhancing the small-scale fluctuations will lead to profound structural changes of the modelled system (e.g., an earth totally covered with ice), the existence of two steady state with the same boundary conditions is not likely.

3 Impact of enhanced small-scale fluctuations on the mean climate

3.1 Introduction

The main objective of this thesis is to investigate the impact of enhanced small-scale fluctuations on the climate sensitivity. Before we actually explore how the climate sensitivity is influenced by enhanced small-scale fluctuations, we will in this chapter compare the mean climate states of all $1\times CO_2$-experiments.

The idea that the representation of dynamical small-scale processes influences the mean state of a model is not new. It is actually closely related to the research question of finding a good parameterisation for the unresolved nonlinear interactions between subgrid scales and resolved scales. Studies by Koshyk and Boer (1995), Stephenson (1995), Kaas et al. (1999) and Frederiksen et al. (2003) show that different parameterisation of the unresolved scale-interactions (which also result in different small-scale fluctuations) can alter large scale quantities. Frederiksen et al. (2003), for example, compares general circulation model experiments employing a standard scale-selective horizontal diffusion scheme and experiments employing a different horizontal diffusion scheme based on closure theory. They find that the two experimental setups show significant differences in the large-scale circulation.

By comparing the mean states of the $1\times CO_2$-experiments `ctrl1x`, `diffus1x_24`, `diffus1x_36`, `noise1x_3`, and `noise1x_6` we analyse how our changes in the representation of dynamical small-scale processes influence the mean climate state. In Section 3.2.1 we first show that reducing the horizontal diffusion or adding white noise to the small scales indeed enhances the small-scale fluctuations. In the subsequent subsections we then compare the atmospheric temperature, clouds, the atmospheric circulation, the ocean circulation and the kinetic energy spectrum of the $1\times CO_2$-experiments.

3.2 Comparison of the 1×CO_2-experiments

3.2.1 Enhanced small-scale variability

From Figure 3.1 we can see that a reduction of the horizontal diffusion or additional noise on the small-scale components in fact enhances the small-scale variability. Figure 3.1a - c) shows the standard deviations of the spectral coefficients of the three prognostic variables: temperature, vorticity, and divergence in the control-experiment (`ctrl1x`). Low wavenumbers correspond to large-scale components and high wavenumbers to small-scale components. Figure 3.1d - i) displays the ratio of the standard deviations from experiments with modified small-scale components to the standard deviations obtained from the control-experiment. As expected the variability of spectral coefficients with high total wavenumbers is significantly enhanced if the horizontal diffusion is reduced or if noise is added to the small-scale components. (The other two experiments `diffus1x_24` and `noise1x_6`, which are not shown, show qualitatively the same behaviour.) Note that the much larger gain of small-scale variability in `noise1x_3` compared to `diffus1x_36` is due to the rather high noise intensity used. By decreasing the noise intensity it would be possible to induce changes of similar magnitude. We chose a rather high noise intensity to ensure that the additional variability is not damped out right away by the horizontal diffusion. The light blue areas at smaller wavenumbers indicate slightly less variability at larger scales due to the reduced horizontal diffusion or the noise.

The question arises, how well do our idealised experiments compare to the situation if the model resolution is actually increased. An experiment with higher resolution of the coupled model (atmosphere: T63L31, ocean: $1.5^\circ \times 1.5^\circ$) includes small-scale processes beyond the truncation scale of T31. In this experiment nonlinear scale-interactions across this scale are possible.

The horizontal diffusion acts by design only on spectral coefficients near the truncation scale. Since the spectral coefficients with total wavenumbers $25 \lesssim l \leq 31$ are in the T63-experiment not close to the truncations scale, these spectral coefficients are in this experiment almost not affected by the damping of the horizontal diffusion. In contrast, in the T31-experiment the spectral coefficients with total wavenumbers $25 \lesssim l \leq 31$ are strongly influenced by the damping of the horizontal diffusion. If we considered only the difference in the damping caused by the different horizontal diffusion in T63 and T31, the variability of spectral coefficients with total wavenumbers $25 \lesssim l \leq 31$ should be much higher in T63 than in T31. The additional resolved scale-interactions in T63, however, partly lead to

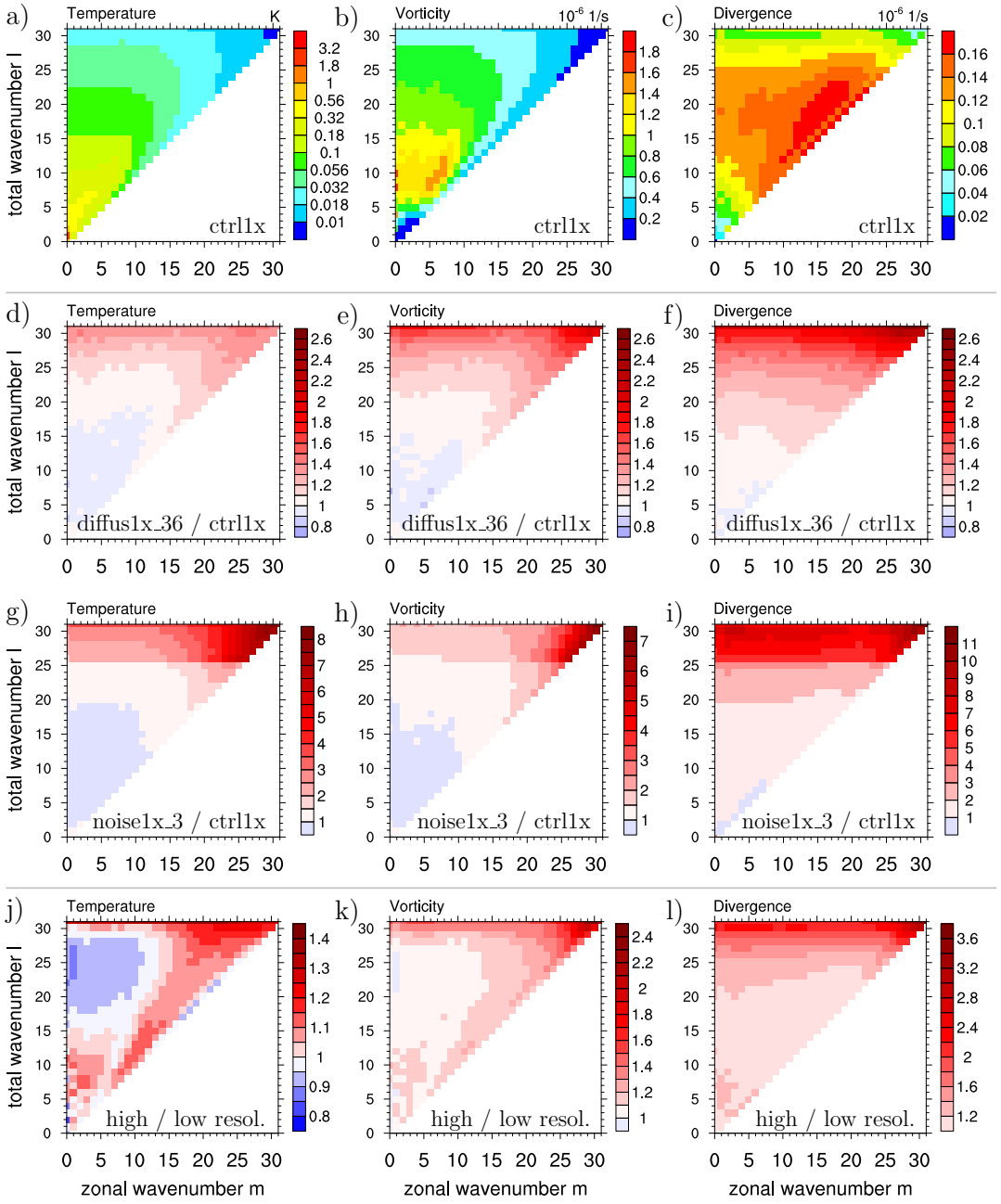

Figure 3.1: *a)-c) Standard deviations of spectral coefficients of experiment* **`ctrl1x`**, *d)-l) Ratio of the standard deviations of the spectral coefficients: d)-f)* **`diffus1x_3/ctrl1x`**, *g)-i)* **`noise1x_36/ctrl1x`**, *j)-l)* **`ctrl1x`***(T63L31)/*`ctrl1x`*(T31L19); All estimates shown here are based on 6-hourly data and 50-year averages at model levels ≈500 hPa. Please note the different colour scales.*

a different picture.

In Figure 3.1j - l) the variability of the two different model resolutions are compared. The usage of 19 levels instead of 31 levels in the T63-experiment leads to similar results as described below. When comparing Figure 3.1d - i) with Figure 3.1j - l) some similarities but also clear differences can be observed. As expected, the increased model resolution leads to enhanced small-scale variability of vorticity and divergence, similar to our idealised experiments. However, there is no indication of reduced variability on large scales, as it is found in the diffusion- and noise-experiments. Moreover, the temperature pattern differs (Figure 3.1 j). Spectral coefficients on smallest scales show a slightly higher variability. Except for total wavenumber $l = 31$, higher variability is mostly found for large zonal wavenumbers m, independent of l. There are also spectral coefficients, in particular those with small zonal wavenumbers and large total wavenumbers, which display less variability.

3.2.2 Temperature

Figure 3.2 and Figure 3.3 show global mean temperature time series of the various experiments obtained from 150 years of integration. At year 1 the experiments with enhanced small-scale fluctuations were branched off the experiment `ctrl1x`. The enhancement of the small-scale fluctuations generally disturbs the equilibrium of the system. After a certain time the system reaches a new equilibrium.

Reducing the horizontal diffusion leads to slightly higher temperatures. The surface temperature increases from 288.0 K in the control-experiment to 288.3 K in `diffus1x_36` (see also Table 3.1). The temperature at 300 hPa rises by 0.6 K. By contrast, in the noise-experiments the temperatures at 300 hPa decrease considerably. The surface temperature in `noise1x_3` remains about the same. In the experiment `noise1x_6` the surface temperature drastically starts to fall to a value of 285.9 K. Although the temperature curve of `noise1x_6` seems to level off, it is not completely clear from Figure 3.3 whether the temperature will drop further.

Figure 3.4 compares zonally averaged temperature cross-sections. We consider time averages of the last 50 years. When reducing the strength of the horizontal diffusion the mean temperature in the troposphere slightly increases. Only near the top of the atmosphere do we observe large differences. Adding noise to the small-scale components, however, leads to major changes in the zonal mean temperatures. In the experiment `noise1x_3` the tropics are up to 3 K cooler, especially, in the upper part of the troposphere. We also observe a cooling in the low- and mid-troposphere near the north pole. When increasing the noise intensity the

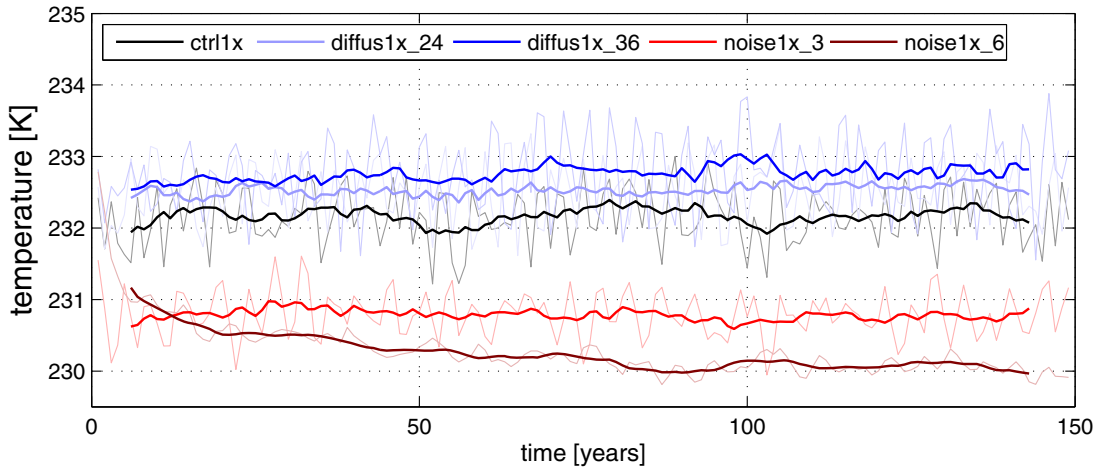

Figure 3.2: *Time series of global mean temperature at 300 hPa of the 1×CO_2-experiments based on yearly averages (thin lines) and 11-year running mean (thick lines)*

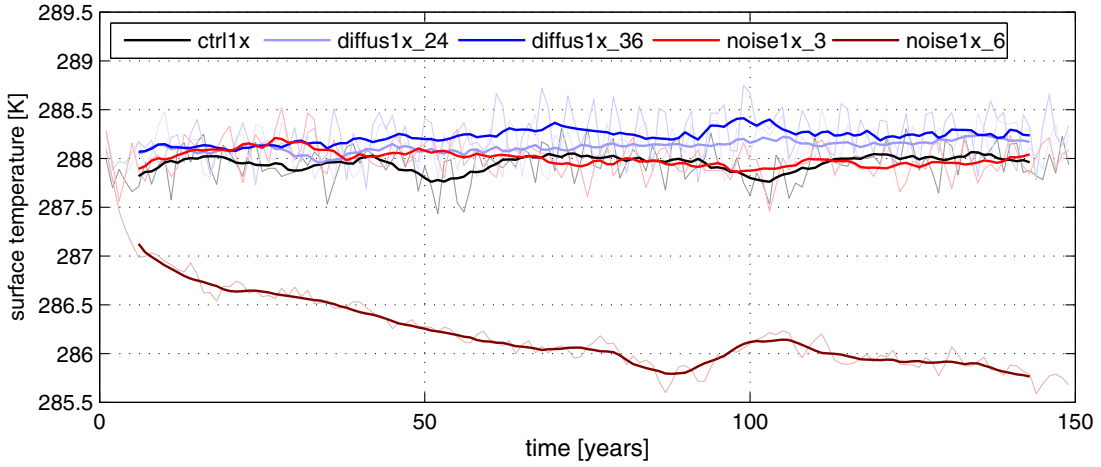

Figure 3.3: *Time series of the global mean surface temperature of the 1×CO_2-experiments based on yearly averages (thin lines) and 11-year running mean (thick lines)*

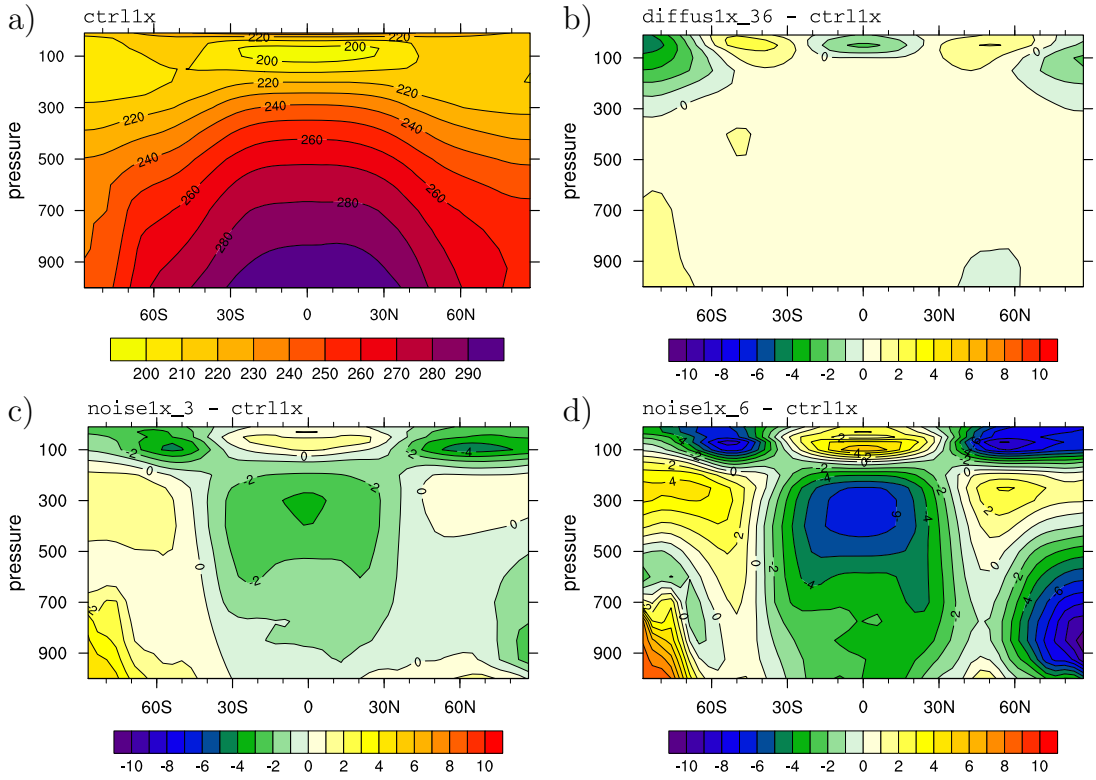

Figure 3.4: *a) Pressure-latitude cross-section of the zonally averaged annual-mean temperature in Kelvin obtained from* **`ctrl1x`***, and the temperature differences of b)* ***`diffus1x_36`*** *-* **`ctrl1x`***, c)* ***`noise1x_3`*** *-* **`ctrl1x`***, and d)* ***`noise1x_6`*** *-* **`ctrl1x`** *also in Kelvin. The results are based on 50-year averages of model years 101-150.*

	T_s	$T300$	q_v
`ctrl1x`	288.0	232.2	26.0
`diffus1x_24`	288.2	232.6	26.4
`diffus1x_36`	288.3	232.8	26.7
`noise1x_3`	287.9	230.8	25.8
`noise1x_6`	285.9	230.1	24.3

Table 3.1: *Time mean of the global mean temperatures at the surface, T_s, and at 300 hPa, $T300$, both in Kelvin, as well as the mean of the global mean vertically integrated water vapour, q_v, in kg/m^2.*

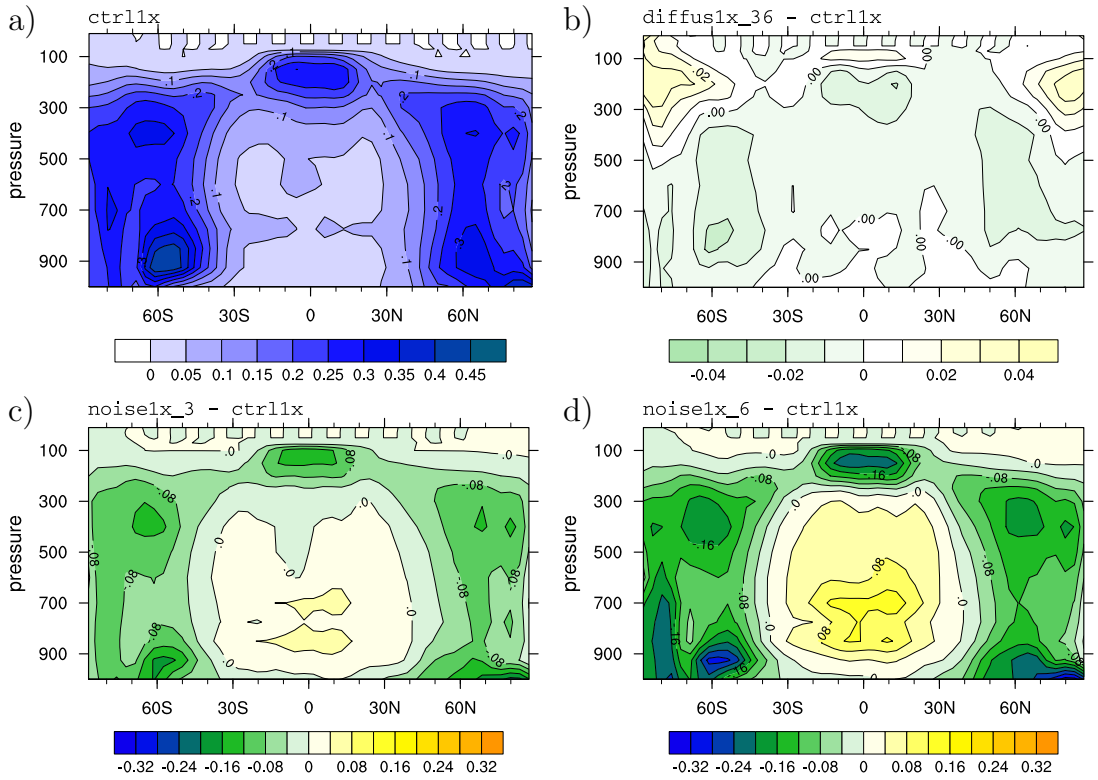

Figure 3.5: *a) Pressure-latitude cross-section of the zonally averaged annual-mean fractional cloud cover obtained from* `ctrl1x`*, and the cloud cover differences of b)* `diffus1x_36 - ctrl1x`*, c)* `noise1x_3 - ctrl1x`*, and d)* `noise1x_6 - ctrl1x`*. The results are based on 50-year averages of model years 101-150.*

difference-pattern is amplified by more than a factor of two.

3.2.3 Clouds

One main reason for the big temperature changes in the noise-experiments are the clouds. From Figure 3.5 it can be seen that also the clouds are significantly influenced by the noise.

In general, clouds influence the earth's radiation budget in two competing ways. First, clouds usually have a higher albedo than the earth's surface. Compared to a clear sky an atmosphere containing clouds reflects more incoming solar radiation, resulting in a cooling effect. In contrast, the second process involved leads to a warming of the atmosphere and the surface. Similar to the greenhouse ef-

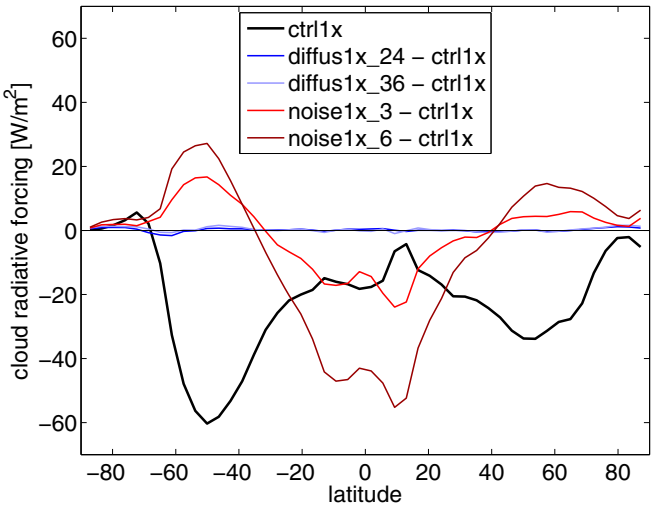

Figure 3.6: *Annual-mean net cloud radiative forcing at the top of the atmosphere of the experiment* ***ctrl1x*** *(black) and the differences between* ***ctrl1x*** *and the four other 1×CO_2-experiments. The curves represent 50-year averages. (The net cloud radiative forcing is defined as the difference between the radiation budget with clouds and without clouds.)*

fect caused by CO_2, clouds absorb and re-emit longwave radiation. A significant amount of outgoing longwave radiation is trapped by the presence of clouds leading to a warming effect.

Numerical experiments using one-dimensional climate models showed that for high clouds the warming effect is larger than the cooling effect. Hence high clouds have a net warming effect. On the other hand middle and low clouds exert a net cooling effect on the climate system. The cooling effect caused by the high albedo of the optically thick middle and low clouds generally outweighs the warming greenhouse effect (Liou, 2002).

In the noise-experiment we find fewer tropical high clouds and more tropical low clouds. Overall this combination results in a cooling of the tropics in comparison to the control-experiment (`ctrl1x`). In the tropics more low clouds amplify the net cooling effect, and the net warming effect of high clouds is reduced. In contrast, in the mid- and high-latitudes the fractional cloud cover is reduced throughout the entire vertical column. The temperature response caused by the changed clouds is not as clear as in the tropics. However, from the change of the mean net cloud radiative forcing (Figure 3.6) we see in the mid-latitudes a warming effect caused by the changed cloud cover in the noise-experiments (red lines). The warming

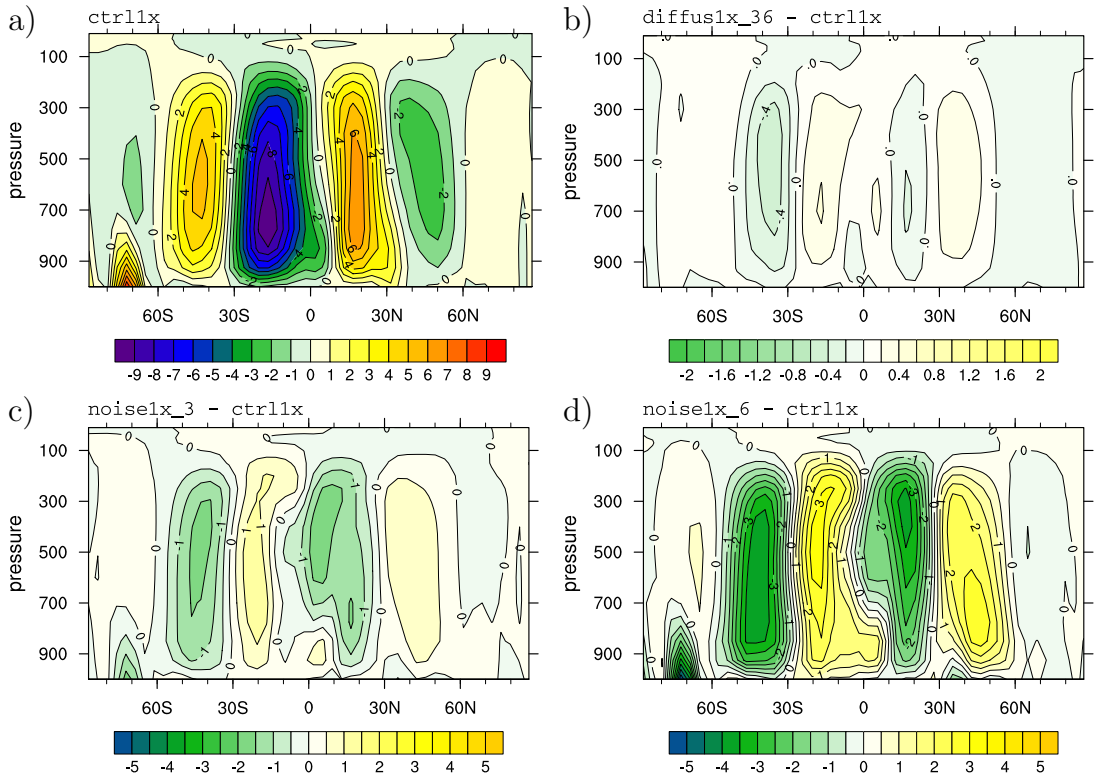

Figure 3.7: *a) Pressure-latitude cross-section of the annual-mean mass stream function in* 10^{10} *kg/s obtained from* **`ctrl1x`**, *and mass stream function differences of b)* **`diffus1x_36`** - **`ctrl1x`**, *c)* **`noise1x_3`** - **`ctrl1x`**, *and d)* **`noise1x_6`** - **`ctrl1x`** *also in* 10^{10} *kg/s. Positive (negative) values in a) indicate clockwise (anticlockwise) circulation. The results are based on 50-year averages of model years 101-150.*

effect is larger in the southern hemisphere than in the northern hemisphere.

3.2.4 General atmospheric circulation

The mean meridional circulation of the 1×CO_2-experiments are compared in Figure 3.7. Similar to the previous figures we find that the changes imposed by reducing the horizontal diffusion on the mean climate state are much smaller than those caused by the noise. In both kinds of experiments, diffusion- and noise-experiments, the Hadley cell and the Ferrel cell are weakened.

The weakening of the Hadley cell in the noise-experiments is related to the changes in the net heating. The clouds decrease the heating in the tropics and

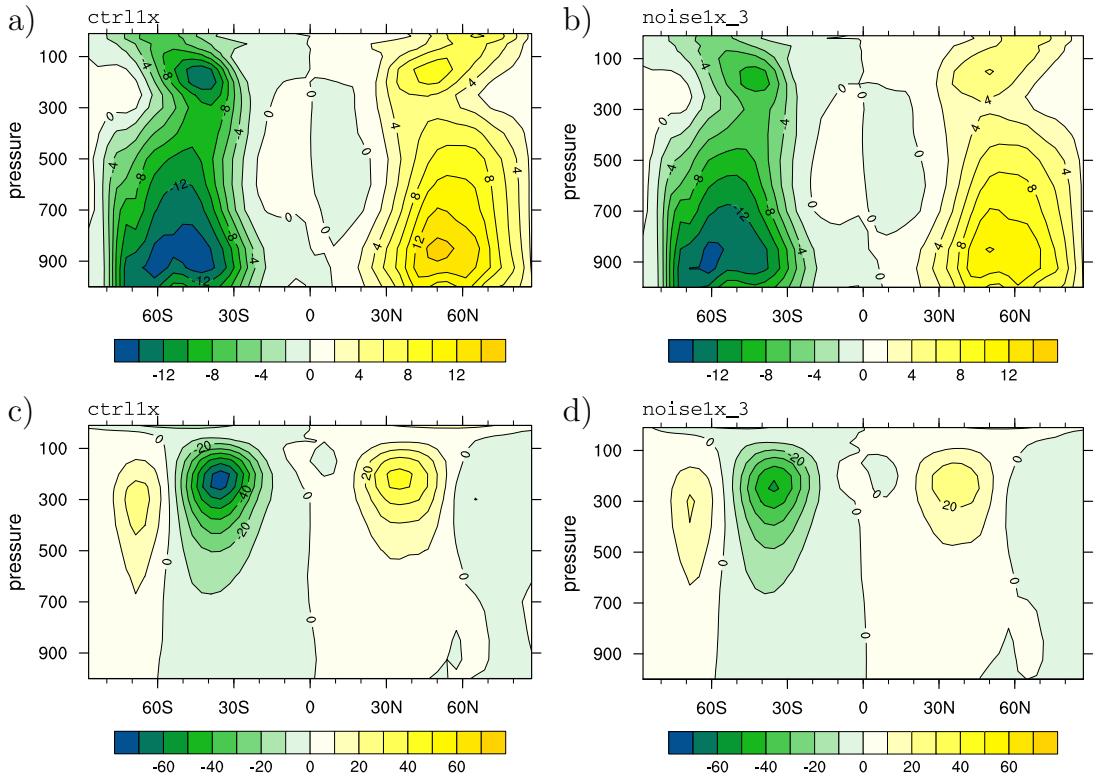

Figure 3.8: *a) and b) transient eddy heat fluxes, $[\overline{T'v'}]$, of* **`ctrl1x`** *and* **`noise1x_3`***; c) and d) transient eddy momentum fluxes, $[\overline{u'v'}]$, of* **`ctrl1x`** *and* **`noise1x_3`***. (The transient eddy fluxes are computed from daily mean values from which the mean annual cycle was subtracted.)*

the cooling in the midlatitudes (Figure 3.6). Thus the forcing of the Hadley cell is weakened. Also the lower water vapour content in the atmosphere (last column of Table 3.1), resulting in less moist convection, has a share in the weakening of the Hadley cell.

The decreased intensity of the Ferrel cell is in line with weaker eddy momentum fluxes and eddy heat fluxes in the two noise-experiments. The transient eddy heat flux $[\overline{T'v'}]$ and the transient eddy momentum flux $[\overline{u'v'}]$ of `ctrl1x` and `noise1x_3` are shown in Figure 3.8. (The prime denotes anomalies of the time average, $x' = x - \overline{x}$; the overbar indicates the time average; the brackets [ ] refer to the zonal average.) The diminished maxima and minima of the eddy fluxes in the noise-experiment implicate a weaker eddy forcing of the Ferrel cell. If, for example, the maximum of the transient eddy heat flux at 50N is weakened, the divergence

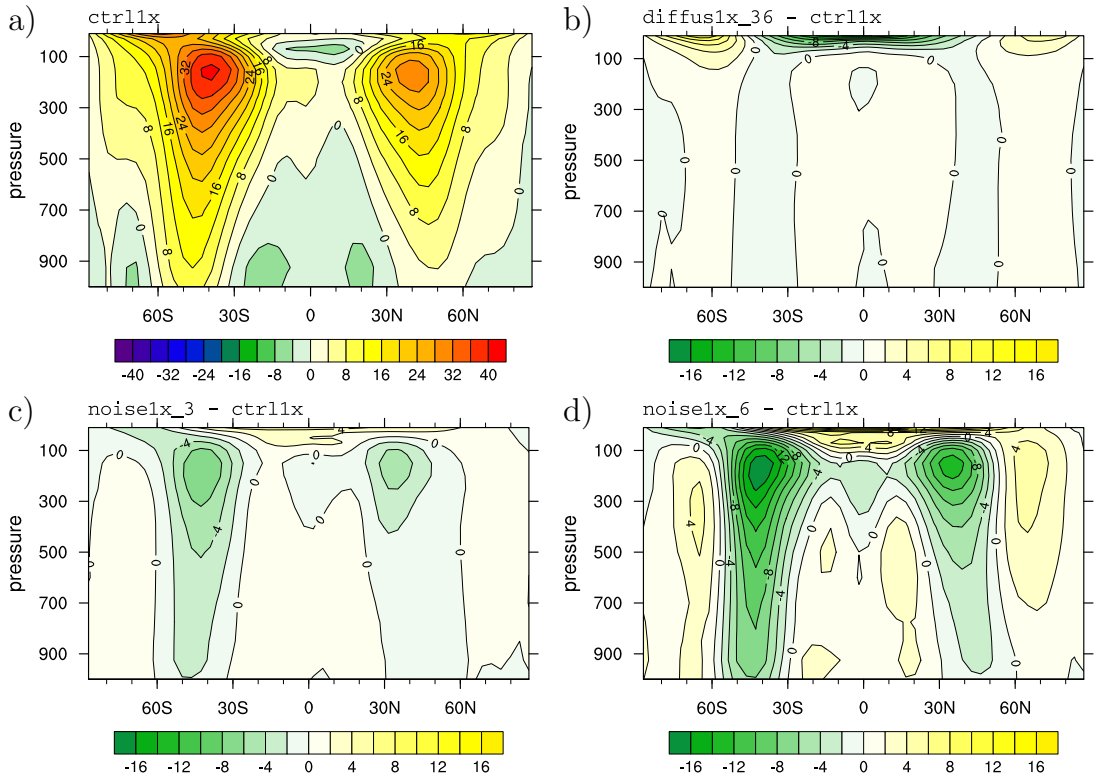

Figure 3.9: *a) Pressure-latitude cross-section of the zonally averaged annual-mean zonal wind component, u, in m/s obtained from* **`ctrl1x`**, *and zonal wind differences of b)* **`diffus1x_36`** *-* **`ctrl1x`**, *c)* **`noise1x_3`** *-* **`ctrl1x`**, *and d)* **`noise1x_6`** *-* **`ctrl1x`** *also in m/s. The results are based on 50-year averages of model years 101-150.*

and the convergence zones south and north of the maximum are weakened, too. Thus the meridional temperature gradient and with it the thermal wind balance is not as much perturbed by the eddy heat fluxes as in the control-experiment. The indirect Ferrel circulation need not be so strong in `noise1x_3` to compensate this perturbation of the thermal wind balance. A similar argument can be given for the eddy momentum fluxes. For more details on the relation of the Ferrel cell and the eddy fluxes see, e.g., Holton (1992).

The zonal mean of the eastward component of the wind, $[\overline{u}]$ (Figure 3.9) is also considerably influenced by the additional noise. The strength of the jets are reduced by 15 % in `noise1x_3` and by 40 % in `noise1x_6`. In the diffusion-experiments the jets are hardly changed. The zonal wind changes are consistent

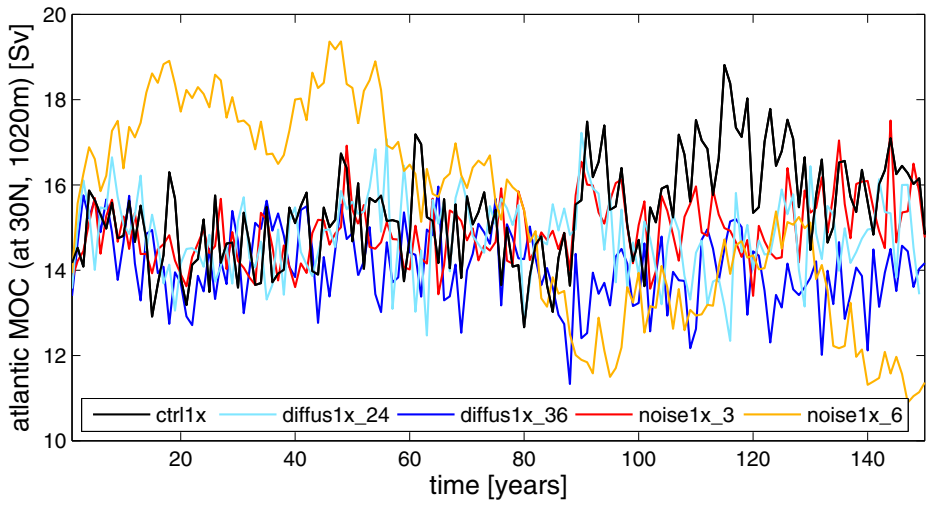

Figure 3.10: *Atlantic meridional overturning at 30°N in a depth of 1020 m in Sv (=10^6 m^3/s), annual means*

with the changes in the meridional temperature gradient caused by the additional noise.

3.2.5 Ocean circulation

Figure 3.10 shows the evolution of the Atlantic meridional overturning circulation (MOC) at 30°N at the depth of 1020 m. In the control-experiment (`ctrl1x`) the Atlantic MOC has a strength of about 15 Sv (1 Sv=10^6 m^3/s) with a standard deviation of 2.3 Sv computed from annual means. In the experiments with reduced horizontal diffusion (`diffus1x_24` and `diffus1x_36`) and with moderate noise (`noise1x_3`) the strength and variability of the MOC is similar to that of `ctrl1x`. We conclude that moderately enhanced atmospheric small-scale variability does not influence the MOC.

In contrast, in the experiment with high noise intensity (`noise1x_6`) we observe considerable changes of the Atlantic MOC (orange line). In response to the strong noise the strength of the Atlantic MOC increases up to about 19 Sv in the first 50 years. In the last 50 years of the 150-year long simulation the MOC strength decreases slightly below the MOC strength of the other experiments (see also Figure 3.11a,b).

Given the large atmospheric changes in the experiment `noise1x_6`, changes in the ocean circulation are not surprising. Further analyses reveal that the ocean

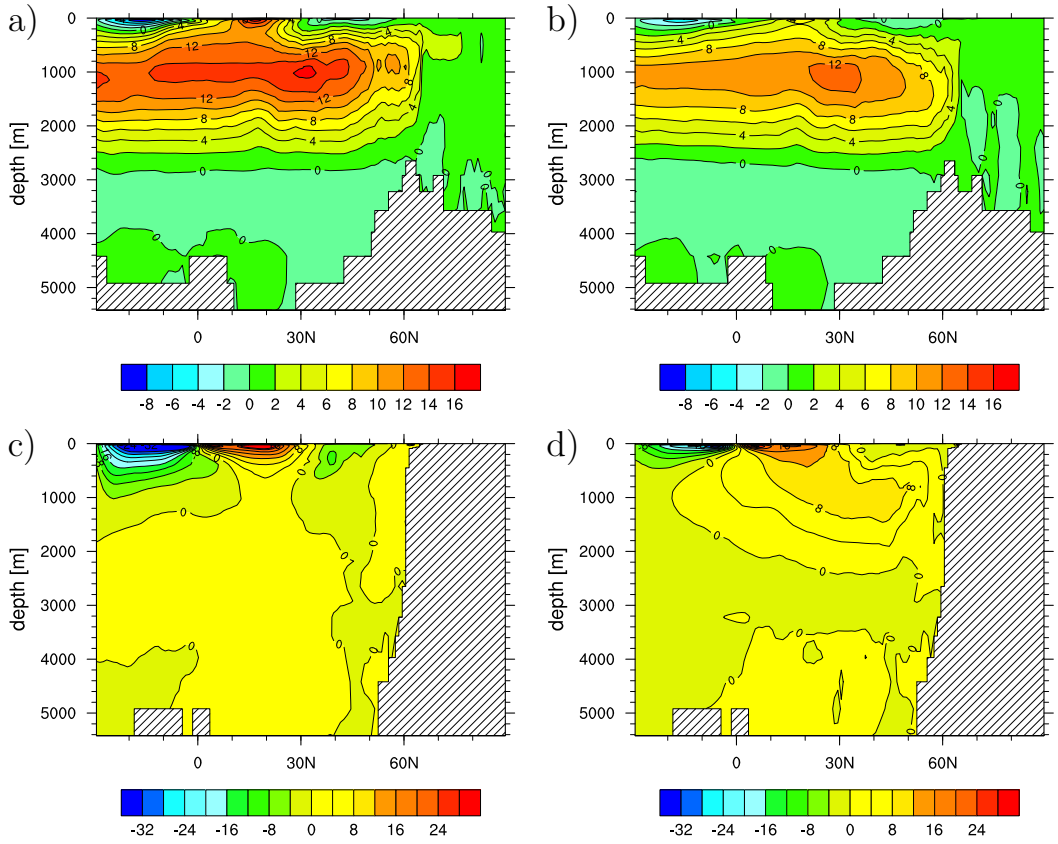

Figure 3.11: *Mean Atlantic meridional overturning circulation in Sv of a)* `ctrl1x` *and b)* `noise1_6`*, as well as mean Pacific meridional overturning circulation in Sv of c)* `ctrl1x` *and d)* `noise1_6`*; All quantities are based on 50-year means of model years 101-150.*

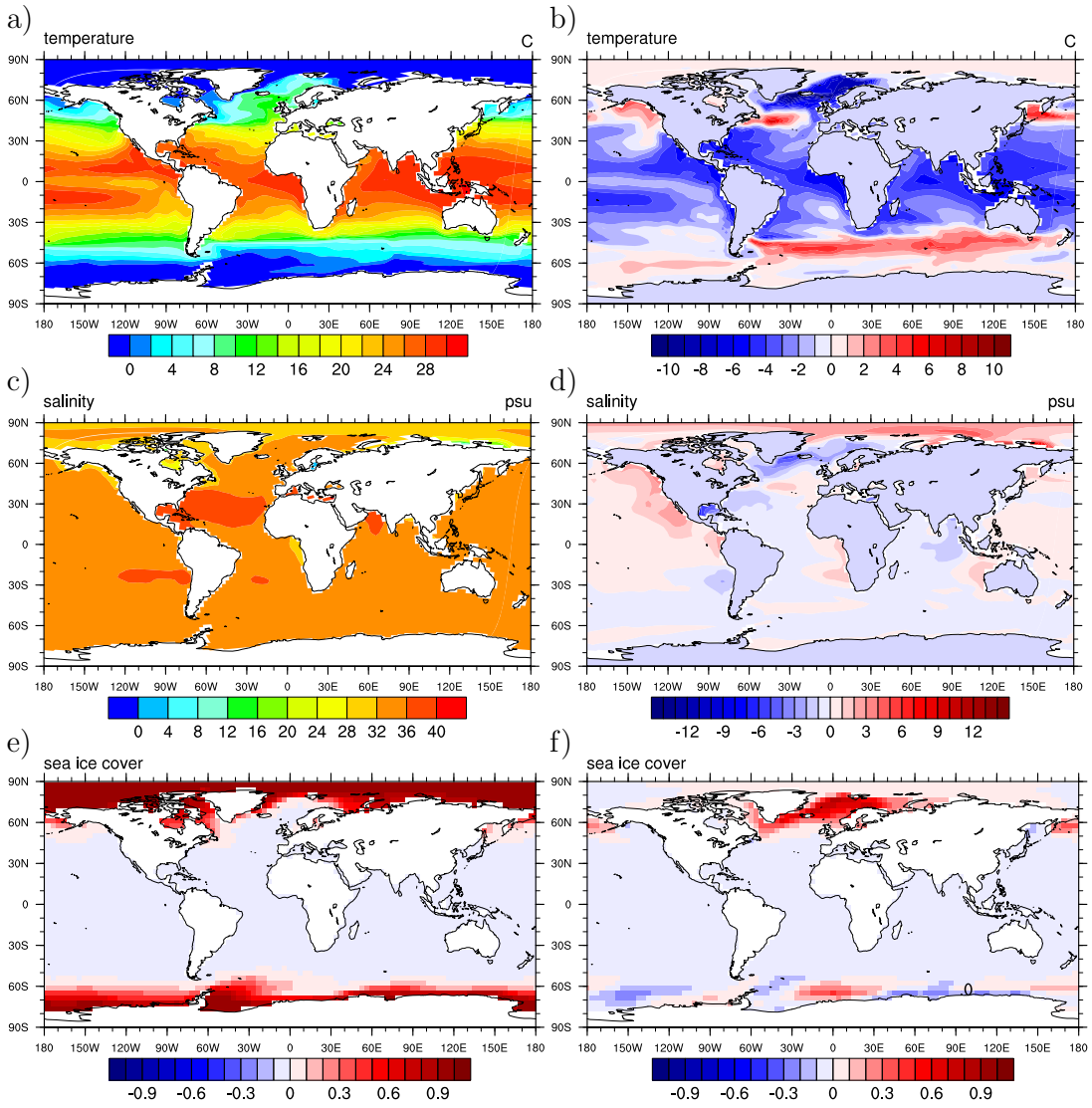

Figure 3.12: *Mean horizontal distributions of* **`ctrl1x`** *(a,c,e) and the difference* **`noise1x_6`**–**`ctrl1x`** *(b,d,f) of a,b) sea surface temperature in °C, c,d) sea surface salinity in psu, and e,f) fractional sea ice cover; All quantities are based on 50-year means of model years 101-150.*

circulation of `noise1x_6` has changed considerably compared to the control experiment. Besides deep water formation in the North Atlantic we find also sinking in the North Pacific. A Pacific overturning circulation develops in the North Pacific (Figure 3.11d).

Since we did not alter the ocean model, the differences found in the ocean circulation must originate from different atmosphere-ocean interactions. The lower atmospheric temperatures in `noise1x_6` generally result in a cooling of the ocean (Figure 3.12a,b). Due to the much lower temperatures in the North Atlantic, sea ice reaches much further South in `noise1x_6` (Figure 3.12e,f). The sea ice acts like a lid over the ocean surface restricting heat and water exchange between atmosphere and ocean. Owing to less evaporation, the North Atlantic freshens (Figure 3.12c,d). In general, the density of sea water depends strongly on its temperature and salinity. The water is the denser, the cooler and saltier it is. Hence, the cooling of the North Atlantic surface water tends to increase the density, but the freshening tends to decrease the density. In the last 50 years of `noise1x_6` the freshening outweighs the cooling, since we find shallower mixing depths in the North Atlantic (not shown) and a weaker Atlantic MOC compared to `ctrl1x`. The convection in the North Pacific is related to higher salinities. The warmer temperatures in this areas do not inhibit the convection.

3.2.6 Kinetic energy spectrum

An important property of the horizontal diffusion is to ensure a realistic kinetic energy spectrum. Kinetic energy spectra derived from observations show generally a spectral slope of ≈ -3 in the total wavenumber range $10 \leq l \leq 30$ (Koshyk and Boer, 1995). A slope of -3 is consistent with an enstrophy-cascading inertial subrange as predicted by the theory of two-dimensional turbulence (Kraichnan, 1967). Reducing the strength of the horizontal diffusion will directly affect the kinetic energy spectrum. Figure 3.13 displays the kinetic energy spectrum at 500 hPa for all 1×CO_2-experiments.

The reduction of the horizontal diffusion leads to an increase of the kinetic energy in small-scale components. While the spectral slope in the experiment `ctrl1x` approximates -3 for total wavenumbers $l \geq 10$, it flattens in the experiments `diffus1x_24` and `diffus1x_36` for total wavenumbers $l > 20$. Besides this difference the spectra of the experiments with reduced horizontal diffusion are very similar to the spectrum of `ctrl1x`.

Adding noise to the small-scale components results in broader changes. The spectral coefficients on which the noise was added ($l \geq 26$) clearly stick out with

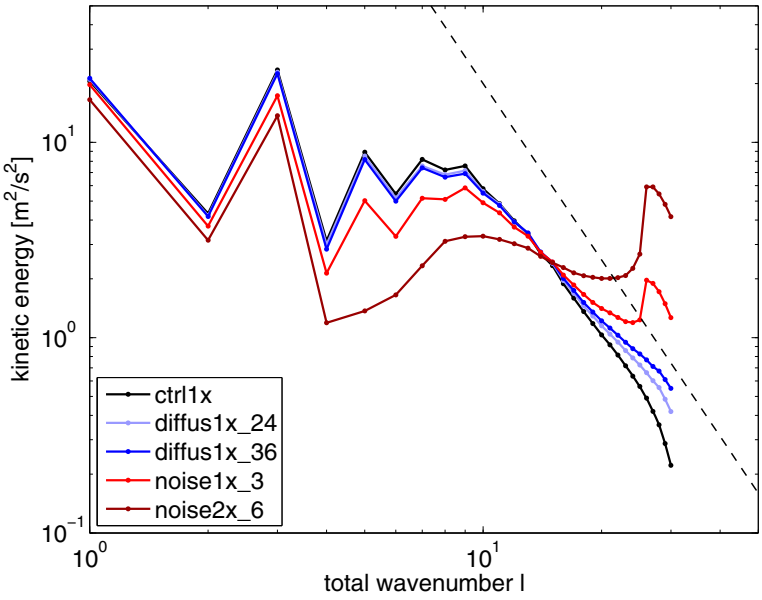

Figure 3.13: *Kinetic energy spectrum at 500 hPa obtained from 6 hourly averages for the different 1×CO_2-experiments; The dashed straight line marks a spectral slope of -3.*

very high values. Overall the kinetic energy is significantly reduced for small wavenumbers ($l < 10$). The very different curve of the noise-experiment with high noise intensity (`noise1x_6`) are consistent with the big changes of the simulated climate found in the previous subsections.

3.3 Discussion

We showed that reducing the horizontal diffusion or adding white noise to the small scales indeed results in enhanced small-scale variability. When noise is added to the small scales the mean climate state is considerably altered. We observe changes in the fractional cloud cover and in the zonal mean temperatures as well as a weakening of the mean meridional circulation and the jets. In the experiment with high noise intensity the ocean circulation changes. Reducing the horizontal diffusion also results in changes of the mean climate state. The changes are, however, by far not as big as in the noise-experiments. Since the noise enhances the small-scale fluctuations much more than does the reduction of the horizontal diffusion, its larger effect on the mean climate state is plausible. A

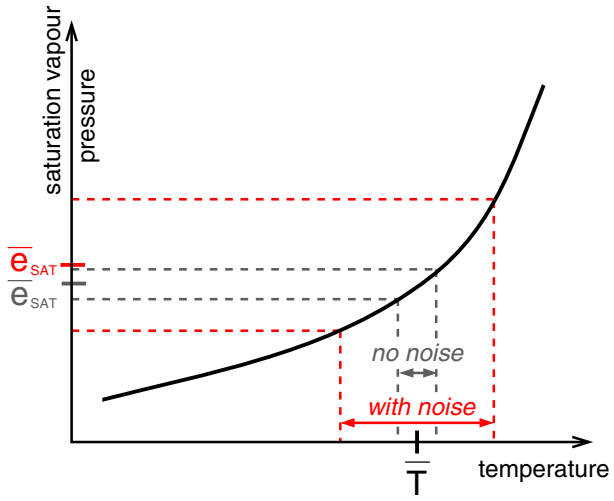

Figure 3.14: *Conceptual illustration how enhanced variability of the temperature caused by additional noise can influence the mean of the saturation vapour pressure e_{SAT}. $\overline{e}_{SAT}$ in black (red) indicates the mean of the saturation vapour pressure in a system without (with) additional noise. $\overline{T}$ is the mean of the temperature, which is not changed by the additional noise.*

smaller noise intensity would scale down the effects on the mean climate.

The changed mean states in the experiments with enhanced small-scale fluctuations are not necessarily more realistic. Especially, the mean state found in the experiment `noise1x_6` is quite unrealistic. The strong noise causes large unrealistic changes in the fractional cloud cover. Compared to observations (Peixoto and Oort, 1993) the atmospheric mean meridional circulation and the jets are too weak in `noise1x_6`. The unrealistic mean state in `noise1x_6` is not surprising since by adding white noise to the system we chose a very simple way of enhancing the small-scale fluctuations, which provides only a crude parameterisation of the induced variability by subgrid-scale processes.

In general, it is difficult to identify the detailed cause-and-effect chain leading to the changes of the mean climate. Since the mean of the noise itself is zero, the nonlinear nature of the climate system must be responsible for the changes.

Nonlinear interactions between temperature and cloud formation are one example how noise with zero mean may alter the mean state. Cloud formation generally depends on the relative humidity RH. When RH reaches values close to 100%, clouds are formed. RH is defined as the ratio of the partial pressure of water vapour e to the saturation vapour pressure e_{SAT}: $RH = e/e_{\mathrm{SAT}}$. The saturation vapour pressure depends exponentially on the temperature. If we now disturb the

temperature T with white noise being symmetrically distributed around the mean temperature, the mean of e_{SAT} will change. A positive anomaly of T leads to a larger disturbance of e_{SAT} than the same negative anomaly (Figure 3.14). In the long run the mean of e_{SAT} in the system with noise is higher than the mean of e_{SAT} in the system without noise. Under the assumption that the partial pressure of water vapour remains unaffected by the noise, RH decreases on average. Hence less clouds form.

Another mechanism for how enhanced variations may influence the mean state is that an important threshold is crossed more frequently. Due to enhanced variability of the temperature the vertical stratification of the atmosphere is more variable. On the one hand this leads more often to an unstable atmosphere, which in turn results in more convection. On the other hand the atmospheric layering is also more often more stable than usual. Unlike the unstable situation, a more stable atmosphere has no direct consequences on, e.g., cloud formation, since the atmosphere is stable most of the time anyway. Thus, if the variability of the lapse rate increases, we expect on average more convection.

Note that the above considerations serve primarily as illustrative examples of how enhanced variability might affect the mean state. Although we, e.g., find reduced cloud cover in many regions of the noise-experiments, we are not sure that the reduction of clouds can completely be explained by the mechanism described above (higher temperature fluctuation $\rightarrow$ lower $e_{\mathrm{SAT}} \rightarrow$ smaller $RH \rightarrow$ less clouds). Even in `noise1x_6` the noise added to the temperature has only an amplitude of 0.06 K. It is likely that other nonlinear processes are also involved. The noise could, e.g., serve as a trigger initiating a positive feedback loop.

4 Impact of small-scale fluctuations on the climate sensitivity

4.1 Introduction

The representations of nonlinear thermodynamical feedback processes (e.g., cloud feedbacks, surface albedo feedback) have a large impact on the modelled climate sensitivity. Different models incorporating various parameterisations simulate different global warming although they are forced in the same way (IPCC (2007)). However, not only the parameterisations of thermodynamical feedback processes are important for the modelled climate sensitivity, also the representation of dynamical small-scale processes near the truncation scale could play a crucial role.

All climate models have finite spatial and temporal resolutions. The impacts of not resolved processes must be parameterised. Different parameterisations of these unresolved scale-interactions could lead to different model sensitivities. Since the implemented parameterisations often do not take the variability induced by subgrid-scale processes into account, we want to investigate the impact of enhanced small-scale fluctuations on the climate sensitivity by artificially increasing the variability near the truncation scale.

The experiments with and without enhanced small-scale fluctuations are described in Chapter 2. For the analyses in this chapter we use from each integration the last 50 years, which are considered to be in quasi-equilibrium. We calculate the response to the doubled CO_2 concentration as the difference between the mean over the last 50 years of the $2\times CO_2$-experiments and the 50-year mean obtained from the respective $1\times CO_2$-experiment.

Section 4.2 shows that enhanced small-scale fluctuations affect the temperature response to a doubled CO_2 concentration. In Section 4.3 we investigate how the thermodynamical feedback processes are changed due to the enhanced small-scale fluctuations. We conclude this chapter with a discussion.

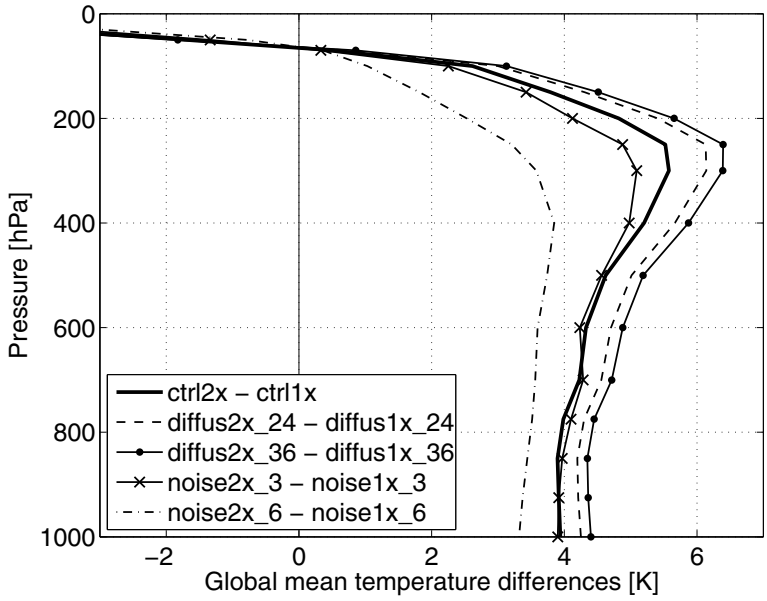

Figure 4.1: *Temperature response to doubled CO_2 concentration (i.e., $T_{2\times CO2} - T_{1\times CO2}$) obtained from experiments with different representations of small scale fluctuations. The results are based on the temperature means over the last 50 years of the integrations.*

4.2 Temperature response

Figure 4.1 shows the temperature response to a doubled CO_2 concentration. Doubling the CO_2 concentration leads to a warming of the entire troposphere for all pairs of experiments.

This warming is stronger in the experiments with reduced horizontal diffusion in comparison to that in the control experiments (`ctrl2x-ctrl1x`). In other words, a reduction of the horizontal diffusion causes an increased climate sensitivity. In general, a larger reduction of the horizontal diffusion results also in a larger increase of the climate sensitivity. Reducing the horizontal diffusion by a factor of two (three) leads to a maximum amplification of the temperature response at 250 hPa by 11% (16%). By contrast, adding white noise to the small scales weakens the temperature response. The temperature response in the experiments with high noise intensity (`noise2x_6 - noise1x_6`) is much smaller than the temperature response of the control experiments. In the experiments with the lower noise intensity (`noise2x_3 - noise1x_3`) the temperature response decreases only in the high troposphere, with a maximum reduction at 200 hPa from 4.8 K to 4.1 K

	1x	2x − 1x	1x	2x − 1x
	T_s	ΔT_s	$T300$	$\Delta T300$
ctrl	288.0	3.8	232.2	5.6
diffus_24	288.2	4.1	232.6	6.1
diffus_36	288.3	4.3	232.8	6.4
noise_3	287.9	3.9	230.8	5.1
noise_6	285.9	3.3	230.1	3.6

Table 4.1: *Time mean of the global mean temperatures at the surface, T_s, and at 300 hPa, $T300$, both in Kelvin. ΔT_s and $\Delta T300$ represent their differences between the 2× CO_2 and 1× CO_2 experiments in Kelvin. All numbers are based on 50-year averages.*

(15%). The changes in the mean temperature responses are statistically significant in all tropospheric levels except for the experiments noise2x_3 - noise1x_3 in the vertical range of 1000 hPa to 450 hPa.

The climate sensitivity at the surface, as defined by the change of the equilibrium surface temperature due to the doubled CO_2 concentration, is 3.8 K in the control integrations (Table 4.1). This value increases to 4.1 K (4.3 K) if the horizontal diffusion is reduced by a factor of two (three). The response of the mean surface temperature in the noise-experiments with moderate noise intensity does not change significantly, but it decreases to 3.3 K in the experiments with high noise intensity.

The surface climate sensitivity varies in the experiments with enhanced small-scale fluctuations by up to 13%. This change of the surface climate sensitivity is not as large as, e.g., changes of the surface climate sensitivity caused by different cloud parameterisations (Soden and Held (2006), Webb et al. (2006)). Soden and Held (2006) reported that inter-model differences in cloud feedbacks provide the largest source of uncertainty in the predictions of the climate sensitivity. They analysed the climate feedbacks in 14 different coupled ocean-atmosphere models forced by the A1B emission scenario of the IPCC[1]. The standard deviation of the cloud feedback in this multi-model ensemble is 0.37 $(W/m^2)/K$. Assuming that the multi-model mean effective feedback λ of 1.27 $(W/m^2)/K$ were enhanced (weakened) by 0.37 $(W/m^2)/K$ due to different cloud feedbacks, the mean surface temperature response $\Delta T_s = \Delta Q/\lambda$ would increase (decrease) by 40% (23%). For this estimation we used the radiative forcing ΔQ=4.3 W/m^2 as given in the

[1]Intergovernmental Panel on Climate Change, IPCC (2007)

mentioned paper.

4.3 Thermodynamical feedback processes

Although we have increased the CO_2 concentration in all experiments by the same amount, the experiments show different temperature responses. Hence the enhanced small-scale fluctuations must have changed the sensitivity of the system to increased CO_2 concentration. Several nonlinear thermodynamical feedback processes influence the climate sensitivity. In this section we want to analyse how these thermodynamical feedback processes, such as those related to the planetary albedo, clouds and water vapour, are altered by the different representations of small-scale fluctuations.

Albedo

To get an impression of how the radiation balances are changed in the different experiments we use a simple global energy balance model (EBM)[2]:

$$SW_{\text{down}}^{\text{TOA}}(1-\alpha_p) = \epsilon\sigma T_s^4 \tag{4.1}$$

where $SW_{\text{down}}^{\text{TOA}}$=341.29 W/m^2 denotes the globally averaged incident shortwave radiation at the top of the atmosphere (TOA). α_p is the planetary albedo, ϵ the effective planetary emissivity, $\sigma = 5.67051\times10^{-8}\,\text{W}/(\text{m}^2\text{K}^4)$ is the Stephan-Boltzmann constant and T_s represents the globally averaged surface temperature. Equation (4.1) describes the balance between the net incoming shortwave radiation and the outgoing longwave radiation at the top of the atmosphere for an earth system in radiative equilibrium.

The planetary albedo α_p is a measure of the amount of shortwave radiation reflected from the earth system. It is defined as the ratio between the globally averaged outgoing shortwave radiation ($SW_{\text{up}}^{\text{TOA}}$) and the globally averaged incident shortwave radiation at the top of the atmosphere: $\alpha_p = SW_{\text{up}}^{\text{TOA}}/SW_{\text{down}}^{\text{TOA}}$. Later we will also refer to the surface albedo: $\alpha_s = SW_{\text{up}}^{\text{BOA}}/SW_{\text{down}}^{\text{BOA}}$, where $SW_{\text{up}}^{\text{BOA}}$ denotes the globally averaged amount of shortwave radiation reflected from the earth's surface and $SW_{\text{down}}^{\text{BOA}}$ is the incoming globally averaged shortwave radiation reaching the earth's surface. (Note that α_p and α_s are not defined as the average of albedos computed for each grid box separately. Rather they are computed as the ratios of the already globally averaged radiation fluxes.) In contrast to α_p,

[2]For a review of EBMs see North et al. (1981).

	1x	2x − 1x	1x	2x − 1x	1x	2x − 1x
	α_p	$\Delta\alpha_p$	α_s	$\Delta\alpha_s$	ϵ	$\Delta\epsilon$
ctrl	0.3166	-0.0095	0.1400	-0.0110	0.5979	-0.0227
diffus_24	0.3161	-0.0103	0.1392	-0.0113	0.5966	-0.0242
diffus_36	0.3163	-0.0113	0.1392	-0.0116	0.5956	-0.0249
noise_3	0.3305	-0.0104	0.1396	-0.0123	0.5865	-0.0221
noise_6	0.3801	-0.0065	0.1514	-0.0149	0.5584	-0.0194

Table 4.2: *Planetary albedo α_p, surface albedo α_s, and effective planetary emissivity ϵ obtained from the 1×CO_2-experiments denoted by '**1x**'. Their differences between the 2×CO_2 and 1×CO_2 experiments are shown in the columns named '**2x − 1x**'. All numbers are based on 50-year averages.*

α_s excludes all reflective processes occurring in the atmosphere (e.g., reflectance of shortwave radiation by clouds). Since $SW_{\text{up}}^{\text{TOA}}$, $SW_{\text{up}}^{\text{BOA}}$, and $SW_{\text{down}}^{\text{BOA}}$ can be diagnosed from the ECHAM5-model output, we are able to compute α_p and α_s for each experiment. Given α_p and T_s we can estimate the effective planetary emissivity ϵ by using the EBM (4.1). The parameter ϵ can principally range from 0 to 1. It accounts for the reduction of outgoing longwave radiation mainly due to greenhouse gases and clouds.

While the planetary albedo of the experiments with 1×CO_2 concentration and reduced horizontal diffusion (`diffus1x_24` and `diffus1x_36`) changed only little compared to `ctrl1x`, α_p considerably increases in `noise1x_3` and `noise1x_6` (Table 4.2). Thus, in the noise-experiments more shortwave radiation is reflected by the earth system leading to a cooling. Because α_s remains almost unaffected in `noise1x_3`, different cloud patterns must be the reason for the high planetary albedo in this experiment (see also Section 3.2.3). In `noise1x_6` an increased surface albedo (i.e., more sea ice and snow) as well as different cloud patterns are responsible for the higher planetary albedo.

Doubling the CO_2 concentration leads to a decrease of α_p by -0.0095 in the control experiments. Compared to the control experiments this decrease of α_p is larger in `diffus_36` by 0.0018. Using the rearranged equation (4.1),

$$T_s = \sqrt[4]{(SW_{\text{down}}^{\text{TOA}}(1-\alpha_p))/(\epsilon\sigma)} \tag{4.2}$$

we estimate the temperature difference ΔT, which would occur, if α_p decreased in the control experiments as much as in `diffus_36`.

$$\Delta T = T_s(\alpha_p^{\text{ctrl1x}} + \Delta\alpha_p^{\text{diffus\_36}}, \epsilon^{\text{ctrl2x}}) - T_s(\alpha_p^{\text{ctrl2x}}, \epsilon^{\text{ctrl2x}}) = 0.2\text{K} \tag{4.3}$$

	1x	2x − 1x	1x	2x − 1x	1x	2x − 1x	1x	2x − 1x
	CRF	ΔCRF	CRF_{SW}	ΔCRF_{SW}	CRF_{LW}	ΔCRF_{LW}	q_v	Δq_v
ctrl	-23.6	-0.72	-52.2	-0.31	28.6	-0.41	25.7	8.4
diffus_24	-23.5	-0.50	-52.2	-0.13	28.7	-0.37	26.4	9.1
diffus_36	-23.5	-0.24	-52.3	+0.13	28.8	-0.37	26.7	9.6
noise_3	-27.4	-0.46	-57.5	+0.12	30.1	-0.58	25.8	7.7
noise_6	-37.5	-1.57	-73.5	-1.14	36.0	-0.43	24.3	6.1

Table 4.3: *Globally averaged net cloud radiative forcing at the top of the atmosphere, CRF, and its shortwave CRF_{SW} and longwave CRF_{LW} part in W/m^2, as well as the globally averaged vertically integrated water vapour content q_v in kg/m^2 for the $1\times CO_2$ experiments. ΔCRF, ΔCRF_{SW}, ΔCRF_{LW}, and Δq_v represent the differences between the $2\times CO_2$ and $1\times CO_2$ experiments also in W/m^2 or kg/m^2. All numbers are based on 50-year averages.*

In (4.3) $\Delta\alpha_p^{\text{diffus\_36}}$ denotes the change in α_p due to a doubled CO_2 concentration in the experiments diffus_36. The above estimate shows that the small difference of 0.0018 between $\Delta\alpha_p^{\text{ctrl}}$ and $\Delta\alpha_p^{\text{diffus\_36}}$ explains an increase of the surface temperature response by 0.2 K. This increase corresponds to 40% of the observed difference of 0.5 K between the responses of ctrl and diffus_36. The stronger surface temperature responses in the experiments with reduced horizontal diffusion can thus be partly explained by changes in the planetary albedo responses $\Delta\alpha_p$. Similar considerations show that the smaller $\Delta\alpha_p$ in noise_6 accounts for 0.3 K (60%) of the differences found in the surface temperature responses between ctrl and noise_6.

The remaining differences are due to altered longwave radiation processes involving water vapour and clouds. These changes of the longwave radiation budget are expressed by the different $\Delta\epsilon$.

Clouds

The changes in fractional cloud cover caused by doubling the CO_2 concentration are shown in Figure 4.2. The patterns of the cloud cover changes due to CO_2 doubling are approximately the same for the different experiments. We find increased fractional cloud cover at high altitudes near the tropopause and mostly reduced fractional cloud cover in the lower troposphere, indicating an upward shift of the clouds. These results are similar to the multi-model mean changes presented in Meehl et al. (2007). The cloud cover changes due to CO_2 doubling are in the

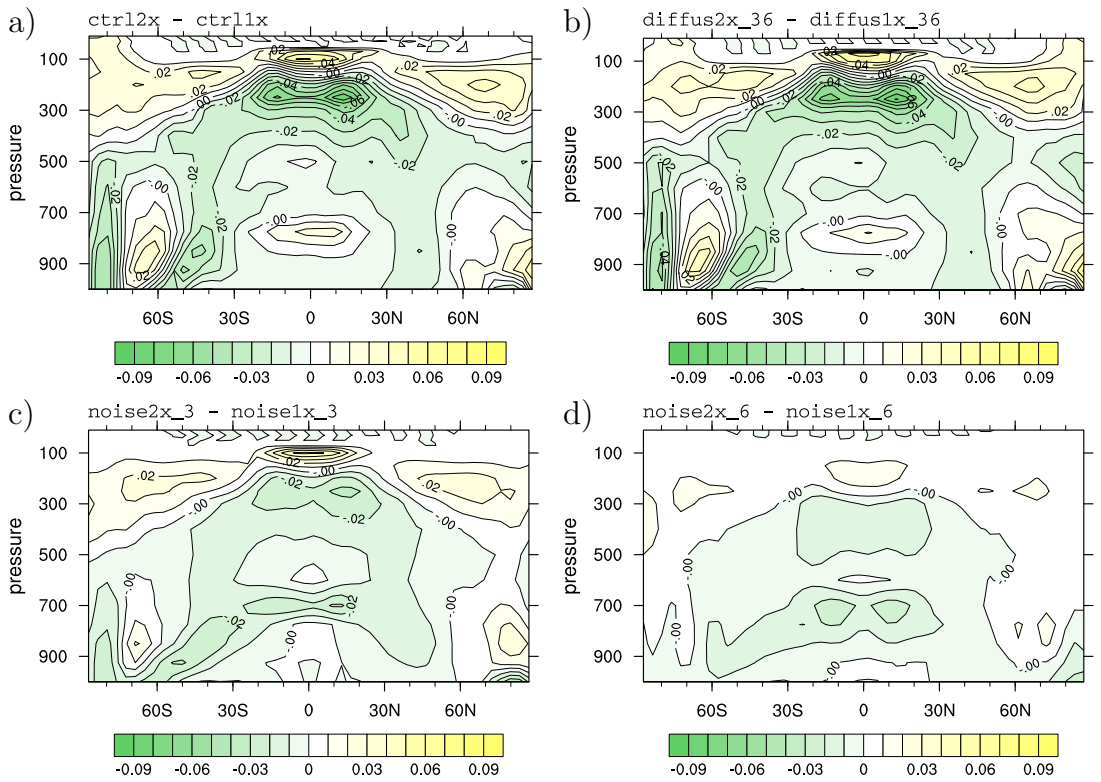

Figure 4.2: *Pressure-latitude cross-section of the response to doubled CO_2 concentration of the zonally averaged fractional cloud cover for a)* `ctrl2x-ctrl1x`*, b)* `diffus2x_36-diffus1x_36`*, c)* `noise2x_3-noise1x_3` *d)* `noise2x_6-noise1x_6`*. The results are based on 50-year averages.*

noise-experiments not as strong as in the control- and diffusion-experiments.

Because of the complicated cloud structures, it is difficult to draw conclusions on how the clouds affect the temperature response, from Figure 4.2 alone. The best way to quantify the effect of the clouds on the temperature response would be to estimate the radiative perturbation caused by the changed clouds ΔC (Wetherald and Manabe, 1988):

$$\delta_C R = R(T^{1x}, C^{1x} + \Delta C, w^{1x}, \alpha_s^{1x}) - R(T^{1x}, C^{1x}, w^{1x}, \alpha_s^{1x}) \tag{4.4}$$

where R is the globally averaged net radiation flux at the top of the atmosphere. T^{1x},C^{1x},w^{1x}, and α_s^{1x} represent temperature, clouds, water vapour and surface albedo of the 1×CO_2-experiment, respectively. The computation of $\delta_C R$ involves offline radiation calculations in which we take all input data from the 1×CO_2-experiment except of the clouds, which are taken from the corresponding 2×CO_2-experiment. Unfortunately, the radiative transfer component of ECHAM5 could not be used in an offline mode without considerable extra effort.

To still get an idea of the effect of clouds on the temperature response we look at the cloud radiative forcing (CRF) at the top of the atmosphere. The CRF is defined as the difference between the radiation budget with clouds and without clouds in a certain experiment. In contrast to $\delta_C R$, CRF depends not only on the clouds but also on non-cloud feedbacks (Soden et al., 2004). The CRF in an atmosphere with, for example, high water vapour content is different than the CRF induced by the same clouds in an atmosphere with lower water vapour content.

Table 4.3 gives the CRF and its difference due to a CO_2 doubling. In the 1×CO_2 concentration control experiment the clouds exert globally averaged a net cooling effect of -23.6 W/m^2 on the climate. As discussed above, if the CO_2 concentration is doubled, the fractional cloud cover changes considerably throughout the troposphere (Figure 4.2a). Due to the altered clouds (and possibly also non-cloud feedbacks) the net cooling effect amplifies by -0.72 W/m^2. Hence the larger negative CRF in `ctrl2x` acts against the global warming caused by the higher CO_2 concentration.

The negative change of CRF, ΔCRF, observed in the experiments `diffus_24`, `diffus_36` and `noise_3` is not as strong as in the control experiments. Thus ΔCRF does not weaken the global warming as much as in `ctrl`. In the experiment `noise2x_6`, however, the cooling effect opposing the global warming is strengthened.

To distinguish between the shortwave and the longwave effect of the clouds onto the radiation budget, we split the net CRF into the shortwave CRF and the

longwave CRF. The shortwave CRF is always negative, since shortwave radiation is mainly reflected back to space by the clouds. In the experiment `ctrl2x` more shortwave radiation is globally reflected by the clouds than in `ctrl1x`. This effect is weakened and even reversed in the experiments with reduced horizontal diffusion or with moderate noise intensities. In the experiment `noise2x_6` the cooling effect by shortwave CRF is intensified.

The longwave CRF is always positive. It describes the absorption and emission of longwave radiation by the clouds similar to the warming effect caused by the greenhouse gases. The change of the longwave CRF caused by doubled CO_2 concentration in `ctrl2x`–`ctrl1x` is negative, resulting in a reduction of the climate sensitivity. Depending on the way of enhancing the small-scale fluctuations this change of the longwave CRF is decreased or increased. In the diffusion-experiments the cooling is decreased, which leads to a warming effect compared to the control experiment. In the noise-experiments the cooling effect is increased.

To summarise, in the experiments with reduced horizontal diffusion the changes of the shortwave and longwave CRF both foster a larger temperature response. In the noise-experiments `noise_3`, however, the changes of the shortwave and longwave CRF take opposite effects, with the shortwave CRF dominating. Hence, if we were considering only the CRF, the experiments `noise_3` would show a larger temperature response. In contrast, the change of the net CRF in the experiments `noise_6` is in line with the weaker climate sensitivity found in Section 4.2.

Water vapour

The mean amount of water vapour in the atmosphere closely depends on the atmospheric temperature. The warmer the air, the more water vapour can be held by the atmosphere. Furthermore, water vapour is an effective greenhouse gas. The combination of these two properties leads to a positive feedback process. If the atmosphere warms due to increased CO_2 concentration, the water vapour content will rise; because of its greenhouse-gas-property a higher water vapour concentration leads to a further warming of the atmosphere. This feedback process is also partly responsible for the different climate sensitivities found in Section 4.2. When the CO_2 concentration is doubled, the globally averaged vertically integrated water vapour content in the control experiments increases by $8.4\,\mathrm{kg/m^2}$ (last column in Table 4.3). In the experiments with reduced horizontal diffusion this value is higher, indicating a stronger feedback, whereas in the experiments with noise it is smaller, implying a weaker feedback.

4.4 Discussion

In this chapter we showed that enhancing the small-scale fluctuations changes the temperature response to a CO_2 doubling. The sign of the change depends on the method used to enhance the small-scale fluctuations. Reducing the horizontal diffusion leads to a strengthening of the temperature response. Adding noise to the small scales tends to weaken the temperature response.

Differences of the two approaches

At first sight it is surprising that the climate sensitivity increases when using a reduced horizontal diffusion but it decreases when adding noise to the small-scale components. Both methods enhance the small-scale variability and should therefore have a similar effect on the climate. However, a closer look at the two methods reveals that they change the small-scale spectral coefficients in very different ways. The reduced horizontal diffusion results in less damping of small-scale eddies. Therefore, small-scale eddies are stronger and can interact more effectively with large-scale processes. These intensified small-scale eddies are correlated in time and across wavenumbers, and they are consistent with the governing equations of the model. In contrast, adding white noise to the small-scale components artificially perturbs the model, and the resulting fluctuations are uncorrelated in time and spectral space.

Direct and indirect effects on climate sensitivity

In Section 4.3 we showed how the changes in albedo, clouds and water vapour content affect the temperature response to doubled CO_2 concentration. Compared to the control experiments we find in the experiments with reduced horizontal diffusion larger decreases of the planetary albedos, smaller reductions of the longwave CRFs and more intense positive water vapour feedbacks. All these effects lead to a stronger global warming. In the experiments `noise_3` the larger decrease of the planetary albedo works against a larger reduction of the longwave CRF and a weaker water vapour feedback, resulting in almost no change of the temperature response at the surface. In the experiments with high noise intensity, `noise_6`, we find a smaller decrease of the planetary albedo and a larger reduction of the longwave CRF as well as a weaker water vapour feedback, leading all to a weaker temperature response.

The only differences in our response experiments are the representations of the small-scale processes. There are basically two ways how the enhanced small-

scale fluctuations can influence the thermodynamical feedback processes described above. First, the thermodynamical feedbacks are directly influenced by the representation of the dynamical small-scale processes. Second, the enhanced small-scale fluctuations change the mean state of the model and owing to the new climate the thermodynamical processes are altered.

To check how important the indirect influence via the altered mean state is, we could perform additional response experiments. In these new experiments all $1\times CO_2$-experiments are tuned, by varying certain model parameters, to have the same climate (e.g., the same global mean surface temperature and similar clouds). In this conceived experiments we would, however, face the problem of distinguishing between the effects of the enhanced small-scale fluctuations and the influence of the varied model parameters on the climate sensitivity. The disentanglement of these different effects would be very difficult.

In general, it is hard to distinguish between the direct and indirect effects of enhanced small-scale fluctuations on the climate sensitivity. We cannot make a definite statement about the mechanisms altering the thermodynamical feedback processes. Nevertheless, since the mean climate states of the noise experiments are much more altered than the mean states of the diffusion experiments (Chapter 3), the noise experiments might be affected more by indirect effects than the runs with reduced horizontal diffusion.

Horizontal diffusion

Our results suggest that a reduction of the horizontal diffusion leads to a higher climate sensitivity. The question arising is, how well established is the strength and structure of the horizontal diffusion. Several studies (e.g., Leith (1971), Koshyk and Boer (1995), Kaas et al. (1999), Frederiksen and Kepert (2006)) sought to improve the parameterisation of the nonlinear interactions between subgrid scales and resolved scales. Besides confirming the idea of damping high wavenumbers stronger than lower wavenumbers, they found also a 'negative damping' at intermediate wavenumbers. This suggests that certain scales are enhanced instead of damped through the scale-interactions with subgrid scales. The damping strength of the horizontal diffusion in climate models is generally tuned to ensure a kinetic energy spectrum close to observations. But, as mentioned by Stephenson (1995), why should the kinetic energy spectrum of a discrete and truncated model (especially near the truncation scale) look like the spectrum of a continuous system? Enhanced small-scale energy might even be necessary to simulate the large-scale circulation and future climate changes correctly.

Given the uncertainty of the form and strength of the horizontal diffusion in climate models, our results suggest that the modelled climate sensitivity to CO_2 forcing does not only depend on parameterisations related to thermodynamical feedback processes but also on the parameterisation of nonlinear interactions between dynamical subgrid-scale processes and resolved scales.

5 Stochastic model for the global mean temperature at 300 hPa

5.1 Introduction

In the previous chapter we found that enhanced small-scale fluctuations influence the temperature response to a CO_2-doubling. To assess whether the influence of enhanced small-scale fluctuations on the temperature response can be explained via the fluctuation dissipation theorem (as mentioned in the introduction (Chapter 1)), we will in this chapter fit a stochastic model to the ECHAM5/MPI-OM data. The stochastic model should reproduce basic statistical properties of the global mean temperature at the pressure level 300 hPa. We choose the temperature at 300 hPa, because at this level the largest response to CO_2 forcing occurs (Figure 4.1).

Stochastic modelling means that certain parts of the system are approximated by a stochastic process. The state of the climate system at a certain time can be represented by a state vector $\vec{x} = (x_1, x_2, ..., x_N)$ consisting of a finite set of variables. The variables $x_1, x_2, ..., x_N$ are, e.g., temperature, wind vectors and humidity at every grid point. In a spectral representation the variables are the spectral coefficients. The time evolution of, e.g., x_1 is generally given by:

$$\dot{x}_1 = f(\vec{x}), \tag{5.1}$$

where $\dot{x}_1$ denotes the time derivative of x_1. $f(\vec{x})$ denotes a generally nonlinear function depending on the state vector. Assuming that x_1 acts on a much longer time scale than the other variables $\vec{x}_{\text{fast}} \equiv (x_2, ..., x_N)$ we can approximate the interactions between $\vec{x}_{\text{fast}}$ and x_1 as noise.

$$\begin{aligned} \dot{x}_1 &= g(x_1) + h(x_1, \vec{x}_{\text{fast}}) && (5.2) \\ &= g(x_1) + \text{noise} && (5.3) \end{aligned}$$

The construction of the second equation above is based on the idea that on time scales relevant for x_1, $\vec{x}_{\text{fast}}$ fluctuate so rapidly that the variables are from one time step to the next not correlated anymore.

If the system includes besides x_1 also other variables $\vec{x}_{\text{slow}}$ acting on similar long time scales as x_1 equation (5.2) can be written as:

$$\dot{x}_1 = \underbrace{g(x_1) + h_1(x_1, \vec{x}_{\text{slow}})}_{g'(x_1)} + h_2(x_1, \vec{x}_{\text{fast}}) \tag{5.4}$$

$$= g'(x_1) + \text{noise} \tag{5.5}$$

In the above case $g'(x_1)$ parameterises the overall effect of the interactions between x_1 and $\vec{x}_{\text{slow}}$.

In this study we are mainly interested in the behaviour of the global mean temperature at 300 hPa. The time evolution of this large-scale variable is, however, a result of complex dynamical and thermodynamical interactions with many other components of the climate system. By using a stochastic model we parameterise small-scale processes as stochastic forcing. Hence we are able to describe the main characteristics of the global mean temperature in a very simple way.

Using stochastic models to describe basic characteristics of physical systems has a long tradition. A prominent example in climate sciences is the stochastic climate model introduced by Hasselmann (1976). Hasselmann's model divides the complex earth system into two parts. The slowly responding climate system (represented, e.g., by the sea surface temperature) is acting as an integrator of the rapidly varying atmospheric weather system, which is modelled as stochastic forcing. Since Hasselmann's paper stochastic models have been used in many other research projects to model atmospheric and oceanic processes. The aim of most studies is to reduce a complex system with many degrees of freedom to simpler stochastic models, which are still able to reproduce the main features of the original system (e.g., Penland and Matrosova (1998), Branstator and Haupt (1998), Vallis et al. (2004)). Several studies used stochastic models based on Hasselmann's to investigate the interplay of ocean and atmosphere in the mid-latitudes (e.g., Barsugli and Battisti (1998)). Those studies mainly focus on the potential predictability of climate variations on seasonal and longer time scales in the mid-latitudes. Stochastic models are also used to explain the El Niño-Southern Oscillation (ENSO) variability (Penland and Sardeshmukh, 1995).

Most of the above-mentioned studies are based on simple linear stochastic models. More recently published results suggest that nonlinear stochastic models might be better suited for certain applications. Berner (2005) used a nonlinear stochastic model to investigate the importance of the nonlinearities in the model parameters when explaining the behaviour of large-scale planetary waves. She concludes that the nonlinearities play an important role. Sura (2003) showed

that the variability of mid-latitude winds can be well described by a univariate stochastic model with a nearly linear deterministic damping term but a state-dependent white noise term. In the tropics, however, it was not possible to fit such a stochastic model to the wind data. As a reason Sura (2003) argued that tropical variability might be non-Markovian.[1] A univariate stochastic model is not able to describe the long-term variability resulting from the interactions between the atmosphere and the tropical ocean.

Using a similar approach as Sura (2003) and Berner (2005) we want to model the global mean temperature at 300 hPa. Because the tropical ocean covers a large part of the earth's surface, the global mean temperature is largely influenced by it. Hence before fitting the stochastic model to our data we will filter out the long-term variability caused by the interactions of the atmosphere with the ocean. We primarily filter out the El-Niño-Southern Oscillation. Later we want to use the stochastic model to analyse the differences in the climate sensitivities of our experiments with and without enhanced small-scale fluctuations (Chapter 6). Therefore filtering out the long-term variability is only suitable for our application, if we assume that the short-term feedback processes (e.g., black-body feedback, cloud feedbacks) are primarily responsible for the amplitude of the climate sensitivity.

In the next section the stochastic model and the fitting method are described. In Section 5.3 we investigate how well the model reproduces the main statistics. A discussion follows in Section 5.4.

5.2 The stochastic model

5.2.1 Nonlinear Langevin equation

As a stochastic model for the global mean temperature at 300 hPa, x, we use a nonlinear Langevin equation:

$$\dot{x}_s(t) = h(x_s) + g(x_s)\eta(t) \qquad \text{[S]}. \tag{5.6}$$

In this equation x_s represents the global mean temperature at 300 hPa from which the mean daily and annual cycles are removed and the long-term variability associated with the interactions between the ocean and the atmosphere are filtered out. The filtering-procedure is described in Appendix A. $\dot{x}_s$ denotes the time

[1] A system is called to be non-Markovian if the future state of the system depends not only on the present state but also on other previous states.

derivative of x_s; t denotes time; $\eta(t)$ represents white noise. White noise is a rapidly fluctuating Gaussian random variable with zero mean and δ-correlation function.[2] $h(x_s)$ and $g(x_s)$ are deterministic functions which need to be estimated. The meaning of [S] will be explained in the next section.

Equation (5.6) models the time evolution of x_s in a compact way. The first term on the right hand side represents the overall effect of the interactions between x_s and variables on similar time scales. The stochastic forcing, $g(x_s)\eta(t)$, comprises mainly the interactions of the small-scale processes with the large-scale variable x_s.

5.2.2 Method: Fitting the stochastic model

To determine $h(x_s)$ and $g(x_s)$ of (5.6) we follow the approach of Siegert et al. (1998). Equation (5.6) is a stochastic differential equation, i.e., a differential equation including a stochastic process. Hence the solution of (5.6) contains a random term. Since for each integration of (5.6) different random numbers are used, each integration represents a different trajectory in phase space. After observing a large number of trajectories we can assign each point x_s in phase space a probability $dw = \rho(x_s)dx_s$ that the infinitesimal interval $(x_s, x_s + dx_s)$ will be visited by the next trajectory. In this way a probability density function $\rho(x_s)$ can be defined for each time step. The time evolution of the probability density function of a Langevin equation is generally governed by a Fokker-Planck equation:

$$\frac{\partial \rho(x_s,t)}{\partial t} = \frac{\partial}{\partial x_s}\left[A(x_s)\rho(x_s,t)\right] + \frac{\partial^2}{\partial x_s^2}\left[B(x_s)\rho(x_s,t)\right] \tag{5.7}$$

in which $A(x_s)$ is called the drift coefficient and $B(x_s)$ is called diffusion coefficient. (For a comprehensive introduction to statistical physics and the Fokker-Planck equation see, e.g., Gardiner (1985) and Risken (1984).)

The coefficients $A(x_s)$ and $B(x_s)$ can directly be estimated from data. The drift coefficient is equal to the local mean tendencies

$$A(x_s) = \lim_{\tau\to 0}\frac{1}{\tau}\left\langle x_s(t+\tau) - x_s(t)\right\rangle\Big|_{x_s(t)=x_s}, \tag{5.8}$$

and the diffusion coefficient is defined as

$$B(x_s) = \lim_{\tau\to 0}\frac{1}{2\tau}\left\langle \left(x_s(t+\tau) - x_s(t)\right)^2\right\rangle\Big|_{x_s(t)=x_s}. \tag{5.9}$$

[2] δ-correlated means that any $\eta(t)$ and $\eta(t')$ are uncorrelated except for $t = t'$. It also implies that $\eta(t)$ has infinite variance. In practise we will always deal with discrete random numbers, which have a finite variance. The concept of white noise is an idealised mathematical formulation of continuous uncorrelated random fluctuations.

$\langle ... \rangle|_{x_s(t)=x_s}$ denote conditional ensemble averages. Our climate experiments are assumed to be stationary and ergodic. Therefore the ensemble averages can be replaced by time averages.

By knowing the Fokker-Planck equation, we can in the univariate case deduce the explicit form of the corresponding Langevin equation. In the Stratonovich[3] system $A(x_s)$ and $B(x_s)$ are related to $h(x_s)$ and $g(x_s)$ in the following way (Risken, 1984)

$$\begin{aligned} A(x_s) &= h(x_s) + g(x_s)\frac{\partial g(x_s)}{\partial x_s}, \\ B(x_s) &= \frac{1}{2}\left(g(x_s)\right)^2. \end{aligned} \tag{5.10}$$

In the Itô system, however,

$$\begin{aligned} A(x_s) &= h(x_s) \\ B(x_s) &= \frac{1}{2}\left(g(x_s)\right)^2 \end{aligned} \tag{5.11}$$

is true. The question arises which of these two definitions should we use for our system. Should the integral of the stochastic term in (5.6) be interpreted in the Stratonovich sense or in the Itô sense?

The issue of Stratonovich or Itô calculus is closely related to the definition of continuous white noise. While the Stratonovich definition implies a small but finite correlation between two random numbers, the Itô definition sticks to the strict mathematical definition that white noise is totally uncorrelated. For a comprehensive definition see Gardiner (1985). Stratonovich calculus should generally be used for systems continuous in time, in which rapid fluctuations with small but finite correlations times are treated as white noise (Penland, 2003). Itô calculus is best suited for discrete systems.

According to the above argumentation our system has to be interpreted in the Stratonovich sense. We want to model the time evolution of the continuous quantity temperature. The white noise term represents the stochastic forcing of the rapidly fluctuating small-scale processes (which have small but finite correlation times) onto the global mean temperature. The [S] in (5.6) symbolises that this is a Stratonovich stochastic differential equation (SDE). In the following an [I] will mark an Itô SDE.

[3]For a short description of the terms: 'Stratonovich' and 'Itô' see next paragraph. A detailed discussion on the differences between Stratonovich and Itô is given in the cited literature (Gardiner, 1985; Risken, 1984).

All Stratonovich SDEs can easily be transformed into Itô SDEs and vice versa. In the Itô system (5.6) can be written as (Gardiner, 1985)

$$\dot{x}_s(t) = h(x_s) + g(x_s)\frac{\partial g(x_s)}{\partial x_s} + g(x_s)\eta(t) \qquad \text{[I]}. \tag{5.12}$$

Equations (5.6) and (5.12) yield the same results, if (5.6) is integrated in the Stratonovich sense and (5.12) is integrated in the Itô sense.

Inserting the definitions (5.10) into the above equation (5.12) yields

$$\dot{x}_s(t) = A(x_s) + \sqrt{2B(x_s)}\eta(t) \qquad \text{[I]}. \tag{5.13}$$

Note that if we had defined our system to be an Itô system, we would use (5.11) with (5.6) marked with [I]. The resulting equation is the same. No matter whether we choose the Stratonovich or the Itô system we always end up with the Itô SDE (5.13). The main difference lies in the interpretation. If we state that our system is a Stratonovich system, $A(x_s)$ is not only determined by the deterministic drift term $h(x_s)$ but also by the noise-induced drift $g(x_s)\frac{\partial g(x_s)}{\partial x_s}$. The noise-induced drift results from the fact that during a change of $\eta(t)$ also $x_s(t)$ changes, and therefore $\langle g(x_s)\eta(t)\rangle$ is no longer zero (Risken, 1984). Empirically it is not possible to separate the deterministic drift and the noise-induced drift when estimating $A(x_s)$ from data. In contrast, if the explicit form of the Langevin equation were given and we wanted to derive $A(x_s)$ and $B(x_s)$ of the corresponding Fokker-Planck equation, it would be important to know whether to use Stratonovich (i.e., relations (5.10)) or Itô (i.e., relations (5.11)) calculus.

The method of fitting the stochastic model to the ECHAM5/MPI-OM data can be summarised as follows

1. Determine x_s by subtracting the mean daily and annual cycle and filtering out the long-term variability from x
2. Estimate $A(x_s)$ and $B(x_s)$ by using their definitions (5.8) and (5.9).
3. Insert $A(x_s)$ and $B(x_s)$ into (5.13)
4. New time series can be generated by integrating (5.13)

5.2.3 Time scale τ

In practice, it is not very straightforward to carry out point 2 of the list above. As can be seen from (5.8) and (5.9) the definitions of the drift and diffusion coefficients

involve the limes of the time lag $\tau \to 0$. When using discrete model output it is not possible to do $\tau \to 0$. We must estimate the drift and diffusion coefficient from:

$$A(x_s) = \frac{1}{\tau} \langle x_s(t+\tau) - x_s(t) \rangle \Big|_{x_s(t)=x_s} \tag{5.14}$$

$$B(x_s) = \frac{1}{2\tau} \left\langle (x_s(t+\tau) - x_s(t))^2 \right\rangle \Big|_{x_s(t)=x_s} \tag{5.15}$$

By using a finite time lag we will introduce a systematic finite-difference error.

The question arises which time lag τ we should actually take for the estimation of the drift and diffusion coefficient. When fitting a stochastic model to a system that is by nature continuous, it is not necessarily the best strategy to use the smallest available time step. By using a stochastic model we assume that we can treat rapid fluctuations with small correlation times, such as small-scale processes, as white noise. To be able to do this approximation we should estimate the parameters for the Fokker-Planck equation not from the smallest available time step (Berner, 2005). In every deterministic system adjacent time steps are highly correlated. We must take care that the time step is sufficient large in the way that the assumption of δ-correlated small-scale fluctuations can be fulfilled.

One way to estimate the appropriate time step is to look at the behaviour of the decorrelation rate at different time lags (DelSole (2000), Berner (2005)). The decorrelation rate α is defined as

$$\alpha(\tau) = -\frac{1}{\tau} \ln c(\tau) \tag{5.16}$$

in which $c(\tau)$ denotes the autocorrelation function at time lag τ. A simple Markov model following the linear Langevin equation

$$\dot{z}_1(t) = -\alpha_0 z_1(t) + \beta_0 \eta(t) \tag{5.17}$$

with α_0 and β_0 being constant, has for example the decorrelation rate $\alpha(\tau) = \alpha_0$. In this model the decorrelation rate α_0 is independent of the time lag τ. DelSole (2000) investigated a "red noise model" in which the white noise term $\eta(t)$ is replaced by random fluctuations $r_\gamma(t)$ with a small but finite decorrelation time τ_γ: $\dot{z}_2(t) = -\alpha_0 z_2(t) + \beta_0 r_\gamma(t)$. In this model the decorrelation rate increases linearly with time lags $\tau < \tau_\gamma$ and asymptotes to α_0 for $\tau > \tau_{\alpha_0} \equiv 1/\alpha_0$. For our results this means, as long as the decorrelation rate increases linearly with time lag we cannot assume that the deterministic small-scale fluctuations can be approximated as white noise because they are not yet decorrelated.

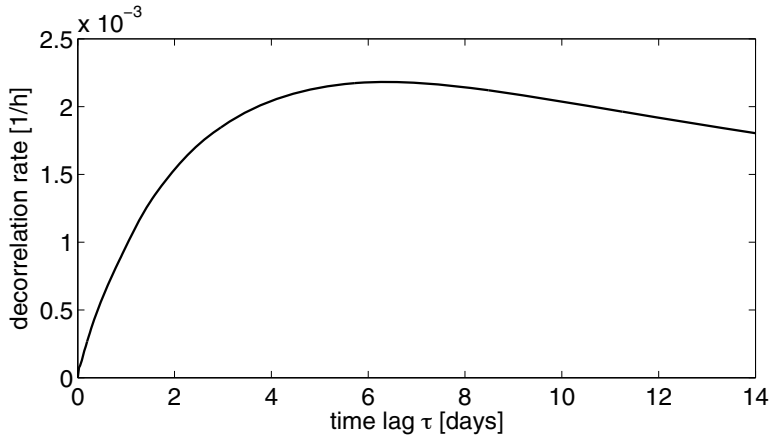

Figure 5.1: *Decorrelation rate of x_s from the control integration with $1\times CO_2$ concentration*

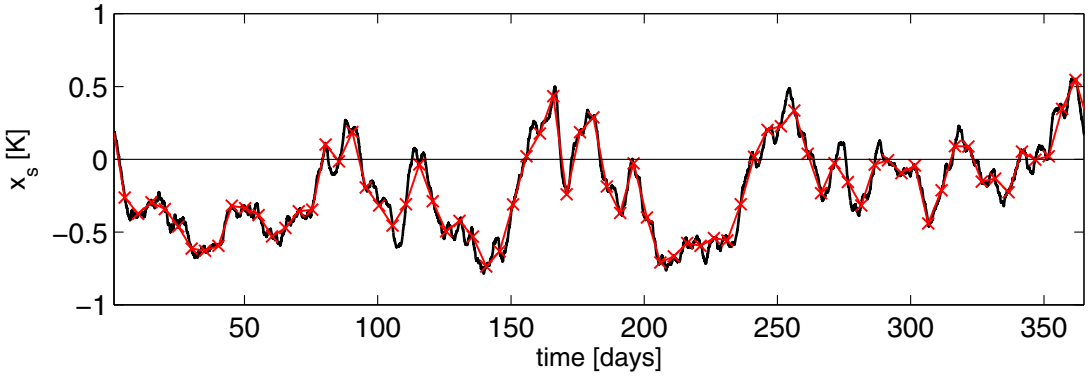

Figure 5.2: *Sample time series of x_s from* `ctrl1x`*, black: values are displayed for each time step (40 minutes), red: values are taken with a time step of 5 days*

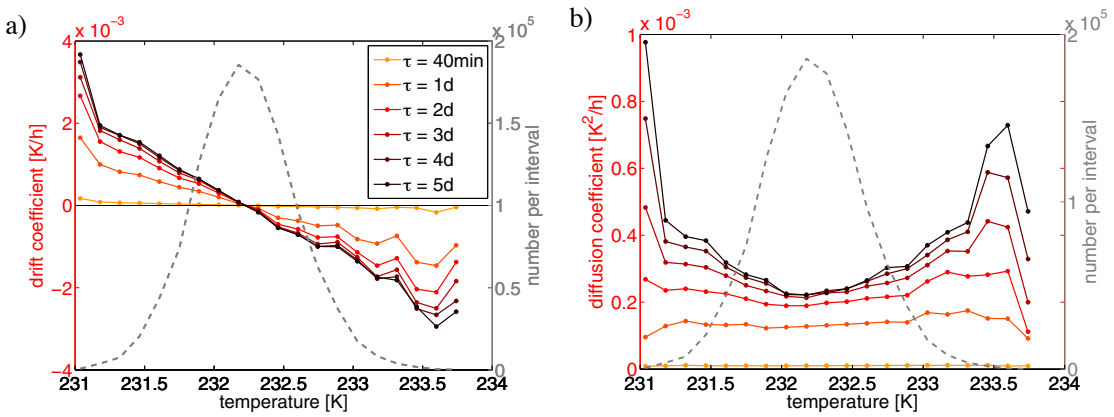

Figure 5.3: *Estimated coefficients of the Fokker-Planck equation for model data x_s obtained from the control integration with $1\times CO_2$ concentration (coloured solid lines). Different curves correspond to different time lags τ. For the evaluation we used one chunk of data including 100 years. The grey dashed line represents the number of data points per interval. a) drift coefficient $A(x_s)$ b) diffusion coefficient $B(x_s)$, same colour scale as in a)*

In Figure 5.1 the decorrelation rate of `ctrl1x` against the time lag is shown. For small time lags the decorrelation rate increases nearly linearly. After reaching a maximum at 5-6 days α slowly decreases again. Because of the above considerations the time lag at which the maximum occurs is chosen as the shortest time step for which the stochastic model can be fitted. A time step of 5 days is large enough to eliminate strong correlations between adjacent time steps and is small enough to still capture the main excursions contributing to the variance of the time series (Figure 5.2).

5.3 Results

5.3.1 $A(x_s)$ and $B(x_s)$

Although we have decided to use $\tau = 5$ days as the appropriate time lag for the estimation of the drift and diffusion coefficients, $A(x_s)$ and $B(x_s)$, we will in the following still have a look at the results with other time lags. In this way we get a feeling for the dependency of the results on the time lag.

We estimate the drift and diffusion coefficient by dividing the phase space into 20 equidistant intervals. The main results described below do not change when we

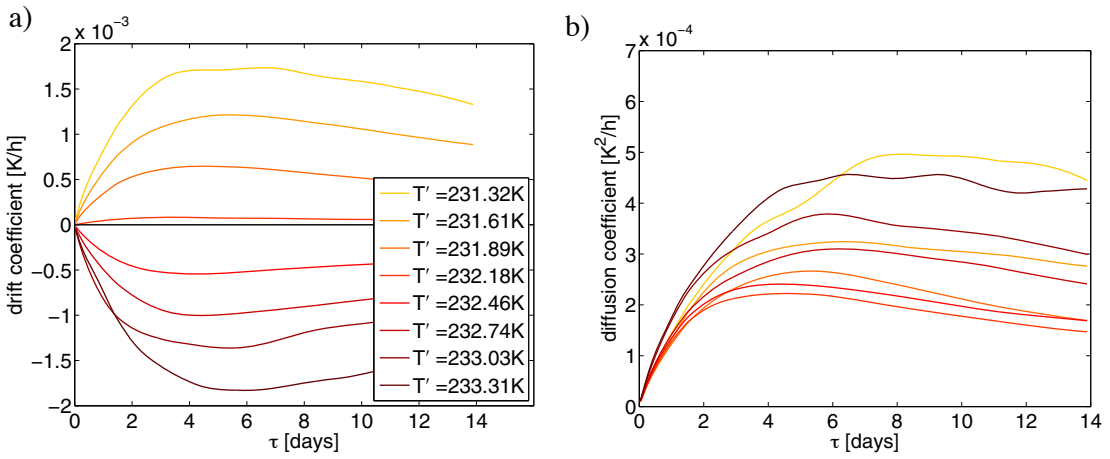

Figure 5.4: *Estimated coefficients of the Fokker-Planck equation for model data x_s obtained from the control integration with $1\times CO_2$ concentration. Different curves correspond to different temperature values. a) drift coefficient $A(x_s)$ b) diffusion coefficient $B(x_s)$*

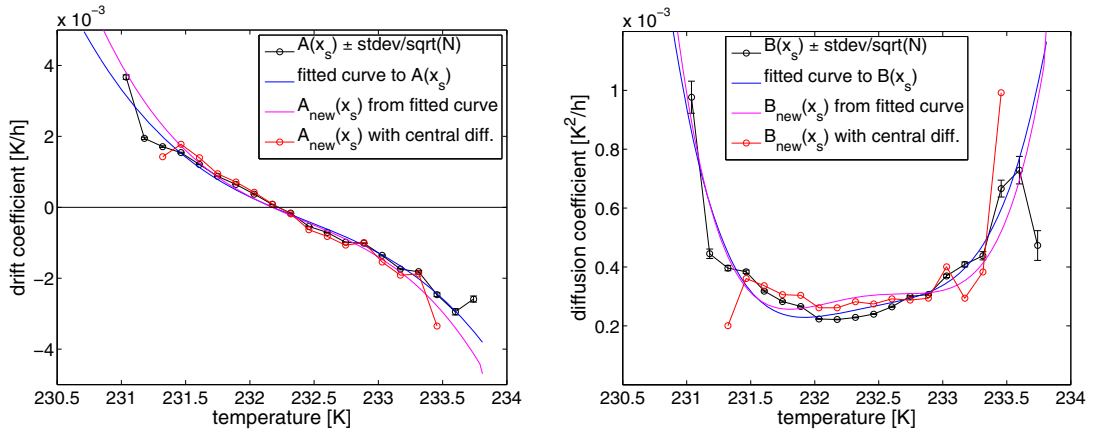

Figure 5.5: *Illustration of the finite-difference error, black: original estimates using Eq.(5.14) and Eq.(5.15) with standard error bars (stddev/$\sqrt{N}$), red: corrected coefficients using centred differences, blue: polynomial fit, magenta: corrected polynomial fit, a) drift coefficient $A(x_s)$ b) diffusion coefficient $B(x_s)$*

use 25, 30 or 35 intervals. Figure 5.3 shows the estimated coefficients $A(x_s)$ and $B(x_s)$ of the Fokker-Planck equation for different time lags τ of the experiment `ctrl1x`. As a first approximation the drift coefficient can be characterised by a straight line. Its slope depends on the time lag τ. With increasing time lag the slope steepens. This steepening abates for larger time lags approaching $\tau = 5$ days.

The diffusion coefficient is by definition everywhere positive. In general, a constant diffusion coefficient would correspond to additive noise in the Langevin equation. Figure 5.3 b) clearly shows that $B(x_s)$ is not constant especially for large time lags. That means that large temperature anomalies are on average accompanied by high noise intensities. Similar to the drift coefficient the change of the diffusion coefficient abates with increasing time lags.

Figure 5.4 shows the drift and diffusion coefficients as functions of time lags. Now different lines correspond to different temperature values, which represent certain points on the x-axis of Figure 5.3. Both $A(x_s)$ and $B(x_s)$ experience strong changes for small time lags. However, at a time lag of 5 days the curves reach extrema and then start to decay very slowly towards zero.

As mentioned in Section 5.2.3, estimating the drift and diffusion coefficient from finite time lags leads to systematic finite-difference errors, since (5.8) and (5.9) are only valid for the limes $\tau \to 0$. The error made can be estimated up to first order (Sura and Barsugli, 2002), and following Berner (2003) we can correct the drift and diffusion coefficient:

$$A_{\text{new}} = A - \frac{1}{2}\left(A\frac{dA}{dx_s} + B\frac{d^2A}{dx_s^2}\right)\tau \tag{5.18}$$

$$B_{\text{new}} = B - \frac{1}{2}\left(A^2 + 2B\frac{dA}{dx_s} + A\frac{dB}{dx_s} + B\frac{d^2B}{dx_s^2}\right)\tau \tag{5.19}$$

When we correct $A(x_s)$ and $B(x_s)$ for the finite-difference error, we derive new drift and diffusion coefficients describing a continuous stochastic process, which has the same or similar statistical properties at time lags $\tau \geq 5\,\text{d}$ as our system at time lags $\tau \geq 5\,\text{d}$.

Because the estimation of the finite-difference error involves the first and second derivatives it is difficult to compute the finite-difference error without introducing new errors. One way is to fit a polynomial function to the data. However, this proves to be difficult if the data show small nonlinear features. The second approach is to compute the derivatives numerically (e.g., by using centred differences). This method leads to a loss of data at the boundaries and can introduce numerical errors larger than the error that we wanted the data to correct for.

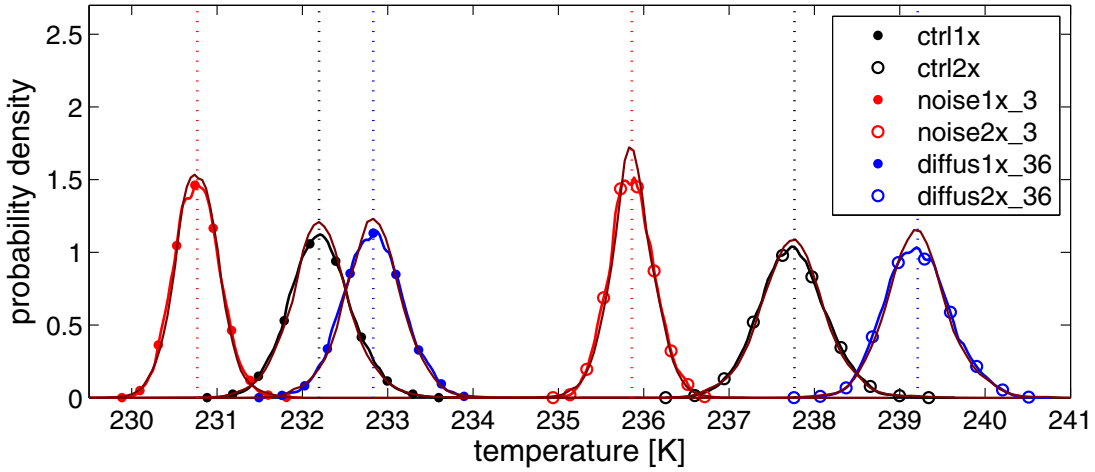

Figure 5.6: *Probability density functions of six different ECHAM5/MPI-OM experiments (black, blue and red lines with closed and open circles) and the corresponding probability density functions of the stochastic models with $\tau = 5$ d (brown lines without circles)*

Figure 5.5 gives an impression of how big the finite-difference errors are. Although the time lag that we use to estimate $A(x_s)$ and $B(x_s)$ is quite large, the error made in the drift coefficient is small. For the diffusion coefficient we find larger errors. $B(x_s)$ is systematically underestimated for small and median temperature anomalies. Since the estimation of the error itself introduces new uncertainties and the finite-errors made are not very large, in the further analysis we will use uncorrected estimates of $A(x_s)$ and $B(x_s)$.

5.3.2 Statistical properties of the fitted stochastic model

To get an impression of how well the nonlinear Langevin equation (5.13) is able to reproduce main statistical properties, we compare in the following x_s, that is the filtered global mean temperature at 300 hPa obtained from ECHAM5/MPI-OM, with data generated by integrating the stochastic model (5.13). The stochastic differential equation is numerically integrated by using the stochastic Euler scheme (Kloeden, 1992).

In Figure 5.6 the probability density functions (PDFs) of six different experiments and the PDFs of the corresponding stochastic models are shown. In general, the PDFs are reproduced well by the stochastic models. However, there is a systematic overestimation of the maximum of the PDF by the stochastic models.

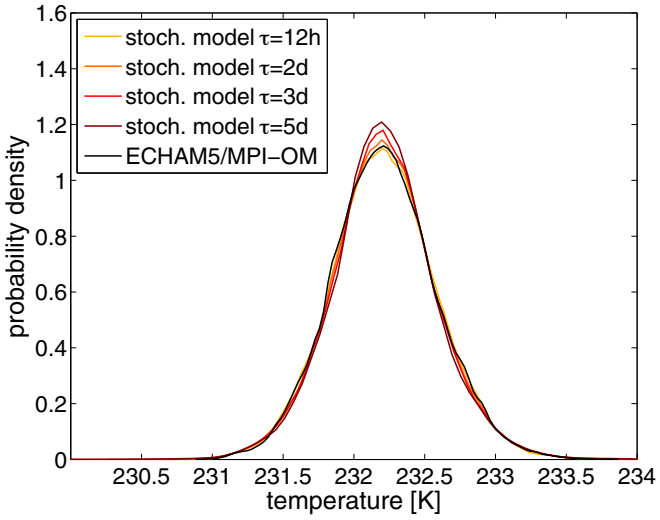

Figure 5.7: *Probability density functions of different stochastic models (coloured lines) and of x_s extracted from* `ctrl1x` *(black line). The coloured lines differ in τ, which is used to evaluate $A(x_s)$ and $B(x_s)$ from* `ctrl1x` *data*

Figure 5.7 compares the probability density function of the experiment `ctrl1x` with PDFs obtained from data generated by different stochastic models. The stochastic models differ only in the time lag τ that was used to estimate $A(x_s)$ and $B(x_s)$. It can be seen that the agreement of the coloured lines (stochastic models) with the black line (ECHAM5/MPI-OM data x_s) worsens with larger time lag τ. In general the kurtosis increases, i.e., the tails become heavier (Table 5.1).

The power spectrum of x_s and of different stochastic models are displayed in Figure 5.8. The spectrum for $\tau = 0.67\,\mathrm{h}$, which matches the smallest available time lag, does not reproduce the spectrum of x_s very well. For $\tau = 5\,\mathrm{d}$ we observe the best agreement in the range of medium and low frequencies. For high frequencies the 5 d-curve disagrees considerably from the x_s-spectrum. This is mainly due to the steep slope of the x_s-spectrum in that frequency-range. Since we fitted the stochastic model to time scales larger than 5 days this discrepancy is not surprising.

The autocorrelation function (Figure 5.9) of the stochastic model fitted to x_s resembles well the autocorrelation function of the filtered ECHAM5/MPI-OM data x_s up to a time lag of $\tau \approx 20$ days. For larger time lags the ECHAM5/MPI-OM data x_s show still some long-term variability, which cannot be simulated by the stochastic model. The stochastic model fitted to x_s reproduces, however, the

	mean	variance	skewness	kurtosis
ECHAM5/MPI-OM (`ctrl1x`)	232.21	0.14	0.14	3.17
stochastic model ($\tau = 12\,\mathrm{h}$)	232.21	0.14	0.10	3.18
stochastic model ($\tau = 2\,\mathrm{d}$)	232.21	0.14	0.11	3.38
stochastic model ($\tau = 3\,\mathrm{d}$)	232.21	0.14	0.11	3.56
stochastic model ($\tau = 5\,\mathrm{d}$)	232.21	0.14	0.10	4.16

Table 5.1: *Statistical moments of the filtered global mean temperature at 300 hPa obtained from* **`ctrl1x`** *and of time series generated by different stochastic models. The stochastic models differ only in the time lag τ used to estimate $A(x_s)$ and $B(x_s)$*

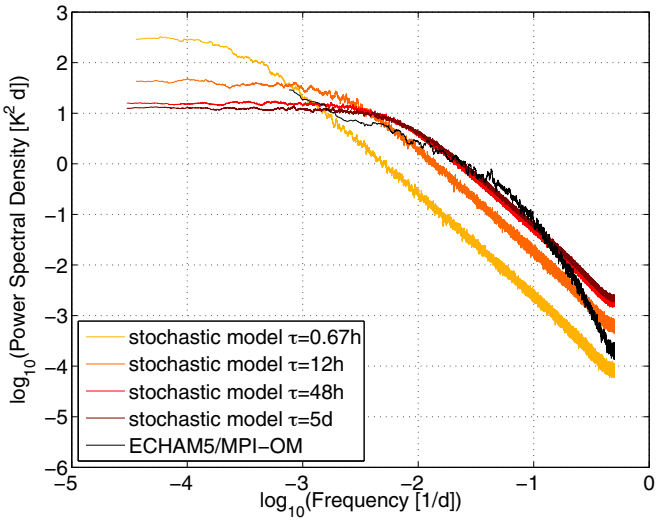

Figure 5.8: *Power spectrums obtained from different stochastic models (coloured lines) and of x_s extracted from* **`ctrl1x`** *(black line). The coloured curves differ in τ which is used to estimate $A(x_s)$ and $B(x_)$ from* **`ctrl1x`** *data.*

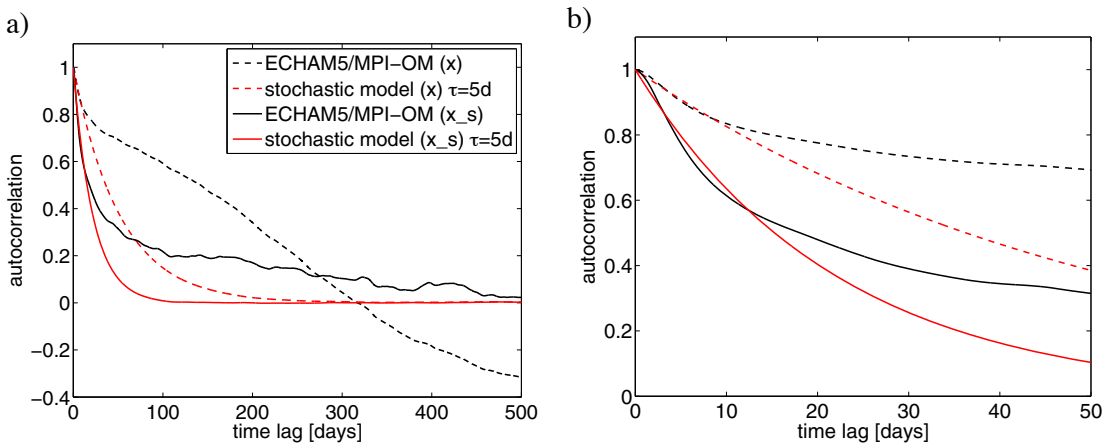

Figure 5.9: *a) Autocorrelation functions of the unfiltered ECHAM5/MPI-OM data x (dashed black) and filtered ECHAM5/MPI-OM data x_s (solid black) as well as the autocorrelation function of the stochastic model fitted to x (dashed red) and x_s (solid red); b) same as a) but with different axes*

time evolution of x_s much better than a stochastic model which was fitted to the unfiltered model data x.

5.4 Discussion

In this chapter we introduced and fitted a stochastic model to the global mean temperature at 300 hPa obtained from `ctrl1x`. Since a univariate stochastic model is not able to reproduce the long-term variability induced by the interactions between the ocean and the atmosphere, we filtered out the long-term variability beforehand. From Figure 5.9 we saw that filtering out the long-term variability is necessary in order to obtain a stochastic model with roughly a similar temporal statistics as the filtered data. Despite the filtering, the autocorrelation function of x_s and of the stochastic model still disagree for larger time lags. To avoid this problem we could filter out not only the long-term variability related to the ocean but all variability longer than for example 1 year. Such a rigorous filtering would change the autocorrelation function both of the stochastic model and of the filtered data at all time lags. The new autocorrelation functions would decay much quicker. We would throw away long-term and medium-term processes that are relevant for the analysis of the system's response to a change in CO_2 concentration. Despite the limitations of the stochastic model we believe that it is still a useful

tool for investigating the impact of small-scale fluctuations on the temperature response to a CO_2 increase (see next chapter).

For the estimation of the model parameters $A(x_s)$ and $B(x_s)$ we decided to use not the smallest available time lag. On the basis of the decorrelation rate we chose the time lag $\tau = 5\,\mathrm{d}$. This time scale is rather large, but the way in which the drift and diffusion coefficient depend on τ supports the choice of $\tau = 5\,\mathrm{d}$. For time lags smaller than 5 days $A(x_s)$ and $B(x_s)$ greatly change with increasing τ. For time lags larger than 5 days the dependency is reversed and much weaker. Furthermore, the power spectrum of the stochastic model with $\tau = 5$ days agrees better with the spectrum of x_s. In contrast, the probability density functions corresponding to stochastic models with time lags close to 5 days experience systematic mismatches. One explanation for this discrepancy is the erroneous computation of the drift and diffusion coefficient due to finite-difference errors. The diffusion coefficient is systematically underestimated and the magnitude of the drift coefficient is too small for large temperature anomalies. These uncertainties could be the reason for too heavy tails of the PDFs, especially since the error grows with increasing time lag.

6 Impact of small-scale fluctuations on the large-scale statistics

6.1 Introduction

One approach to finding a connection between the small-scale variability and the large-scale response of the global mean temperature to increased CO_2 concentration can be made via the fluctuation dissipation theorem (FDT). The FDT originates from statistical physics. Although the climate system does not satisfy all conditions required for the theorem, Leith (1975) first argued that the FDT could be used to approximate the climate response to small changes in external forcings. Since Leith's paper several studies obtained promising results when testing the FDT in climate-like systems (Bell (1980), North et al. (1993), Cionni et al. (2004), Langen and Alexeev (2005)). Gritsun and Branstator (2007) introduced a less restrictive derivation of the FDT than Leith, which is better suited for the climate system. They also find the FDT to be a useful tool in approximating the response of a climate model to changed external conditions.

The fluctuation dissipation theorem states that the response of a system to a changed external forcing can directly be deduced from the statistics of the *unperturbed* system. This is possible because the recovery of the system from an artificial perturbation is assumed to have about the same temporal behaviour as the recovery from a natural fluctuation. Although the climate system is in a stationary state, it is frequently driven away from its mean state due to internal instabilities. The way in which the system returns from these excursions back to the mean state is determined by the overall effect of several feedback processes. The FDT assumes that these same feedback processes also determine the response of the system to small artificial impulsively-forced perturbations. Hence from observing the naturally fluctuating system and with that the stability-altering feedback processes (i.e., processes that determine how the system in equilibrium reacts to an impulsively-forced perturbation (Bates, 2007)), we can draw conclusions about the sensitivity of the system to a constant increment in external forcing.

If in our experiments the enhanced small-scale fluctuations affected the statis-

tics of the global mean temperature in the unperturbed system, the temperature response to increased CO_2 concentration would also be influenced. In other words, because the climate response depends on the statistical properties of the pre-industrial climate, the response would be changed, if the statistical properties were varied by enhanced small-scale fluctuations. Indeed, a study by von Storch (2004) indicates that stronger small-scale fluctuations can lead to different statistics of large-scale variables.

In this chapter we want to analyse whether enhanced small-scale fluctuations alter the statistical properties of the global mean temperature in our experiments and thereby cause different climate sensitivities. We also hope to gain insight into the different behaviour of the two different ways of enhancing the small-scale variability, which are reducing the horizontal diffusion or adding white noise to the small-scale components.

In the next section we argue that a linear stochastic model will be sufficient for our application. We also derive a simple form of the FDT and show how the temperature response can depend on the statistics of the unperturbed system. In Section 6.3 we describe how the parameters of the stochastic model are affected by a CO_2 doubling and enhanced small-scale fluctuations.

6.2 Method

6.2.1 Linear stochastic model with additive noise

In Figure 5.3 (previous chapter) we saw that the drift coefficient pictures as a first approximation a straight line. The diffusion coefficient, however, indicates multiplicative noise. The question arises, how important are the small deviations of the drift coefficient from a straight line and the temperature-dependency of the diffusion coefficient for our application. Using a Langevin equation with a linear drift coefficient and with additive noise would very much simplify the analysis.

Inserting a linear drift coefficient ($A(x_s) = -\alpha x_s + F$) and a constant diffusion coefficient ($B(x_s) = B = \frac{1}{2}g_0^2$) into the stochastic model (5.13) yields the linear Langevin equation

$$\dot{x}_s(t) = -\alpha x_s + F + g_0\,\eta(t). \tag{6.1}$$

We estimate the parameters α and F by linearly least-squares fitting $-\alpha x + F$ to the original drift coefficient (Figure 6.1). The linear Langevin equation (6.1) has the variance

$$\sigma^2 = \frac{g_0^2}{1-(1-\alpha)^2}.$$

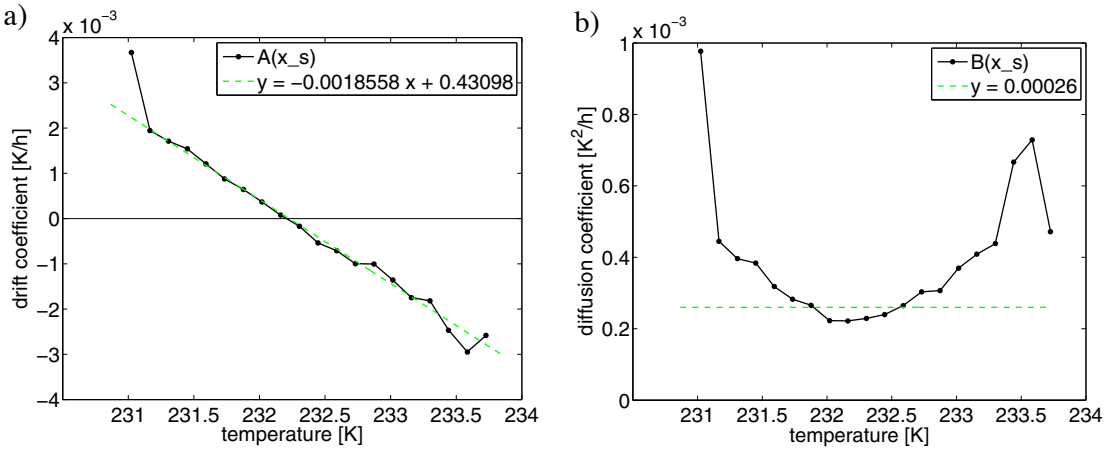

Figure 6.1: *Coefficients of the Fokker-Planck equation of* `ctrl1x` *for time lag* $\tau = 5d$ *(solid black) and the corresponding linear fits used for the linear stochastic model (dashed green). a) drift coefficient* $A(x_s)$*, b) diffusion coefficient* $B(x_s)$

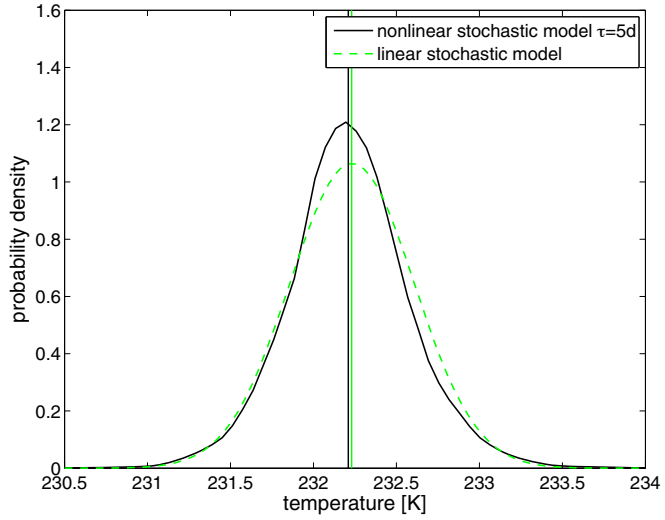

Figure 6.2: *Probability density function of the full nonlinear stochastic model (solid black) and of the linear stochastic model with additive noise (dashed green). Both models are fitted to* x_s *obtained from* `ctrl1x`*. The vertical lines mark the time means of the stochastic processes.*

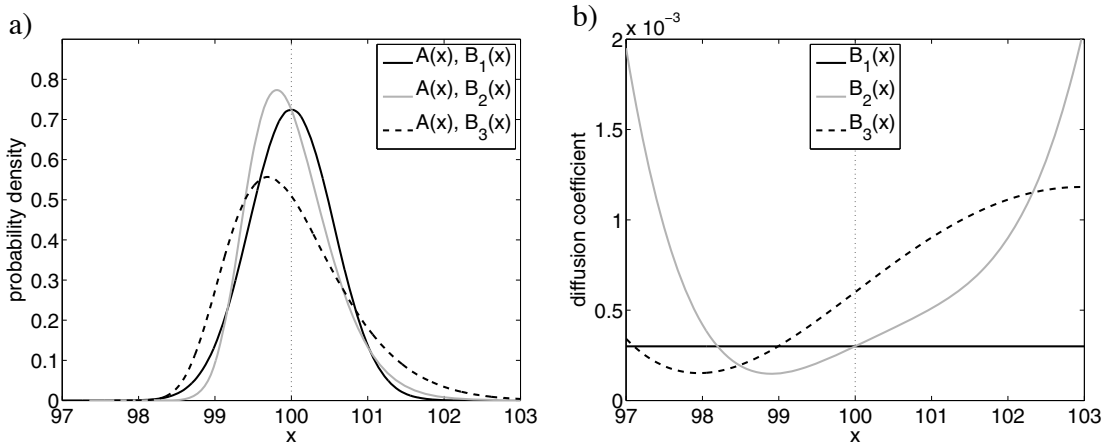

Figure 6.3: *a) Probability density function of three fictitious Langevin equations with the same linear drift coefficient* $A(x) = -1 \cdot 10^{-3}x + 0.1$ *and different nonlinear diffusion coefficients shown in b); The vertical dotted line marks the mean of the stochastic processes.*

By choosing $g_0 = \sqrt{\sigma^2_{nlin}[1-(1-\alpha)^2]}$ we ensure that the stochastic process described by (6.1) has the same variance σ^2_{nlin} as the nonlinear stochastic model (5.13).

The probability density function (PDF) of the new linear Langevin equation (6.1) is normally distributed. It differs considerably from the PDF of the nonlinear stochastic model (Figure 6.2). Unlike the variance, the mean of (6.1) is not tuned to be the same as that of the nonlinear stochastic model. The difference between the two means tells us how big the impact of the nonlinearities in the drift coefficient on the mean value is. From Figure 6.2 we see that the mean temperature of the linear stochastic process (6.1) is almost the same as the mean in the nonlinear case. It is only 0.02 K higher in comparison to the nonlinear model.

The difference between the means is small, because the drift coefficient obtained from the ECHAM5/MPI-OM data is already almost linear. Generally, if the drift coefficient of the nonlinear stochastic process (5.13) is linear, the mean is always independent of the form of the diffusion coefficient. Figure 6.3a) illustrates this statement by means of three example stochastic processes. All shown PDFs result from stochastic processes with the same linear drift coefficient but very different diffusion coefficients (Figure 6.3b). Although the PDFs deviate from each other, they all have the same mean marked by the dotted line.

We conclude, since the drift coefficient of our data is nearly linear, the temperature dependency of the diffusion coefficient is not important for our application.

We are only interested in the mean and its change due to increased CO_2 concentration. If we, however, cared, e.g., about extreme values, the form of the diffusion coefficient would play a crucial role.

6.2.2 Response to a change in external forcing

Given the linear stochastic model with additive noise we can derive formulas for the mean and the mean response to changed external forcing. Applying a time average on (6.1) yields

$$\overline{\dot{x}_s(t)} = -\alpha\overline{x_s} + F + \overline{g_0\,\eta(t)}. \tag{6.2}$$

Since the system is stationary, the average of the time derivative $\overline{\dot{x}_s(t)}$ is zero. The third term on the right hand side involving white noise also vanishes, because g_0 is a constant and $\eta(t)$ has zero mean. We get:

$$\mu_1 \equiv \overline{x_s} = \frac{F}{\alpha} \tag{6.3}$$

The time mean μ_1 is solely determined by the parameters F and α. In a descriptive, physical sense their meaning can be seen as follows. F represents a constant forcing on x_s, which results from external factors such as CO_2 concentration and solar irradiance. Note that F is generally not independent of the climate state $\vec{x}$. The radiative forcing related to the CO_2 concentration depends for instance on the temperature and cloud distribution. The parameter α is on the other hand related to the internal feedbacks and interactions in the system. The term $-\alpha x_s$ is often referred to as statistical dissipation or damping. The negative slope $-\alpha$ ensures the stationarity of the system. It always drives the system back towards its mean. α is a measure for the climate's 'spring constant' as introduced in the introduction (Chapter 1).

Doubling the CO_2 concentration modifies the forcing F in equation (6.2) to $F + \Delta F$. After a certain time the system will reach a new equilibrium μ_2:

$$\mu_2 = \frac{F + \Delta F}{\alpha}$$

The response $\Delta\mu$ to the doubled CO_2 concentration is determined by:

$$\Delta\mu \equiv \mu_2 - \mu_1 = \frac{\Delta F}{\alpha} \tag{6.4}$$

The above relation represents a very simple form of the fluctuation dissipation theorem. Note that it is only valid if the CO_2 increase does not alter the statistical damping coefficient α. In general, equation (6.4) means, from knowing the

statistics of the unperturbed system, namely α, and the change in external forcing ΔF, we can determine the mean response $\Delta\mu$. Thus, if the enhanced small-scale fluctuations in, e.g., the diffusion-experiments decreased α, the higher temperature response in the diffusion-experiments could be explained with the aid of the fluctuation dissipation theorem.

In the following we will estimate for each experiment the drift coefficient and its slope $-\alpha$. By comparing the results we see whether the enhanced small-scale fluctuations alter the statistics of x_s and with it the response $\Delta\mu$. We determine the drift coefficient from the last 100 years of data of each experiment (model years 51–150 corresponding to $\approx 1,314,000$ time steps) by using relation (5.14) with $\tau = 5$ days. To get a good estimate of the slope $-\alpha$, we take the mean of three linear least-squares fits differing in the number of data points used. For the fitting we omit the outer points, namely on each edge 5, 6, or 7, since we are interested in the slope drawn by the inner points.

6.3 Results

6.3.1 Impact of increased CO_2 concentration

Figure 6.4 shows the drift coefficient $A(x_s)$ obtained from the control experiments with $1\times CO_2$ concentration and with $2\times CO_2$ concentration. As expected from the above given meaning for F and α, the increased CO_2 concentration results mainly in a horizontal shift of the drift coefficient. The external forcing F is increased. The slope of the drift coefficient $-\alpha$ changes only little. We find $\alpha_{\text{ctrl1x}} = 1.84 \times 10^{-3}\,1/\text{h}$ and $\alpha_{\text{ctrl2x}} = 2.03 \times 10^{-3}\,1/\text{h}$. To get an idea of the uncertainties involved when estimating α, we perform a non-parametric statistical test.

As null hypothesis we assume that α_{ctrl2x} is not significantly different from α-estimates obtained from `ctrl1x` solely. In other words, the difference between α_{ctrl1x} and α_{ctrl2x} occurred just by chance. We extend the experiment `ctrl1x` by 650 years and split the now 800 year long `ctrl1x`-experiment into 71 chunks of data. Each chunk has a length of 100 years and overlaps the previous chunk by 90 years. For each chunk we estimate the statistical damping coefficient α as described above. The 71 resulting values are estimates of the parameter α_{ctrl1x}, which we could have gotten, if we by chance had used another chunk of 100y-data instead of year 51–150 of the `ctrl1x`-experiment. Since each chunk contains also data from adjacent chunks, the estimates are not independent. We include estimates obtained from overlapping chunks, because we also want to account for

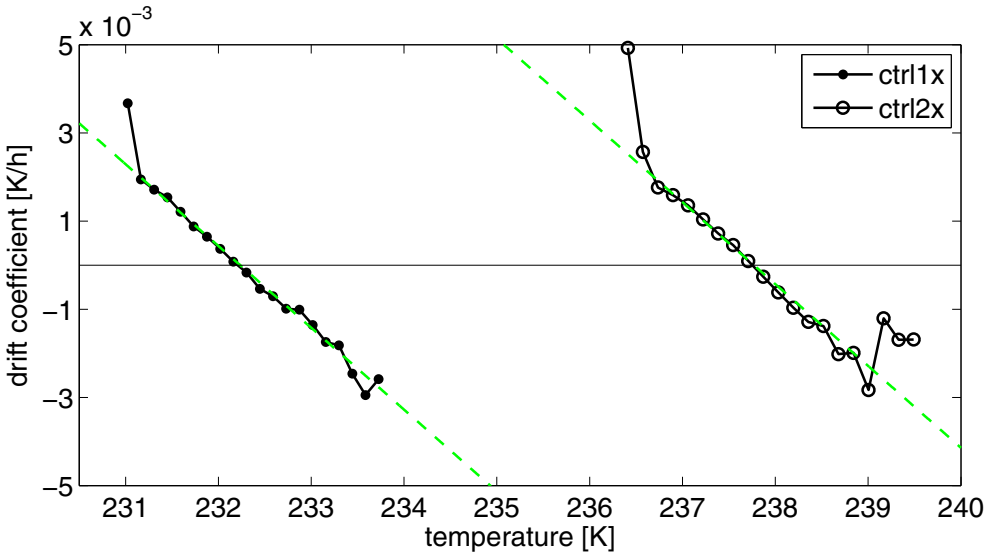

Figure 6.4: *Drift coefficients $A(x_s)$ of the experiments* `ctrl1x` *(closed circles) and* `ctrl2x` *(open circles) as well as a linear fit of* `ctrl1x` *(green dashed line on the right). The left green dashed line displays the linear fit of* `ctrl1x` *shifted along the x-axis.*

the uncertainty introduced, when data from somewhat shifted chunks are used.

The empirical cumulative distribution function obtained from the 71 α-estimates is shown in Figure 6.5. The vertical dotted lines mark the 2.5th and 97.5th percentiles. If α_{ctrl2x} were smaller than the 2.5th percentile or larger than the 97.5th percentile, we would reject the null-hypothesis with 5% risk and accept the alternative hypothesis that α_{ctrl2x} is statistically significant different from α_{ctrl2x}. The dashed vertical line marks the estimate of α_{ctrl2x}. It lies within the uncertainty range of α_{ctrl1x}. Hence we conclude, a higher CO_2 concentration does not significantly alter α. Our results are consistent with equation (6.4). The response $\Delta\mu$ is mainly due to an increase of F.

6.3.2 Impact of small-scale fluctuations

Considering the relation (6.4) we find three possible ways in which the climate response $\Delta\mu$ can be influenced via enhanced small-scale fluctuations:

case 1: The enumerator ΔF could be changed by the different representation of small-scale fluctuations. In other words, ΔF results not only from changes

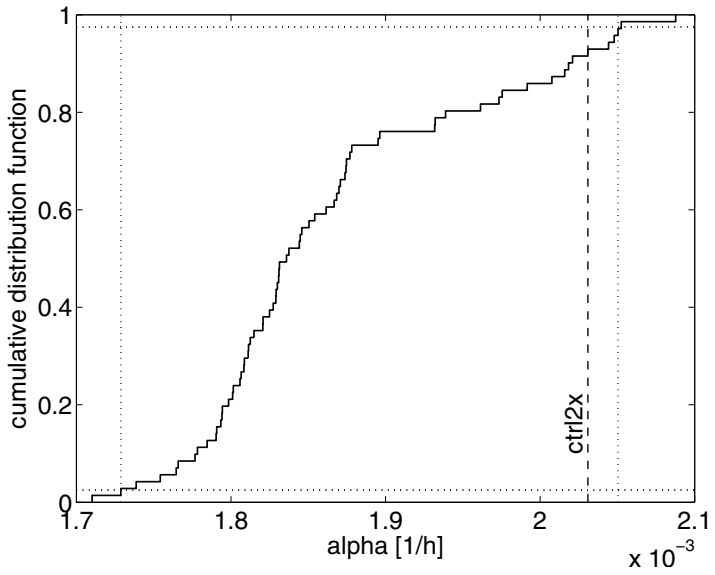

Figure 6.5: *Cumulative distribution function (cdf) of the parameter α obtained from the experiment* `ctrl1x`*. The cdf is estimated from 71 drift coefficients, which were calculated by using 71 overlapping 100-year chunks. The dotted, vertical lines mark the 2.5th and 97.5th percentiles. The dashed vertical line corresponds to the estimate of α for* `ctrl2x`

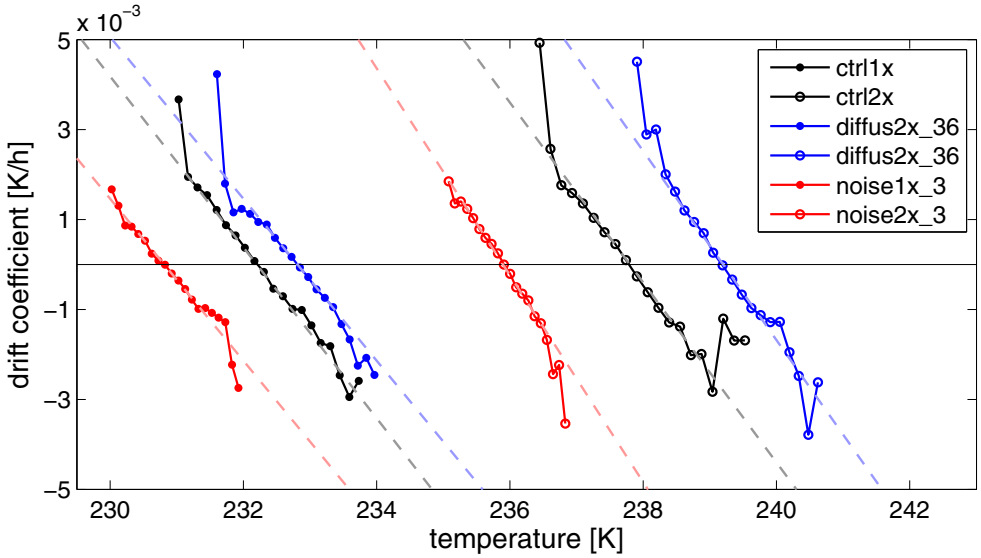

Figure 6.6: *Drift coefficients $A(x_s)$ of the experiments* `ctrl1x` *(black closed circles),* `ctrl2x` *(black open circles),* `diffus1x_36` *(blue closed circles),* `diffus2x_36` *(blue open circles),* `noise1x_3` *(red closed circles) and* `noise2x_3` *(red open circles); The dashed lines show linear fits of the respective drift coefficient.*

in CO_2 concentration but also from the representation of small-scale fluctuations.

case 2: The enhanced small-scale fluctuations could lead to a larger or smaller statistical dissipation coefficient α. The 'spring constant' of the system were changed. As discussed in the introduction this would mean that the statistics of the global mean temperature are altered.

case 3: Both α and ΔF are influenced by the representation of the small-scale fluctuations.

Figure 6.6 shows the drift coefficients $A(x_s)$ of the control experiments and experiments with enhanced small-scale fluctuations. Similar to the impact of doubled CO_2 concentration on $A(x_s)$ the drift coefficients are primarily shifted along the x-axis. A closer comparison of the slopes reveals differences between the experiments (Table 6.1).

From Figure 6.7 we see which changes of α are significant and which not. Overall we find distinct behaviours of the diffusion-experiments and the noise-experiments. Reducing the horizontal diffusion does not significantly change the

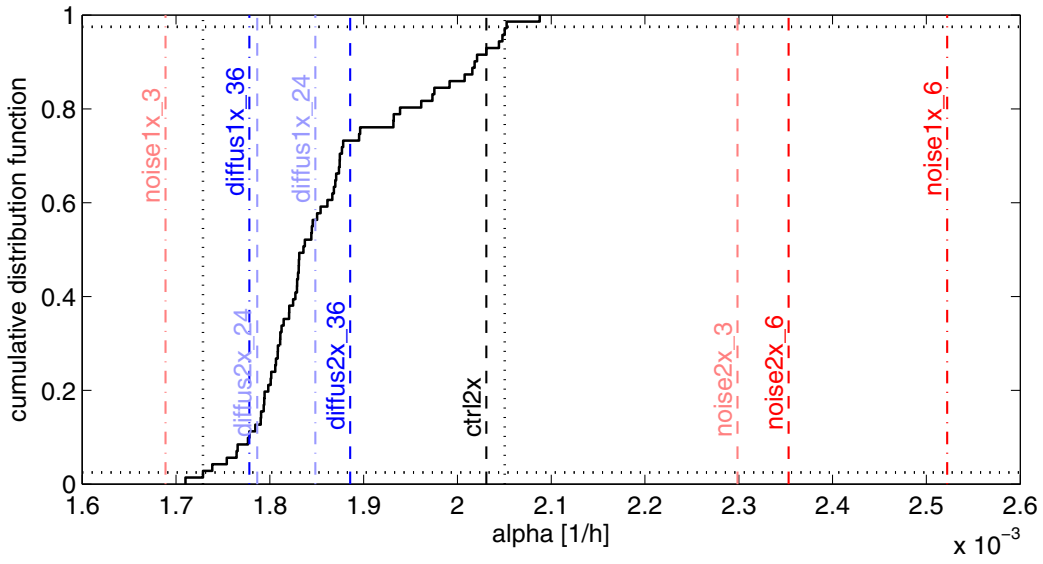

Figure 6.7: *Cumulative distribution function (cdf) of the parameter α obtained from the experiment* ***ctrl1x*** *as shown in Figure 6.5. The dotted, vertical lines mark the 2.5th and 97.5th percentiles. The dashed vertical lines correspond to the estimates of α for different experiments (see also Table 6.1)*

	α [10^{-3} 1/h]		$\Delta\mu$ [K]	ΔF [10^{-3} K/h]
experiment	1xCO_2	2xCO_2	$2\text{xCO}_2 - 1\text{xCO}_2$	$2\text{xCO}_2 - 1\text{xCO}_2$
`ctrl`	1.87	2.03	5.6	10.5
`diffus_24`	1.85	1.79	6.1	11.4
`diffus_36`	1.78	1.89	6.4	12.0
`noise_3`	1.69	2.30	5.1	–
`noise_6`	2.52	2.35	3.6	8.8

Table 6.1: *Estimates of the statistical dissipation coefficient α, global mean temperature response at 300 hPa to a doubling of CO_2 $\Delta\mu$, and the parameter ΔF defined in Eq.(6.4); The value of α_{ctrl1x} corresponds to the mean obtained from the 71 α-estimates used to create the cumulative distribution function in Figure 6.5. All other statistical dissipation coefficients are estimated from 100-year long data chunks. For the sets of experiments* ***ctrl****, **diffus_24**, and **diffus_36** ΔF is evaluated by using $\overline{\alpha}_{\text{ctrl1x}} = 1.87 \times 10^{-3}$ 1/h and $\Delta\mu$ of each set of experiments. For **noise_6** ΔF is evaluated by using $(\alpha_{\text{noise1x\_6}} + \alpha_{\text{noise2x\_6}})/2 = 2.44$.*

statistical damping coefficient. Adding noise to the small scales, however, may result in a different statistical damping. With the exception of the experiment `noise1x_3` all noise-experiments have a larger α. This means that the slopes of the corresponding drift coefficients are steepened. Thus the noise strengthens the statistical damping of the global mean temperature at 300 hPa. On average the system with noise is stronger driven back towards the mean state than the system without noise.

Getting back to the question of how the enhanced small-scale fluctuations alters the climate response $\Delta\mu$, we conclude that for the diffusion-experiments case 1 is true. Since the reduction of the horizontal diffusion does not change α, ΔF must be different. The difference must result from the representation of small-scale fluctuations, since otherwise $\Delta\mu$ in the diffusion-experiments would be the same as $\Delta\mu$ in the control experiments. For the noise-experiments it is more complicated. For the set of experiments with moderate noise (`noise2x_3` – `noise1x_3`) none of the above cases is applicable. Since α changes from the $1\times CO_2$-experiment to the $2\times CO_2$-experiment, relation (6.4) is not valid. The experiments `noise1x_3` and `noise2x_3` violate the assumption that a CO_2-doubling does not change the statistical damping coefficient. We cannot say whether the change in $\Delta\mu$ is caused by changes in α or ΔF. For the set of experiments with strong noise (`noise2x_6` – `noise1x_6`) cases 2 or 3 may be true, assuming that $\alpha_{\text{noise1x\_6}}$ and $\alpha_{\text{noise2x\_6}}$ are not significantly different. (Seeing the uncertainty range of `ctrl1x` this is a reasonable assumption.) The statistical damping coefficient in `noise1x_6` and `noise2x_6` changed, but we have to check whether the change of the statistical damping coefficient alone is responsible for the decrease of $\Delta\mu$ by 2 K.

For the experiments in which $\alpha_{\text{1xCO2}} = \alpha_{\text{2xCO2}}$ (within the range of uncertainty) we evaluate ΔF using (6.4): $\Delta F = \Delta\mu \cdot \alpha$ (Table 6.1). Since we found that the statistical damping coefficients α are within the uncertainty range equal in the sets of experiments `ctrl`, `diffus_24`, and `diffus_36`, we use for the diffusion-experiments also $\overline{\alpha}_{\text{ctrl1x}} = 1.87 \times 10^{-3}\,1/\text{h}$. $\overline{\alpha}_{\text{ctrl1x}}$ denotes the mean of the 71 α-estimates used to create the cumulative distribution function in Figure 6.5. For the set of experiments `noise_6` we evaluate ΔF by using the average of $\alpha_{\text{noise1x\_6}}$ and $\alpha_{\text{noise2x\_6}}$. We get $\Delta F_{\text{noise\_6}} = 8.8 \times 10^{-3}\,\text{K/h}$, which is smaller than $\Delta F_{\text{ctrl}} = 10.5 \times 10^{-3}\,\text{K/h}$. Hence we infer that in the set of experiments `noise_6` the noise changes the statistical damping coefficient α as well as the change in the forcing ΔF. Case 3 of the above consideration applies.

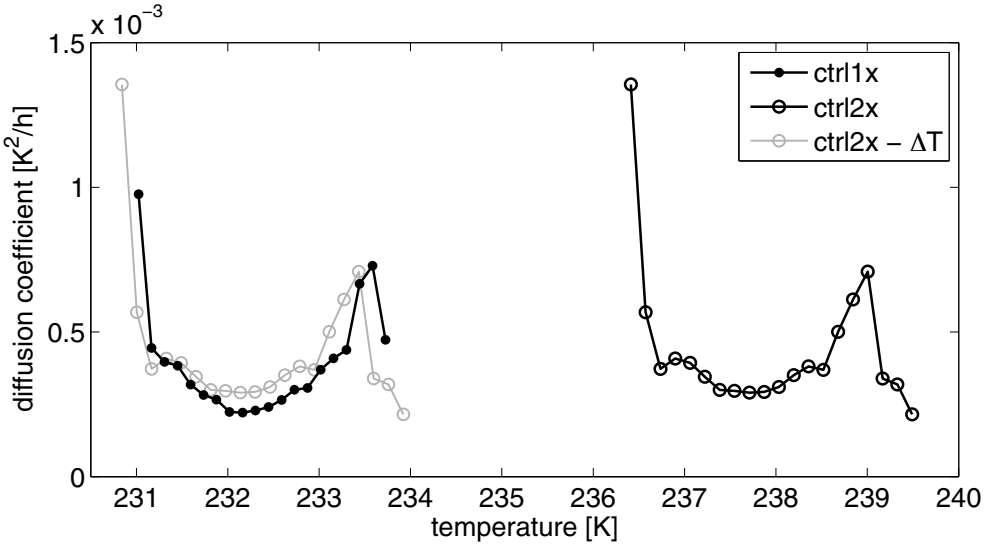

Figure 6.8: *Diffusion coefficient $B(x_s)$ of the experiments* `ctrl1x` *(closed circle) and* `ctrl2x` *(open circle); For comparison the grey curve displays the diffusion coefficient of* `ctrl2x` *minus the temperature response caused by the CO_2 increase.*

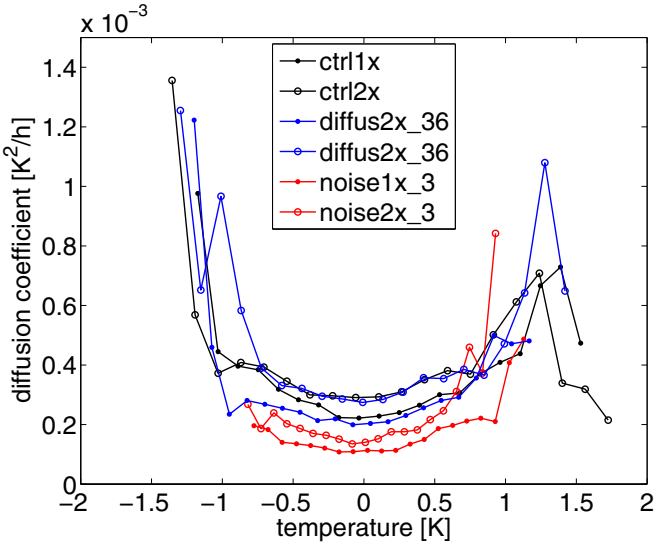

Figure 6.9: *Diffusion coefficients $B(x_s)$ of the experiments* `ctrl1x` *(black closed circles),* `ctrl2x` *(black open circles),* `diffus1x_36` *(blue closed circles),* `diffus2x_36` *(blue open circles),* `noise1x_3` *(red closed circles) and* `noise2x_3` *(red open circles)*

6.3.3 Diffusion coefficients

For the sake of completeness we show the diffusion coefficients $B(x_s)$ of the experiments `ctrl1x` and `ctrl2x` in Figure 6.8. When doubling the CO_2 concentration the shape of the diffusion coefficient (black line with open circles) stays mostly the same as in the experiment with $1\times CO_2$ (line with closed circles). The diffusion coefficient of `ctrl2x` is shifted towards higher temperatures. A closer comparison of the diffusion coefficient from `ctrl1x` and `ctrl2x` reveals slightly larger values for small temperature anomalies in the experiment `ctrl2x`.

Figure 6.9 shows the diffusion coefficients of the same experiments considered in Figure 6.6. For better comparability all coefficients were computed from anomalies, which results in an alignment around zero on the x-axis. In general the diffusion coefficients of the $2\times CO_2$-experiments are larger than the diffusion coefficients of the corresponding pre-industrial runs. Whereas the experiments with reduced horizontal diffusion show roughly similar results as the control experiments, the coefficients of the noise-experiments are significantly smaller.

6.4 Discussion

Doubling CO_2 concentration

In this chapter we investigated how a doubled CO_2 concentration and enhanced small-scale fluctuations affect the statistical properties of the global mean temperature at 300 hPa as modelled by a linear Langevin equation. As expected, when doubling the CO_2 concentration the statistical damping ($-\alpha x$) remains within the uncertainty range unchanged in most experiments. The change in external forcing leads primarily to an increase of the constant forcing F. In the experiments with moderate noise intensity (`noise_3`) the higher CO_2 concentration, however, alters the statistical damping. This finding indicates that in `noise_3` doubling the CO_2 concentration essentially changes the statistics of the global mean temperature at 300 hPa. The 'spring constant' varies with external forcing. The fluctuation dissipation theorem is not applicable in `noise_3`.

Enhancing small-scale fluctuations

The reaction of the system to enhanced small-scale fluctuations depends on the method used to enhance the small-scale fluctuations. Reducing the horizontal diffusion mainly affects ΔF. The statistical damping is not changed in the diffusion-experiments. In contrast, when we add white noise to the small scales the statis-

tical damping is different. In the experiments with high noise intensity the higher statistical damping is partly responsible for the decreased sensitivity of the system to a CO_2-doubling.

When the statistical damping is changed, the enhanced small-scale fluctuation change the 'spring constant' of the system. The 'spring constant' describes how fast the stationary system returns from a natural fluctuation to its mean. Generally, changes in the 'spring constant' are related to changes in internal feedback and interaction processes. For example, negative cloud feedbacks acting in the stationary system could be strengthened resulting in an overall larger negative feedback towards the mean. The system then returns faster from a natural disturbance to its mean.

When ΔF is changed due to enhanced small-scale fluctuations, the small-scale fluctuations do not alter the temporal behaviour of x_s in the unperturbed system but they directly change the mean response of the system to CO_2 doubling. A change in ΔF indicates that the change in $\Delta\mu$ cannot be (solely) explained by changes in the internal feedback processes. We distinguish between the internal feedback processes present in the stationary undisturbed system and feedback processes only acting when the CO_2 concentration is increased. The change in ΔF indicates that the latter feedback processes are altered independently of the internal feedbacks.

Validity of the FDT

During this study we assumed that the fluctuation dissipation theorem (FDT) and with it relation (6.4), $\Delta\mu = \Delta F/\alpha$, is applicable to our system. The FDT as given in the form here is only valid if we can describe the main statistical properties of the global mean temperature at 300 hPa by the linear Langevin equation (6.1). From Figure 5.9 we see, however, that the autocorrelation function of the unfiltered global mean temperature at 300 hPa is not decaying exponentially. Filtering out the long-term variability related to the atmosphere-ocean interactions improves the picture, but especially for larger time lags the autocorrelation function decays too slow.

The Langevin equation is only a crude approximation. An imperfect representation of the autocorrelation function means that equation (6.1) is not an appropriate model. Thus the application of the FDT to the global mean temperature is questionable. However, to truly test the validity of relation (6.4) we would need to obtain independent estimates of $\Delta\mu$, α, and ΔF. Whereas we are able to determine $\Delta\mu$ and α, it is difficult to estimate ΔF. We determined ΔF by using the

relation (6.4). Thus ΔF is not an independent parameter. ΔF directly depends on $\Delta\mu$ and α.

Note that ΔF is not equal to the radiative imbalance ΔQ at the top of the atmosphere arising from CO_2 doubling if everything else is held constant. We can relate ΔF to ΔQ by defining a transfer factor k: $\Delta Q = k\Delta F$. k describes how the radiative forcing ΔQ in W/m^2 translates to ΔF in K/s. k includes, for example, the ocean's heat uptake, but it also includes atmospheric feedback processes, which determine how strongly the global mean temperature at 300 hPa is affected by changes in the radiative forcing.

Time scale

For the estimation of the 'spring constant' we focus on the fast atmospheric variability and filter out large parts of the long-term variability related to the ocean, because we assume that the short-term atmospheric feedback processes are most relevant for the climate change to CO_2-doubling. The importance of fast atmospheric feedback processes is supported by the findings that, e.g., the parameterisations of cloud formation play a crucial role in modelling the correct climate sensitivity (Bony et al., 2006). The long-term response of the ocean on the global mean temperature is included in ΔF. In contrast to our approach, Schwartz (2007, 2008) argues that the long time scales related to the ocean are most important for the climate change occurring on a multidecadal time scale.

7 General conclusions and outlook

7.1 Conclusions

Since all climate models used for climate change studies have finite spatial and temporal resolutions, the effects of subgrid-scale processes on the resolved scales must be parameterised. Most of these parameterisations do not take into account the variability that is induced by subgrid-scale processes. In this study we investigated how enhanced small-scale variability influences the modelled climate response to increased CO_2 concentration. To enhance the small-scale fluctuations we reduced the horizontal diffusion or added white noise to spectral coefficients with high total wavenumbers in ECHAM5/MPI-OM.

Enhancing the small-scale variability affects the mean climate state

We find that enhancing the small-scale variability changes the mean climate state. The $1\times CO_2$-experiments with noise have noticeably different mean climate states compared to the $1\times CO_2$-control-experiment without noise. Reducing the horizontal diffusion also alters the mean climate state, but the changes are not as large as in the noise-experiments. The larger effect of the noise is due to the rather high noise intensities. In this study the noise enhances the small-scale fluctuations much more than the reduction of the horizontal diffusion. Experiments with lower noise intensity would result in smaller changes of the mean climate states.

The representation of small-scale fluctuations matters for the modelled climate sensitivity

Furthermore, we find that the representation of small-scale fluctuations matters for the modelled climate sensitivity to a CO_2 doubling. The representation of dynamical small-scale processes should therefore be considered as a source of uncertainty for the modelled climate sensitivity.

Reducing the horizontal diffusion in ECHAM5/MPI-OM by a factor of two (three) enhances the equilibrium climate sensitivity at the surface by 8% (13%). Since the form and the strength of the horizontal diffusion is generally not very

certain, it is important to note that changes in this parameterisation also affect the model's response to increased CO_2 concentration.

Adding noise to the small scales also affects the temperature response to CO_2 doubling. In the experiment with moderate noise intensity the temperature response is mainly changed in the middle and upper troposphere. The surface climate sensitivity remains unaffected. The decrease of the surface climate sensitivity in the experiment with high noise intensity is likely caused by the strongly modified mean climate state of the $1\times CO_2$ experiment. Compared to the observed present climate the mean climate state of `noise1x_6` is not very realistic. The climate sensitivity of `noise2x_6`–`noise1x_6` might therefore be not applicable for the prediction of the future climate change.

The impact of the enhanced small-scale fluctuations on the modelled climate sensitivity is not as large as, e.g., the impact of different cloud parameterisations. To reduce the uncertainty of predicted climate change, future research should therefore first focus on improving the representation of thermodynamical feedback processes in climate models.

A Langevin equation is suitable to only a limited extent for the representation of the global mean temperature at 300 hPa

To better understand how small-scale fluctuations alter the climate sensitivity, we fitted a linear Langevin equation to the global mean temperature time series at 300 hPa of each experiment and estimated the statistical damping coefficient α for each experiment. A *linear* Langevin equation is sufficient since the drift coefficients obtained from the temperature time series are approximately linear. The slope $-\alpha$ of the drift coefficient is a measure for the 'spring constant'. It describes how fast the system is, on average, driven back towards its mean state after experiencing a natural fluctuation.

Before fitting the stochastic model to the data we filtered out the long-term variability induced by atmosphere-ocean interactions. This is necessary because the univariate stochastic model is not able to reproduce such long-term fluctuations. Since we assume that the strength of the short-term atmospheric feedback processes are most relevant for the climate change to CO_2 doubling, we believe this approach is suitable. While the stochastic model reproduces the probability density distribution well, the autocorrelation function is less satisfactory represented for large time lags.

We are able to distinguish between two mechanism of how the small-scale fluctuations influence the climate sensitivity

The analysis based on the diagnostic of the statistical damping coefficient α and the parameter ΔF makes it possible to distinguish between two mechanisms of how the climate sensitivity can be influenced by the small-scale fluctuations. Enhanced small-scale fluctuations can influence the climate sensitivity via altering the 'spring constant', i.e., feedback and interaction processes that are present in the unperturbed system, or the small-scale fluctuations alter the feedback and interaction processes that are directly coupled to the CO_2 increase.

Reducing the horizontal diffusion does not alter the 'spring constant', but adding noise to the small scales changes it

Reducing the horizontal diffusion does not significantly alter the 'spring constant', i.e. the statistical damping coefficient α. Adding white noise to the small scales influences the statistical damping coefficients. In the noise-experiments with moderate noise intensity the statistical damping coefficients change from the $1\times CO_2$- to the $2\times CO_2$-experiment. In the noise-experiments with high noise intensity the statistical damping coefficients are considerably higher than in the control-experiments.

A comparison of these findings with the results from Chapter 3 reveals that changes of the statistical damping coefficient coincide with changes of the mean climate state in $1\times CO_2$-experiments. Compared to the $1\times CO_2$-control-experiment the mean climate state of the diffusion-experiments is hardly changed. The statistical damping coefficients of the diffusion-experiments remain also unaffected. On the other side the mean climate state of the $1\times CO_2$-noise-experiment with high noise intensity (`noise1x_6`) is very different to that of `ctrl1x`, and also the statistical damping coefficient in `noise1x_6` is altered. The change in α indicates that the temporal behaviour of the global mean temperature at 300 hPa is different. The internal feedback processes determining the way in which the system returns from a natural fluctuation to its mean are changed.

The results of the noise-experiments with moderate noise intensity (`noise_3`) lie between the diffusion-experiments and the experiments with strong noise. The moderate noise alters the mean climate state more strongly than the reduced horizontal diffusion but less than the strong noise. Since the statistical damping coefficients of `noise_3` change when the CO_2 concentration is increased, the fluctuation dissipation theorem (FDT) is not applicable in these experiments. The change in the statistical damping indicates that the mean temporal behaviour and

with it the internal feedback processes are changed when increasing the CO_2 concentration. Since the FDT is only valid for small changes in the external forcing, the dependence of the statistical damping on the CO_2 concentration might be an indicator that the change in external forcing caused by the CO_2 doubling is too large. It remains, however, an open question why the CO_2 doubling should be a too strong forcing in `noise_3` but not in the other experiments.

Changes in the temperature response are (partly) due to changes in feedback processes, which cannot be observed in the unperturbed system

We assume that the temperature response $\Delta\mu$ is determined by $\Delta\mu = \Delta F/\alpha$. Since in the diffusion-experiments α is not changed although $\Delta\mu$ increases, ΔF must be changed. ΔF is also changed in the noise-experiments with high noise intensity. The larger α in `noise_6` is not sufficient to explain the decrease of the climate response.

ΔF represents the change of the net forcing on the global mean temperature at 300 hPa. Differences in ΔF are due to changes in feedback processes, which cannot be observed in the unperturbed system. Feedback processes, which are only acting when the CO_2 concentration is increased, are altered.

7.2 Outlook

Although we investigated in Chapter 4 which physical feedback processes are influenced by the enhanced small-scale fluctuations, the exact cause-and-effect-chain leading to the different climate sensitivities remains unclear. In general, it is very difficult and maybe impossible to disentangle the processes leading to a higher/lower climate sensitivity when enhancing the small-scale variability. The difficulties arise from the complex interactions between the nonlinear processes acting in the climate system. To get a more quantitative idea how strong each thermodynamical feedback process changed, offline radiative transfer calculations (as done in Colman (2003), Soden and Held (2006)) could be used for measuring the climate change feedbacks in each pair of experiments. In this way we could quantify the effects of the enhanced small-scale fluctuations on each climate feedback altering the climate response to CO_2 doubling.

Future work could also focus on relating the parameters of the stochastic model to the physics of the system. We, for example, stated that the statistical damping is related to the internal feedback processes, which are always present in the stationary system. Showing that one or more of these internal feedback processes

is actually different in a system with higher/lower statistical damping, would demonstrate that this physical interpretation is justified.

It would also be interesting to see how the climate sensitivity was influenced in experiments with lower noise intensity than used in `noise_3`. From the small effect found in the experiments with moderate noise (`noise2x_3`–`noise1x_3`) we expect that the climate sensitivity would not be influenced by a lower noise intensity. It is, however, also possible that such an experiment would react more like the experiments with reduced horizontal diffusion resulting in an increase of the climate sensitivity.

Our results show that the representation of small-scale fluctuations near the truncation scale influences the modelled climate response to higher CO_2 concentrations. The representation of small-scale processes is generally more realistic in climate models with high spatial and temporal resolutions. But since numerical climate models will always have finite resolutions we encourage the development and improvement of stochastic parameterisations schemes to ensure the proper inclusion of small-scale variability.

A Filtering out the long-term variability

In the following we describe the derivation of x_s from the global mean temperature at 300 hPa x. We assume, the time anomalies of the global mean temperature at 300 hPa, $x' = x - \overline{x}$, can be divided into two parts:

$$x' = x'_s + x'_l \tag{A.1}$$

where x'_s describes the part which is associated with the internal short-term atmospheric variations and x'_l is related to the long-term variations of the atmosphere caused by the interactions of the atmosphere and the ocean. To estimate x'_l we assume a linear relationship between x'_l and the anomalies of the global mean sea surface temperature (SST) y'.

$$x' = x'_s + \beta y' \tag{A.2}$$

Before carrying out a least-squares fit a 90 day-running mean is applied to the data. In this way we can assure that we get hold just of the long-term variations. Under the assumption that x'_s and y'_{90d} are uncorrelated β can be estimated by using:

$$\beta = \frac{\langle x'_{90d}\, y'_{90d} \rangle}{\langle {y'_{90d}}^2 \rangle}, \tag{A.3}$$

where x'_{90d} and y'_{90d} denote the time series on which a 90 day-running mean was applied. We determine x'_s by subtracting the scaled SST anomalies from x'

$$x'_s = x' - \beta\, y'_{90d} \tag{A.4}$$

The filtered global mean temperature at 300 hPa, x_s, can now be defined as

$$x_s = x'_s + \overline{x} = x - \beta y'_{90d} \tag{A.5}$$

Figure A.1 shows the autocorrelation functions of x' and x'_s. The major part of the longterm variability is filtered out by the filtering procedure. Some mediumterm variability remains, however, in the system.

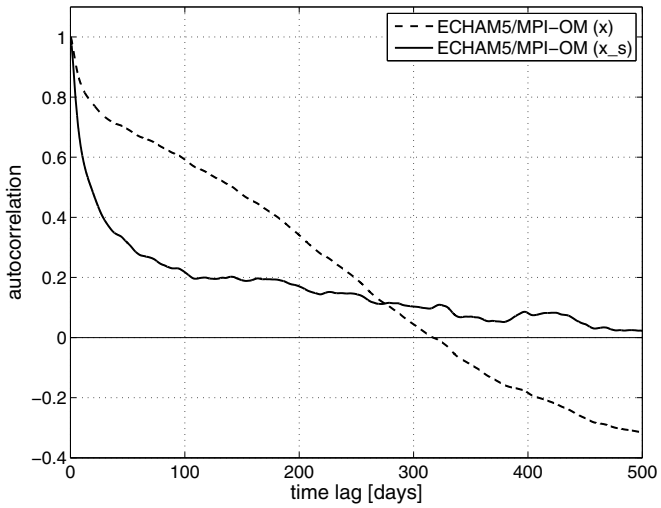

Figure A.1: *Autocorrelation function of filtered and unfiltered ECHAM5/MPI-OM data*

Bibliography

Barsugli, J. J. and D. S. Battisti, 1998: The basic effects of atmosphere-ocean thermal coupling on midlatitude variability. *J. Atmos. Sci.*, **55 (4)**, 477–493.

Bates, J. R., 2007: Some considerations of the concept of climate feedback. *Quart. J. Roy. Meteor. Soc.*, **133 (624)**, 545–560.

Bell, T. L., 1980: Climate sensitivity from fluctuation dissipation: Some simple model tests. *J. Atmos. Sci*, **37**, 1700–1707.

Bengtsson, L., K. I. Hodges, M. Esch, N. Keenlyside, L. Kornblueh, J. J. Lu, and T. Yamagata, 2007: How may tropical cyclones change in a warmer climate? *Tellus*, **59 (4)**, 539–561.

Berner, J., 2003: Detection and stochastic modelling of nonlinear signatures in the geopotential height of an atmospheric general circulation model. Ph.D. thesis, Mathematisch-Naturwissenschaftliche Fakultät, Rheinische Friedrich-Wilhelms-Universität Bonn.

Berner, J., 2005: Linking nonlinearity and non-gaussianity of planetary wave behavior by the Fokker-Planck equation. *J. Atmos. Sci.*, **62 (7)**, 2098–2117.

Bony, S., et al., 2006: How well do we understand and evaluate climate change feedback processes? *J. Climate*, **19 (15)**, 3445–3482.

Branstator, G. and S. E. Haupt, 1998: An empirical model of barotropic atmospheric dynamics and its response to tropical forcing. *J. Climate*, **11 (10)**, 2645–2667.

Buizza, R., M. Miller, and T. N. Palmer, 1999: Stochastic representation of model uncertainties in the ECMWF Ensemble Prediction System. *Q. J. R. Meteorol. Soc.*, **125**, 2887–2908.

Cionni, I., G. Visconti, and F. Sassi, 2004: Fluctuation dissipation theorem in a general circulation model. *Geophys. Res. Lett*, **31**, L09 206, doi: 10.1029/2004GL019739.

Colman, R., 2003: A comparison of climate feedbacks in general circulation models. *Climate Dyn.*, **20 (7-8)**, 865–873.

DelSole, T., 2000: A fundamental limitation of markov models. *J. Atmos. Sci.*, **57 (13)**, 2158–2168.

Frederiksen, J. S., M. R. Dix, and A. G. Davies, 2003: The effects of closure-based eddy diffusion on the climate and spectra of a GCM. *Tellus Series A-Dynamic Meteorology and Oceanography*, **55 (1)**, 31–44.

Frederiksen, J. S. and S. M. Kepert, 2006: Dynamical subgrid-scale parameterizations from direct numerical simulations. *J. Atmos. Sci.*, **63 (11)**, 3006–3019.

Gardiner, C. W., 1985: *Handbook of Stochastic Methods: For Physics, Chemistry, and the Natural Sciences*. Springer.

Gent, P. R., J. Willebrand, T. J. McDougall, and J. C. McWilliams, 1995: Parameterizing eddy-induced tracer transports in ocean circulation models. *J. Phys. Oceanogr.*, **25 (4)**, 463–474.

Gritsun, A. and G. Branstator, 2007: Climate response using a three-dimensional operator based on the fluctuation-dissipation theorem. *J. Atmos. Sci.*, **64 (7)**, 2558–2575.

Hasselmann, K., 1976: Stochastic climate models Part I. Theory. *Tellus*, **28 (6)**, 473–485.

Holton, J. R., 1992: *An Introduction to Dynamic Meteorology*. 3d ed., Academic Press.

IPCC, 2007: *Climate Change 2007: The Physical Science Basis. Contribution of Working Group I to the Fourth Assessment Report of the Intergovernmental Panel on Climate Change*. Cambridge University Press, Cambridge, United Kingdom and New York, NY, USA.

Jungclaus, J. H., et al., 2006: Ocean circulation and tropical variability in the coupled model ECHAM5/MPI-OM. *J. Climate*, **19 (16)**, 3952–3972.

Kaas, E., A. Guldberg, W. May, and M. Deque, 1999: Using tendency errors to tune the parameterisation of unresolved dynamical scale interactions in atmospheric general circulation models. *Tellus Sesies A-Dynamic Meteorology and Oceanography*, **51 (5)**, 612–629.

Kiehl, J. T., C. A. Shields, J. J. Hack, and W. D. Collins, 2006: The climate sensitivity of the Community Climate System Model version 3 (CCSM3). *J. Climate*, **19 (11)**, 2584–2596.

Kloeden, P., 1992: *Numerical Solution of Stochastic Differential Equations*. Springer, Berlin.

Kloster, S., K. D. Six, J. Feichter, E. Maier-Reimer, E. Roeckner, P. Wetzel, P. Stier, and M. Esch, 2007: Response of dimethylsulfide (DMS) in the ocean and atmosphere to global warming. *Journal of Geophysical Research-Biogeosciences*, **112 (G3)**, G03 005.

Knutti, R., G. A. Meehl, M. R. Allen, and D. A. Stainforth, 2006: Constraining climate sensitivity from the seasonal cycle in surface temperature. *J. Climate*, **19 (17)**, 4224–4233.

Koshyk, J. and G. Boer, 1995: Parameterization of dynamical subgrid-scale processes in a spectral GCM. *J. Atmos. Sci.*, **52 (7)**, 965–976.

Kraichnan, R. H., 1967: Inertial ranges in two-dimensional turbulence. *Phys. Fluids*, **10 (7)**, 1417–1423.

Langen, P. L. and V. A. Alexeev, 2005: Estimating $2\times CO_2$ warming in an aquaplanet GCM using the fluctuation-dissipation theorem. *Geophys. Res. Lett.*, **32**, L23 708, doi:10.1029/2005GL024136.

Leith, C., 1975: Climate response and fluctuation dissipation. *J. Atmos. Sci*, **32**, 2022–2026.

Leith, C. E., 1971: Atmospheric predictability and 2-dimensional turbulence. *J. Atmos. Sci.*, **28 (2)**, 145–161.

Liou, K. N., 2002: *An Introduction to Atmospheric Radiation*, International Geophysics Series, Vol. 84. 2d ed., Academic Press.

Marotzke, J. and M. Botzet, 2007: Present-day and ice-covered equilibrium states in a comprehensive climate model. *Geophys. Res. Lett.*, **34 (16)**, L16 704.

Marsland, S. J., H. Haak, J. H. Jungclaus, M. Latif, and F. Roske, 2003: The Max-Planck-Institute global ocean/sea ice model with orthogonal curvilinear coordinates. *Ocean Modelling*, **5 (2)**, 91–127.

May, W. and E. Roeckner, 2001: A time-slice experiment with the ECHAM4 AGCM at high resolution: the impact of horizontal resolution on annual mean climate change. *Climate Dyn.*, **17 (5-6)**, 407–420.

Meehl, G., et al., 2007: *Climate Change 2007: The Physical Science Basis. Contribution of Working Group I to the Fourth Assessment Report of the Intergovernmental Panel on Climate Change*, chap. Global Climate Projections. Cambridge University Press, Cambridge, United Kingdom and New York, NY, USA.

Murphy, J. M., D. M. H. Sexton, D. N. Barnett, G. S. Jones, M. J. Webb, and M. Collins, 2004: Quantification of modelling uncertainties in a large ensemble of climate change simulations. *Nature*, **430 (7001)**, 768–772.

North, G. R., R. E. Bell, and J. W. Hardin, 1993: Fluctuation dissipation in a general circulation model. *Climate Dyn.*, **8**, 259–264.

North, G. R., R. F. Cahalan, and J. A. Coakley, 1981: Energy-balance climate models. *Rev. Geophys.*, **19 (1)**, 91–121.

Peixoto, J. P. and A. H. Oort, 1993: *Physics of Climate*. American Insitute of Physics.

Penland, C., 2003: A stochastic approach to nonlinear dynamics: A review (extended version of the article - "noise out of chaos and why it won't go away"). *Bulletin of the American Meteorological Society*, **84 (7)**, 925–925.

Penland, C. and L. Matrosova, 1998: Prediction of tropical atlantic sea surface temperatures using linear inverse modeling. *J. Climate*, **11 (3)**, 483–496.

Penland, C. and P. D. Sardeshmukh, 1995: The optimal-growth of tropical sea-surface temperature anomalies. *J. Climate*, **8 (8)**, 1999–2024.

Piani, C., D. J. Frame, D. A. Stainforth, and M. R. Allen, 2005: Constraints on climate change from a multi-thousand member ensemble of simulations. *Geophys. Res. Lett.*, **32 (23)**, L23 825.

Pohlmann, H., F. Sienz, and M. Latif, 2006: Influence of the multidecadal Atlantic meridional overturning circulation variability on European climate. *J. Climate*, **19 (23)**, 6062–6067.

Risken, H., 1984: *The Fokker-Planck Equation: Methods of Solution and Applications*. Springer.

Roeckner, E., et al., 2003: The atmospheric general circulation model ECHAM5 Part I - Model description. Tech. Rep. 349, Max Planck Institut for Meteorology.

Roeckner, E., et al., 2006: Sensitivity of simulated climate to horizontal and vertical resolution in the ECHAM5 atmosphere model. *J. Climate*, **19 (16)**, 3771–3791.

Schwartz, S. E., 2007: Heat capacity, time constant, and sensitivity of Earth's climate system. *J. Geophys. Res.*, **112 (D24)**, D24S05.

Schwartz, S. E., 2008: Reply to comments by G. Foster et al., R. Knutti et al., and N. Scafetta on "Heat capacity, time constant, and sensitivity of Earth's climate system". *J. Geophys. Res*, in press., doi:10.1029/2008JD009872.

Seiffert, R., R. Blender, and K. Fraedrich, 2006: Subscale forcing in a global atmospheric circulation model and stochastic parametrization. *Quart. J. Roy. Meteor. Soc.*, **132 (618)**, 1627–1643.

Seiffert, R. and J. S. von Storch, 2008: Impact of atmospheric small-scale fluctuations on climate sensitivity. *Geophys. Res. Lett.*, **35 (10)**, L10 704.

Siegert, S., R. Friedrich, and J. Peinke, 1998: Analysis of data sets of stochastic systems. *Phys. Lett. A*, **243 (5-6)**, 275–280.

Soden, B. J., A. J. Broccoli, and R. S. Hemler, 2004: On the use of cloud forcing to estimate cloud feedback. *J. Climate*, **17 (19)**, 3661–3665.

Soden, B. J. and I. M. Held, 2006: An assessment of climate feedbacks in coupled ocean-atmosphere models. *J. Climate*, **19 (14)**, 3354–3360.

Stephenson, D. B., 1995: The impact of changing the horizontal diffusion scheme on the northern winter climatology of a general circulation model. *Quart. J. Roy. Meteor. Soc.*, **121 (521)**, 211–226.

Sura, P., 2003: Stochastic analysis of southern and pacific ocean sea surface winds. *J. Atmos. Sci.*, **60 (4)**, 654–666.

Sura, P. and J. Barsugli, 2002: A note on estimating drift and diffusion parameters from timeseries. *Phys. Lett. A*, **305 (5)**, 304–311.

Valcke, S., A. Caubel, D. Declat, and L. Terray, 2003: OASIS3 Ocean Atmosphere Sea Ice Soil User's Guide. Tech. rep., CERFACS, Toulouse, France.

Vallis, G. K., E. P. Gerber, P. J. Kushner, and B. A. Cash, 2004: A mechanism and simple dynamical model of the north atlantic oscillation and annular modes. *J. Atmos. Sci.*, **61 (3)**, 264–280.

von Storch, J. S., 2004: On statistical dissipation in GCM-climate. *Climate Dyn.*, **23 (1)**, 1–15.

von Storch, J. S. and H. Haak, 2008: Impact of daily fluctuations on long-term predictability of the atlantic meridional overturning circulation. *Geophys. Res. Lett.*, **35 (1)**, L01 609.

Webb, M. J., et al., 2006: On the contribution of local feedback mechanisms to the range of climate sensitivity in two GCM ensembles. *Climate Dyn.*, **27 (1)**, 17–38.

Wetherald, R. T. and S. Manabe, 1988: Cloud feedback processes in a general-circulation model. *J. Atmos. Sci.*, **45 (8)**, 1397–1415.

Acknowledgements

I would like to thank all people, who encouraged and supported me during my PhD work. Without you I never had started this thesis and finished it.

In particular, I thank my supervisor, Jin-Song von Storch. She was always receptive to my scientific questions, problems, ideas and doubts. Thank you for many helpful discussions and the continuous support throughout the last years.

Furthermore, I am very grateful to the other two members of my advisory panel, Johann Jungclaus and Klaus Hasselmann, for their scientific advice, ideas and guidance.

I thank Jochem Marotzke, who reviewed this thesis as primary referee.

Many thanks go to all current and former members of the ocean group at the Max Planck Institute for Meteorology. I enjoyed being part of this interdisciplinary group and benefited from many discussions during the weekly group meeting and outside it.

For scientific and technical support I thank Erich Roeckner, Johannes Quaas, Dirk Notz, Michael Botzet, Helmuth Haak, and Monika Esch.

Special thanks go to Malte Heinemann, Lorenzo Tomassini, Daniel Hernandez Decker, Hui Wan, Claas Teichmann and Heinz Jürgen Punge for reading parts of the manuscript. Their suggestions greatly improved the thesis.

I thank the International Max Planck Research School on Earth System Modelling for giving me the opportunity to carry out my PhD studies. I am grateful to Antje Weitz and Cornelia Kampmann, who were always prepared to provide organisational support and advise.

I thank CIS for their technical support and patience. I thank the library and the administrative staff for their support.

Die gesamten Veröffentlichungen in der Publikationsreihe des MPI-M
„Berichte zur Erdsystemforschung“,
„Reports on Earth System Science“,
ISSN 1614-1199

sind über die Internetseiten des Max-Planck-Instituts für Meteorologie erhältlich:

http://www.mpimet.mpg.de/wissenschaft/publikationen.html


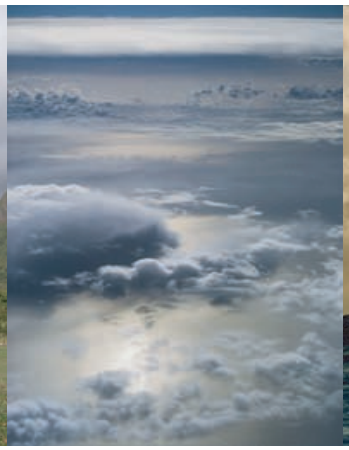


ISSN 1614-1199